THE ROLE OF OXIDATIVE STRESS IN ABDOMINAL AORTIC ANEURYSM DEVELOPMENT: MOLECULAR AND MECHANICAL EFFECTS IN THE ORIGINS OF ANEURYSMAL DISEASE

A Dissertation
Presented to the
Academic Faculty

by

Kathryn A. Maiellaro, M.E.

In Partial Fulfillment
of the Requirements for the Degree
Doctor in Philosophy in the
Wallace H. Coulter Department of Biomedical Engineering

Georgia Institute of Technology

August 2008

THE ROLE OF OXIDATIVE STRESS IN ABDOMINAL AORTIC ANEURYSM DEVELOPMENT: MOLECULAR AND MECHANICAL EFFECTS IN THE ORIGINS OF ANEURYSMAL DISEASE

Approved by:

W. Robert Taylor, M.D., Ph.D
School of Medicine
Emory University

John N. Oshinski, Ph.D
Department of Biomedical Engineering
Georgia Institute of Technology

Rudolph L. Gleason, Jr., Ph.D
Department of Biomedical Engineering
Georgia Institute of Technology

Raymond P. Vito, Ph.D
Department of Biomedical Engineering
Georgia Institute of Technology

Kathy K. Griendling, Ph.D
School of Medicine
Emory University

Date Approved: June 16, 2008

ACKNOWLEDGEMENTS

It is difficult for me, if not laughable, to include only myself as the author of this thesis, when so many others have contributed to the final product. Be it through help with experiments, scientific guidance, chats about interpreting the data, encouragement, or just getting me over the graduate slump with friendship, I have many people to thank. I would like to thank first and foremost my mentor Bob Taylor. At our first meeting I knew that Bob would become somewhat of a father figure, and in that way would guide my graduate studies not just by what was best for his lab, but for what was best for me and my life. Of course there's the joke that I told him from Day 1 (I would say "requested of him") that I would be graduating in 5 years. This of course has been brought up at every one-on-one meeting, random exchange in the hallway, and even during my committee meetings. In the end, I am so thankful that Bob actually respected my request. He has been a wonderful guide over the past 4 years: letting me make big (expensive!) mistakes and not making me feel inferior for it, and letting me take the reins in the last year or so to design and execute experiments in the way I best see fit. I have learned so much from him and I leave the lab thinking, "Man! Now that I know what I'm doing, I could accomplish so much more if I could go back and do this all over again!" That's the point of this whole process I guess. Mission accomplished.

I also express great gratitude to my dissertation committee for their guidance over the years. It must be difficult to advise a BME student, who walks the line between engineering and biology, not necessarily exploring one of the two to the fullest depth. My mentors demonstrated that biology and engineering principles are intertwined, one dependent on the other, and all questions must be addressed with that concept in mind.

Dr. Ray Vito, Dr. Rudy Gleason, and Dr. John Oshinski were superb advisors for engineering aspects. Under their guidance I feel that the work presented here is solidly based in engineering fundamentals. I am particularly thankful to Dr. Gleason and his graduate trainee William Wan, for allowing me to use their biaxial testing set-up. While not the core of my thesis, the experiments performed on this system have provided a spring board for future work. William was so patient and helpful as I learned to use the set-up, and I am grateful for his kindness and support. I would particularly like to express my admiration to Drs. Griendling and Gleason, as they have demonstrated such a successful balance between work and family. It is an example that I will bring with me into my own career and I thank them for showing me that such a balance is possible (albeit with a lot of work I'm sure).

Of course I can't thank enough the people with whom I worked with everyday, Team Taylor! Work is so much better when it doesn't feel like work, but just a get together of your friends. This camaraderie is as much a testament to the type of students who enter into the Wallace H. Coulter Department of Biomedical Engineering, as well as the ability of Bob to hire intelligent, down-to-earth trainees. I met one of my best friends Patrick Cowan in the Taylor Lab. What a great opportunity to come to work everyday to see your best buddy! Patrick taught me not to sweat everything so much, and that the most productive work is mixed with lots of fun. When Patrick moved to bigger and better things to enter grad school, my chronic laughter-induced stomach ache carried on in cahoots with Craig Duvall, Scott Robinson, Nick Willett, and Ebony Washington. These friends have truly propelled me through graduate school. If I didn't have them to joke with, party with, and talk science with, I wouldn't have enjoyed it my time here half

as much, and the quality of my work would have suffered. Craig, thanks for returning my email 5 years ago when I was looking into possible labs. You helped me make the perfect choice of lab and I got you as a friend- what a deal! Scott, Chuck Norris of Emory Cardiology, you will tear this section apart with your teeth when you read this, but you have proved to be a true friend, one I can count on. By being the only one to celebrate my birthday (you too Ebony!), to providing the deep fryer, to helping trouble-shoot my PCR, to our conversations (read- all the times we made fun of each other) through the portal, I know you're a good friend (and you can't do anything to change my mind!! Ha!!). Nick, I can leave here knowing that all of your research potential can be attributed to my good tutelage. I'm going to try to emulate your cool-under-pressure, as I know you work so hard, while keeping yourself as laid-back as possible. Ebony, I agree with you to keep "always smiling." Thank you for being my girlfriend among all these boys. I think I would have gone crazy without you.

Finally, I'd like to appreciate 2 special Taylorites, without whom most my work could not have be accomplished. Dr. Daiana Weiss has provided immeasurable knowledge and skill throughout my time here. When you need to work with animals, you need to know Daiana. Daiana has the magic touch when it comes to science, so much so that I didn't trust my own hands for certain experiments, i.e. I wouldn't have dared to extract RNA from my precious catalase mice. I feel like Daiana truly wanted me to succeed here, and that she often took my success as a reflection of her own. That is such a wonderful trait of a mentor. Giji Joseph, the histology guru, has also been instrumental in regards to my work. She has also been a wonderful companion in room 326! I will

really miss talking to her. Daiana and Giji, thanks so much for your time and expertise. I am so grateful to both of you. Your stamp is definitely all over this thesis.

To the original blue-cheesers Craig, Matt Rhyner, Angela Lin, and Scott, to the Disciples of Cheesus, including Angie Gulino and Torrence Welch, and to all other cheese-lovers- it shouldn't be legal to have so much cheesy goodness on one table. I'd particularly like to thank Matt and Corinne Rhyner for introducing me to my fiancé Tom Rafferty. There is not much more I can say about that except that I am so happy you did, and that my life is better for knowing the two of you. An even before meeting Tom, you opened your house to some of my greatest memories of grad school- chili cook-offs, lumberjack competitions, and BBQs!

I would like to thank my parents Ed and Rachel, who weren't initially too crazy about me entering into a Ph.D program. But it was their guidance that prompted me to challenge myself beyond what I think I can do, and so when I noticed that I excelled at school, I just kept going (and going, and going, and going). And so I know it's been a long road for us, but it's been a trip worth making. I could not have made it through without your support and love. And I'm happy that I obtained my degree before I got married, so that I can enjoy being *Dr. Maiellaro*. It would have been a shame to replace my surname after all we've been through and how long it's taken me to get to this point. Besides, what's the fun of having a last name that people can actually pronounce?!

And lastly I'd like to apologize to my fiancé Tom for that last name comment! Tom has been with me step-by-step during these past months, keeping me sane and pulling me back from the edge. He has maintained my spirits and made sure I didn't

worry myself into a panic attack. Thank you Tom, for your support and love, but mostly for your friendship, which is truly special.

TABLE OF CONTENTS

ACKNOWLEDGEMENTS iii

LIST OF TABLES xiii

LIST OF FIGURES xiv

SUMMARY xvii

CHAPTER 1: SPECIFIC AIMS 1

1.1 Introduction 1

1.2 Aim 1 1

1.3 Aim 2 2

1.4 Aim 3 2

1.5 Significance and Innovation 3

CHAPTER 2: BACKGROUND AND LITERATURE REVIEW 5

2.1 AAA Epidemiology 5

2.2 AAA Pathology 6

2.3 AAA Biology 7

2.3.1 Physical Remodeling 7

2.3.2 Matrix metalloproteinases 8

2.3.3 Reactive Oxygen Species 12

2.4 Catalase and AAA 14

2.5 Animal Models of AAA Formation 17

2.6 AAA Biomechanics 18

2.6.1 Modeling the Mechanical Behavior of Large Arteries 20

CHAPTER 3: BIOMECHANICAL AND MOLECULAR CHARACTERIZATION OF THE EARLY MURINE AAA 26

3.1 Introduction 26

3.2 Methods 26

3.2.1 Animals 27

3.2.2 Models of Aneurysm Formation 27

3.2.3 Wire Myography 27

3.2.4 Vessel Isolation and Mechanical Testing 28

3.2.5 Magnetic Resonance Angiography 30

3.2.6 Ultrasound Imaging 30

3.2.7 Histological Analysis 31

3.2.8 Statistical Analysis 31

3.3 Results 31

3.3.1 Aortic ring testing 31

3.3.2 Mechanical Testing 34
3.3.2.1 Experimental design and aortic preparation 34
3.3.2.2 Optimization of P-D data acquisition 34
3.3.2.3 Compliance mechanics of AAA models 37
3.3.2.4 Compliance mechanics in apoE$^{-/-}$ mice 42
3.3.3 In vivo validation 44
3.3.3.1 In vivo validation: MRI 44
3.3.3.2 In vivo validation: Ultrasound 47
3.3.4 Microstructural Analysis 49
3.3.4.1 Incidence of AAA formation 49
3.3.4.2 Microstructure of established aneurysms 50
3.3.4.3 Microstructure of Small AAA 53
3.3.4.4 Microstructure of the Pre Aneurysm 56

3.4 Discussion 59

CHAPTER 4: H_2O_2 IS MECHANISTICALLY LINKED TO AAA BIOMECHANICAL REMODELING 63

4.1 Introduction 63

4.2 Animals 65

4.3 Methods 65
4.3 1 Aortic Preparation and Set-Up 65
4.3.2 Measurement of Opening Angle 66

4.3.3 Measurement of Collagen Content 67

4.3.4 Gelatin Zymography 67

4.3.5 Histological Analysis 68

4.3.6 Quantiative real-time PCR 69

4.3.7 Statistical Analysis 70

4.4 Results 70

4.4.1 Circumferential mechanical behavior 70

4.4.2 Collagen content SMC-Cat and WT 74

4.4.3 H_2O_2 scavenging blunts increased opening angle 75

4.4.4 Media directs mechanical changes in AAA formation 77

4.4.5 Medial H_2O_2 scavenging and altered collagen gene transcription 80

4.4.6 MMP-9 activity in SMC-Cat aortas 83

4.5 Discussion 85

CHAPTER 5: THE ADVENTITIA IS AN IMPORTANT LOAD BEARING CONSTITUENT OF THE ARTERIAL WALL 92

5.1 Introduction 92

5.2 Methods 93

5.2.1 Animals and Reagents 93

5.2.2 Circumferential mechanic 94

5.2.3 Collagenase digestion of adventitia 94

5.2.4 Histological Analysis 95

5.2.5 Vascular contractility after collagen digestion 95
5.2.6 Multiaxial Mechanical Testing 96
5.3 Results 96
5.3.1 Adventitia dispersion alters mechanical behavior 96
5.3.2 Collagenase digestion is specific to the adventitia 99
5.3.3 VSMC contractility is maintained after adventitia digestion 100
5.3.4 P-D response after adventitia digestion 102
5.4 Disussion 105
CHAPTER 6: SUMMARY, LIMITATIONS, AND FUTURE CONSIDERATIONS . 110
6.1 Summary 110
6.2 Limitations and Future Directions 111
6.2.1 Aim 1 111
6.2.2 Aim 2 113
6.2.3 Aim 3 116
6.3 Conclusion 118
APPENDIX A 120
REFERENCES 122
VITA 134

LIST OF TABLES

TABLE 2.3.1 MMPs and TIMPS in AAA Development 11

TABLE 2.4.1 Matrix genes downregulated in the SMC-Cat aorta. 17

TABLE 3.2.1 In vivo pre-stretch 38

TABLE 3.2.2 Baseline maximum compliance of control mice. 38

TABLE 3.3.1 Aortic compliance measured by MRI. 46

TABLE 3.3.2 Aortic compliance measured by ultrasound. 48

TABLE 3.4.1 Indidence of AAA and dissection in murine models. 49

LIST OF FIGURES

FIGURE 2.3.1 Vascular Reactive Oxygen Species 13

FIGURE 2.4.1 En face WT apoE$^{-/-}$ aorta 16

FIGURE 2.4.2 En face SMC-Cat aorta..... 16

FIGURE 2.6.1 Axial and circumferential forces on an artery. 23

FIGURE 3.1 Isolated Vessel Testing Set-Up 29

FIGURE 3.1.1 Force versus deformation behavior of aorta rings. 32

FIGURE 3.1.2 Force versus deformation curves from aortic rings. 33

FIGURE 3.2.1 Representative pressure ramp and diameter response. 35

FIGURE 3.2.2 Optimization of mechanical testing..... 35

FIGURE 3.2.3 Preconditioning cycles. 36

FIGURE 3.2.4 Typical P-D response. 37

FIGURE 3.2.5 Local compliance versus pressure curve. 39

FIGURE 3.2.6 Pressure versus diameter response in the accelerated model 40

FIGURE 3.2.7 Compliance-pressure response at 12 days..... 40

FIGURE 3.2.8 Compliance-pressure response at 6 days..... 41

FIGURE 3.2.9 P-D response of the angII/HF model..... 41

FIGURE 3.28 Verhoff van Geison image of angII/HF after 9 days. 57

FIGURE 3.3.1 Compliance versus pressure behavior apoE$^{-/-}$ + angII/HF 43

FIGURE 3.3.2 MR Angiogram..... 45

FIGURE 3.3.3 MR Angiogram of AAA..... 45

FIGURE 3.3.4 Black-blood MR images of the abdominal aorta..... 47

FIGURE 3.3.5 Doppler Ultrasound imaging of the abdominal aorta. 48

FIGURE 3.4.1 Representative image of a healthy aorta. 50
FIGURE 3.4.2 Representative image of an established AAA. 50
FIGURE 3.4.3 Representative images of healthy aortic microstructure. 52
FIGURE 3.4.4 Cross-section of the healthy aortic microstrucure. 52
FIGURE 3.4.5 Representative image of the microstructure of an established AAA. 53
FIGURE 3.4.6 Representative en face image of early AAA dilation. 54
FIGURE 3.4.7 Representative images of small AAA. 55
FIGURE 3.4.9 Elastin staining of accelerated model of AAA. 58
FIGURE 4.4.1 In vivo pre-stretch of WT and SMC-Cat aorta. 71
FIGURE 4.4.2 Mechanical behavior of WT versus SMC-Cat aortas. 72
FIGURE 4.4.3 Collagen content and picro-sirius red staining 75
FIGURE 4.4.4 Collagen content after angII/HF treatment. 76
FIGURE 4.4.5 Representative images of opening angles. 77
FIGURE 4.4.6 Thickness of aortic media and adventitia. 79
FIGURE 4.4.7 Elastin fragmentation. 80
FIGURE 4.4.8 Quantitative RT-PCR of matrix genes. 82
FIGURE 4.4.9 MMP activity 84
FIGURE 5.3.1 Circumferential strain and local compliance 97
FIGURE 5.3.2 Histological analysis of control and collagenase digested aortas 100
FIGURE 5.3.3 Baseline and PE-induced tension in aortic rings 101
FIGURE 5.3.4 Contractile response of aortic rings to 10μM PE. 102
FIGURE 5.3.5 Biphasic diameter repsonse at altered axial stretch. 103
FIGURE 5.3.6 Example of pressure versus axial force behavior. 103

FIGURE 5.3.7 P-D response after collagenase digestion. 104

FIGURE 5.3.8 Pressure versus axial force behavior after collagenase digestion..... 105

FIGURE 6.2.1 Multiphoton excitation confocal microscopy. 113

FIGURE 6.2.2 Stress and stretch in the unloaded and loaded configurations. 115

FIGURE 6.2.3 Lysyl oxidase isoform expression in aortic tissue. 117

FIGURE 6.2.4 Expression of lysyl oxidase isoforms 118

SUMMARY

The etiology of abdominal aortic aneurysms (AAA) is characterized by localized extracellular matrix (ECM) remodeling and vessel dilation attributable to degeneration of elastin and collagen. Population-based studies have shown that AAA account for nearly 1% of all deaths with an incidence of up to 13% in males over age 65. The central theme of this thesis is to identify the earliest molecular and biomechanical determinants of aneurysm formation.

Our initial motivator was the lack of information defining the underlying mechanisms of AAA formation. To determine these events we used isolated vessel testing and histological analysis to study the mechanical and morphological evolution of AAA. These factors were measured in murine models of reproducible AAA formation. From this study, we determined 1) that molecular events precede mechanical events in AAA progression and 2) aortic circumferential mechanics are well conserved during AAA pathogenesis.

Next we sought to explore the mechanistic link between oxidative stress and AAA development. To determine this relationship we used isolated vessel testing as well as measurement of aortic residual circumferential strain, a measure of stress modulation due to ECM alteration and vascular adaptation. To isolate the role of oxidative stress in these studies we used a line of transgenic mice with vascular smooth muscle cell-specific overexpression of the antioxidant catalase. The results of this study suggest that oxidative stress-mediated elastin degeneration within the aortic media is etiologic of altered aortic mechanics.

Lastly, we sought to determine the independent mechanical contribution of the aortic adventitia and media tunica to overall aortic behavior. To accomplish this goal we compared the circumferential and axial mechanical behavior of aortas with and without collagenase treatment. The data demonstrated that the adventitia regulates the circumferential behavior of the aorta by preventing overstretch and the media regulates the axial behavior by maintaining tensile loading.

In conclusion, this thesis demonstrates 1) that detecting early aneurysm progression in the form of mechanical or geometric changes may miss the window in which aneurysm pathology may be potentially reversed, 2) that mitigating oxidative stress within the aortic wall may provide protection against AAA, and 3) the adventitia is an important load bearing constituent of the arterial wall and plays a role in vascular adaptation to altered mechanical states. Overall our results impact understanding of early aneurysmal pathogenesis and in doing so may facilitate the development of preventative therapies for AAA progression and rupture.

CHAPTER 1

SPECIFIC AIMS

1.1 Introduction

The ability to prevent abdominal aortic aneurysm (AAA) formation lies in our understanding of the critical signals and events involved in aortic dilation and remodeling. AAA growth is rarely accompanied by noticeable symptoms and therefore often goes undetected before rupture. Nearly 1% of all deaths result from aortic rupture (1). Management of small aneurysmal dilation includes clinical monitoring of growth rate, while extensive dilations may require invasive surgery to resect or remove the aneurysmal tissue. With the ultimate goal to detect and prevent AAA, the objective of this investigation is to identify the earliest molecular and biomechanical determinants of aneurysm formation. The working hypothesis is that oxidative stress is mechanistically linked to the biomechanical remodeling involved in aneurysm formation. We specifically seek to determine how the mechanical response of the aorta changes as it enlarges into an aneurysm. It is expected that this characterization will reveal the earliest events that provoke aneurysm formation, ultimately motivating new clinical interventions in AAA treatment. Our objective and hypotheses have been investigated through the following specific aims.

1.2 Specific Aim 1

Define the fundamental biomechanical changes in the pre-aneurysmal aorta.

The objective of this specific aim is to determine the biomechanical changes of the aorta prior to aneurysm formation. The hypothesis is that alterations of the aorta before aneurysm formation are detectable and quantifiable. Aortic compliance will be

measured using murine models of both accelerated and pathophysiologic aneurysm formation. The expectation is that pre-aneurysmal aortic events include temporally decreased compliance that will be detected within a timeframe of 12 days after treatment.

1.3 Specific Aim 2

Determine the functional importance of oxidative stress in modulating the biomechanical changes in the aorta that occur prior to aneurysm formation.

Based on previous evidence of increased reactive oxygen species (ROS) production in established aneurysms, we hypothesize that ROS produced by smooth muscle cells in the vessel wall provide a critical signal that potentiates mechanical changes in the pre-aneurysmal aortic wall. Investigation of this aim will utilize an existing colony of apolipoprotein E deficient mice which specifically over-express the antioxidant catalase in vascular smooth muscle cell. Aortas from these mice will be subject to mechanical testing as described in Aim 1 as well a detailed morphologic analysis of the matrix. Our expectation is that increased generation of ROS predisposes the vessel to matrix remodeling, which alters aortic mechanics and subsequently promotes AAA formation.

1.4 Specific Aim 3

Define the contribution of the tunica adventitia to the aortic mechanical response.

Motivated by constitutive models that theoretically isolate the mechanical contribution of the media and adventitia independently, as well as by increasing interest in the functional relevance of the adventitia to cardiovascular disease, we hypothesize that the adventitia contributes significantly to the mechanical behavior of the aorta. We developed a novel technique that allows subtractive evaluation of the mechanical

contribution of the adventitia to the composite behavior of the aorta by unshielding the tunica media of its adventitial reinforcement. Our expectation is that degradation of the adventitia will affect increased compliance at low pressures and decreased compliance at high pressures representative of physiologic loading.

Significance and Innovation

This work is innovative in that it is the first investigation of the transition mechanics that link the healthy aorta to the early AAA. To our knowledge the studies presented here provide the first mechanistic discussion of early aneurysmal remodeling mediated by deleterious vascular restoration of the homeostatic mechanical state Focusing our studies on early disease pathogenesis allows detection of events whose progression can be blunted, or even reversed. We demonstrate a causal link between oxidative stress-mediated medial elastin fragmentation and propensity toward aneurysm formation. Targeting therapeutic interventions toward the tunica media could therefore become the basis for prevention.

The experiments designed within this project have achieved significant gains towards understanding the interplay between matrix biology and aortic mechanics, and provides results which not only help to define the pathogenesis of AAA, but also suggest that clinical screening for AAA should ultimately incorporate criteria other than aortic geometry and growth rate as the basis. The interrelationship between the molecular mechanisms and biomechanics is a fundamentally important question addressed by this thesis. The experiments discussed yielded the following outcomes. First, we demonstrated that molecular and cellular mediators promote deleterious matrix remodeling before mechanical alterations can be detected with *ex vivo* or *in vivo*

methodologies. Second, we found a direct link between upregulation of reactive oxygen species and the onset of elastin degradation, an established hallmark of AAA. Third, we showed that the adventitia is an important load bearing constituent of the arterial wall and plays a role in vascular adaptation to altered mechanical state. This final result allowed speculation of the mechanism of increased collagen deposition in the adventitia of early and established aneurysmal dilations. Overall our results impact our understanding of early aneurysmal pathogenesis and in doing so may potentially participate in the development of preventative therapies for AAA.

CHAPTER 2
BACKGROUND AND LITERATURE REVIEW

2.1 AAA Epidemiology

Population-based studies have shown that AAA account for nearly 1% of deaths with an incidence of up to 13% in males over age 65 (1). The current mortality associated with AAA in the US is estimated to be approximately of 15,000/year. The risk of AAA in white males is elevated as compared to black males who have a hazard ratio of 0.57 compared to white men (2). In women the incidence of AAA is much lower, mostly likely due to hormonal differences. Of all other risk factors including hypertension, family history, and previous stroke or coronary heart disease, tobacco use is the strongest factor (3) for AAA development with a hazard ratio greater than 6.0 for heavy smokers (2). Traditionally, AAAs with a minimum diameter of greater than 5 cm are thought to pose the greatest risk for rupture and this measurement is used as the clinical endpoint for reparative therapy.

Often patients with AAA present with a "leaking" aneurysm or frank rupture, which is associated with a very high mortality rate. In the clinical setting, it is typical that primarily patients with a family history of aneurysm ultimately seek ultrasound specifically for AAA detection. The majority of affected patients, however, receive no screening, and the aorta dilates silently and dangerously.

It is clear that aneurysm formation is a disease that affects both the molecular and mechanical properties of the arterial wall. To move toward better approaches to prevent AAA, we must first define the molecular mechanisms of AAA formation which correlate temporally with the altered biomechanics of aortic remodeling and dilation. Until recently, most research has focused on characterizing the biology and biomechanics of

the aneurysmal aorta in the setting of established aneurysms (4-7). However, as predictive medicine evolves as the gold standard in healthcare and imaging methodologies offer greater resolution, there has been a push to define subclinical origins of disease. We are motivated by the striking lack of information defining pre-aneurysmal aortic events, which should reveal essential information about the pathophysiologic mechanisms of formation of AAA and hopefully advance our predictive capabilities.

2.2 AAA Pathology

AAA are characterized in part by localized remodeling and vessel dilation attributable to degeneration of elastin and collagen, the structural proteins in the aortic wall (8-10). In humans, aneurysms usually form in the infrarenal aorta, distal to the renal arteries and proximal to the iliac bifurcation. In mice, however, aneurysms form predominantly in the suprarenal aorta with occasional presentation in the arch and thoracic region. We believe this spatially isolated aneurysm development is closely related to the pathophysiology of the disease.

Aortic aneurysms have been classified based on the shape of vessel dilation. Saccular aneurysms have a balloon-like appearance expanding primarily in the radial direction. Fusiform aneurysms are not localized to one aortic region, but manifest as a dilatation spanning more than one region, such as from the upper thoracic region down to the low suprarenal region. These shapes do not relate to specific cardiovascular disease. In addition, aneurysm dilation is not usually symmetric, resulting in a complex aortic geometry. This asymmetry is due to a combination of the localization of disease in the tissue, the organs/tissues surrounding, and the tethering along the vertebral column. The vertebral column limits expansion in the posterior direction forcing the aorta to dilate

anteriorly. The dilated aorta pushes against the abdominal organs, which alter aortic geometry to an even greater extent. Ultimately, the result of these pathological alterations is a spatially weakened aortic region that varies in geometry, size, and wall mechanics in each patient affected.

2.3 AAA Biology

2.3.1 Physical remodeling

Physical remodeling of the aorta is tied to alterations in the extracellular matrix (ECM). Studies in our laboratory have shown that inhibition of native elastin and collagen covalent crosslinking promotes ECM breakdown into fully dilated aneurysms in as few as 12 days (discussed in *Animal Models of AAA Formation*). These data strongly support the link between disturbance of the ECM structural proteins and aneurysmal disease, which is mediated at the cellular and molecular level of the vessel. It has been established that elastin degradation is a hallmark of AAA, however, that alone should not precipitate aortic dilation as collagen has been shown to be stiffer than elastin at physiologic pressures. Therefore, by intuition, collagen should prevent radial expansion (11). The layers of the vessel, the adventitia, media, and intima, change in histologically different manners in the remodeling response. As the aorta expands the adventitia thickens and becomes highly populated with inflammatory cells. Existing collagen becomes highly crosslinked compared to newly synthesized collagen (12). The media appears hypertrophic and the resident elastic laminae appear degenerated and disconnected. In aneurysms associated with atherosclerotic lesions, the aortic intima is severely disrupted and fibrous. However, aneurysms and lesions are not always mutually present, leaving the biology of the aneurysmal intima unclear. In summary, while the

morphology of AAA is relatively well described, the pathogenesis of these phenotypic changes is not. Even more unclear is how the individual layers change during the pathology from healthy to aneurysmal aorta. This thesis attempts to define these changes and link them to the manifestation of aneurysmal mechanical events.

2.3.2 Matrix-metalloproteinases

In addition to investigating the biomechanical events that precede aneurysm formation, we also seek to determine the critical molecular signals that promote elastin and collagen breakdown. The major targets in this proposed research are matrix-metalloproteinases (MMPs) and ROS. MMP activity is conferred by a very large family of over 20 isoforms. They are secreted in pro-form by mesenchymal and inflammatory cells alike, including vascular smooth muscle cells (VSMCs), fibroblasts, macrophages, and neutrophils. As such they are involved in many cellular processes, including migration, extracellular matrix (ECM) deposition, and apoptotic clean-up. Their natural inhibitors are a small family of tissue inhibitors of MMPs (TIMPs).

Reactive oxygen and nitrogen species (ROS, RNS) have been demonstrated to regulate MMP transcription and activation. Both superoxide anion ($O_2^{-\bullet}$) and hydrogen peroxide (H_2O_2) have been shown to activate MMP secretion by vascular smooth muscle cells (VSMCs) (13). These authors were the first to demonstrate the capacity of peroxynitrite ($^{-}$OONO) to activate the latent form of MMP-2 into the active enzyme. Moreover, they showed that modulation of MMP-2 activity was dependent on $O_2^{-\bullet}$ and H_2O_2. H_2O_2 affects activity biphasically, imparting increased activation at low concentrations and inhibiting activation at high concentrations. In addition, H_2O_2 is specifically linked to increased release of polymorphonuclear cell-derived MMP-9 (14),

which was shown to be completely blunted in the presence of catalase, the antioxidant which metabolizes H_2O_2 to water and oxygen. The mechanism of this regulation is likely via H_2O_2 activation of *ras* and the mitogen activated protein-kinase pathway (15) and subsequent phosphorylation of redox sensitive transcription factors such as nuclear factor-κB (NF-κB) (16, 17) and ets-1 (14, 15)). Indeed NF-κB has been shown to regulate genes that mediate aneurysmal dilation and its inhibition has been shown to reverse small aortic dilatations induced by aortic elastase infusion (18). Specific activation of the pro-form of MMP-9 was established in neuronal cells (19). Activation is conferred by irreversible S-nitrosylation of a prodomain cysteine that coordinates Zn^{2+} in the active site. This nitrosylated cysteine is then oxidized into a stable sulfenic acid. It is assumed that homologous MMPs are activated in the same manner. Thus, both MMP expression and post-translational activation is conferred by oxidative and nitrosative stress.

MMP-2 and MMP-9 are the most frequently detected proteolytic species in developing and established AAA. MMP-2 is a Type IV collagenase with elastolytic activity as well. Activation within the aneurysm has been associated with early origins of progression correlating with increases in membrane tethered (MT)-MMP-1 (also called MMP14), which is a known activator of MMP-2 (20-22). Most interesting is upregulation of MMP-2 in satellite locations away from the AAA. MMP-2 was found in VSMCs of the inferior mesenteric vein and culture of these cells showed augmented invasive behavior (23). Although a recent review of MMP expression and activity in AAA presents MMP-2 activity as isolated to early stage AAA (24), other investigators have shown it is expressed and active in all stages of AAA development (Table 1), even

demonstrating a positive correlation with AAA size (25). Therefore, the temporal activation pattern of MMP-2 is still undefined.

Expression of MMP-9 on the other hand has been demonstrated to be highly upregulated in late stage disease and at the site of rupture. MMP-9 expression has been repeatedly demonstrated to be robustly upregulated in aneurysmal tissue compared to control (Table 2.3.1). Seminal work demonstrating a causative role for MMP-9 showed first that MMP-9-deficient mice developed significantly smaller aneurysmal dilations than control in elastase-induced experimental aneurysms (26). Continuing investigation in this model showed that MMP-$9^{-/-}$ mice receiving WT bone marrow post-nonlethal irradiation showed marked development of AAA, while the converse experiment in which WT mice received MMP-$9^{-/-}$ marrow did not induce aneurysm formation. These results indicate that MMP-9 causality is independent of its cellular source, be it mesenchymal or from inflammatory infiltrate. Intriguing in the scope of preventative therapeutics, MMP-9 protein has been detected in human plasma samples at presentation of both aortic rupture (27) and endovascular leak following endovascular graft placement (28). Moreover, the risk of AAA development has been significantly correlated with MMP-9 polymorphisms. Overall the current opinion regarding MMP-9 is that it correlates positively with AAA size, and more specifically, is possibly associated with rupture-prone AAA.

The temporal mechanism of MMP recruitment in the development and progression of AAA, despite the abundance of investigation into specific MMPs and inhibitors, is unfortunately undefined. Table 2.3.1 provides a list of reported MMPs and the aneurysmal state in which they have been associated. It is clear, however, that there is no temporal growth chart for AAA development and the terms “early,” “small,” and “large,” are arbitrarily used to provide some context for aneurysm development. The myriad and complexity of MMP contributions allows speculation that the focus should move away

from the absolute presence of MMPs toward tracking those MMPs associated with aneurysmal growth rate.

Table 2.3.1. Summary of recent (within current decade) studies on the effective contribution of MMPs and Tissue Inhibitors of MMPs (TIMP) to aneurysm development. MMP family members found in Early (Dilation less than 2 times normal diameter), Established (dilation greater than 2 times normal diameter), and Ruptured AAA are included, although the spectrum of MMP activation makes such limitation arbitrary. The effect of MMP- or TIMP-gene disruption on aneurysm outcome is included bottom row. Unless indicated, the MMP listed was found at the protein or mRNA level within aortic aneurysmal tissue. The species human (h) or murine (m) precedes the MMP family member.

Early AAA (Dilation < $2xD_o$)	pro-hMMP2 mMMP9 hMMP14		Vinh A et al 2008 Vinh A et al 2008, Miyake et al 2007 Nishimura K et al 2003
Established AAA (Dilation > $2xD_o$)	MMP-1 active mMMP2 mMMP-3 mMMP-9 hMMP-9 mMMP-12 hMMP-13 hMMP-14 TIMP-3		Annabi B et al 2002 Vinh A et al 2008, Peterson E et al 2002 Silence J, 2001 Vinh A et al 2008 Freestone T et al 1995, Saito et al 2002, Annabi B et al 2002 Longo GM et al 2005, Annabi B et al 2002 Tromp G et al 2004 Annabi B et al 2002 Annabi B et al 2002
Ruptured	hMMP-8 hMMP-9 hMMP-1 hMMP-9	 In plasma In plasma	Wilson WRW et al 2006 Wilson WRW et al 2006, Peterson E et al 2002 Wilson WRW et al 2008 Wilson WRW et al 2008
Effect of gene deficiency on AAA development	TIMP-$1^{-/-}$ TIMP-$2^{-/-}$ MMP-$3^{-/-}$ MMP-$9^{-/-}$ MMP-$12^{-/-}$	↑AAA ↓AAA ↓AAA ↓AAA ↓AAA	Silence J et al 2002 Xiong W et al 2006 Silence J et al 2001 Pyo et al 2000 Longo GM et al 2005

AAA formation has been investigated using animal models deficient in MMP and tissue inhibitors of MMPs, including MMP-$2^{-/-}$, MMP-$9^{-/-}$, MMP-$12^{-/-}$, and TIMP-$1^{-/-}$. mice (29, 30). These models suggest that MMP-2, -9, and -12 (a macrophage-specific MMP) are necessary for early aneurysmal progression, but still require other elastolytic enzymes or combined MMP actions to induce full aortic expansion. The concept that combinations of MMPs are necessary for both early and mature AAA formation is

supported by studies with ApoE$^{-/-}$/TIMP-1$^{-/-}$ double knock out mice (10, 31), in which MMP-1 and MMP-3 have been implicated synergistically in advanced AAA progression. The fact that elastolysis is necessary, but not sufficient to enhance AAA progression, supports our belief that other factors such as spatial location along the aorta and altered mechanical properties must complete the cascade to force the weakened vessel into a state of active remodeling and aneurysmal expansion.

2.3.3 Reactive oxygen species

Reactive oxygen species are highly reactive and unstable oxidants whose summed effect is called oxidative stress. Oxidative stress has been implicated in disease pathologies ranging from hypertension to Parkinson's disease. The primary reactive oxygen species are shown in Figure 2.2.1. Endothelial cell production of nitric oxide (NO) leads to endothelium-dependent vessel dilation. Although vasodilation is generally an anti-atherogenic event, NO can also react with $O_2^{-\bullet}$ to form $ONOO^-$, a molecule that is highly pro-atherogenic. Highly reactive, but short lived $O_2^{-\bullet}$ can be converted into H_2O_2 by the antioxidant superoxide dismutase (SOD). The antioxidant catalase metabolizes H_2O_2 into H_2O and molecular oxygen (O_2). ROS production occurs in all vascular cell types as well as in multiple intracellular locations, such as the mitochondria and the membrane-associated NAD(P)H oxidase. The NAD(P)H oxidase has been implicated in many forms of cardiovascular disease including atherosclerosis and angiogenesis. It is a membrane-bound receptor complex which generates $O_2^{-\bullet}$ and H_2O_2 when bound by angiotensin II (angII) (32). $O_2^{-\bullet}$ and H_2O_2 production in the vessel wall leads to multiple cellular responses including VSMC differentiation, growth, and even apoptosis (33, 34). In fact, studies suggest that not only the presence, but also the quantity of ROS

production correlates with vascular pathology. Low concentrations of ROS can function as intracellular second messengers to mediate normal vascular smooth muscle cell growth, while high concentrations of ROS can be toxic and signal cellular apoptosis (35).

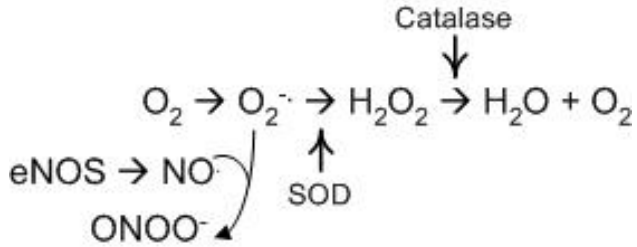

Figure 2.3.1. Vascular ROS. Oxygen is converted to superoxide ($O_2^{-\cdot}$) by oxidases. Superoxide dismuthase (SOD) converts $O_2^{-\cdot}$ to H_2O_2 and catalase converts H_2O_2 to its H_2O and O_2 components. NO is produced by endothelial cell nitric oxide synthase (eNOS). NO and $O_2^{-\cdot}$ react to form peroxynitrite ($ONOO^-$) a highly reactive mediator of lipid peroxidation. Figure adapted from (33).

Oxidative stress in vascular walls has been strongly linked to ECM degeneration leading to atherosclerosis (13, 33, 36, 37). Important for our discussion is the demonstration that ROS are significantly increased in established AAA (36, 38, 39) and promote ECM degradation by upregulating MMP activity via the NAD(P)H oxidase (13, 40). The basic mechanism of ECM degeneration by ROS is considered similar in both atherosclerosis and aneurysmal disease. Since VSMCs and endothelial cells are adherent cells, a complete underlying protein structure of elastin, collagen, and other matrix components is crucial to maintain organization of the medial layers. Oxidative disturbance of the ECM promotes endothelial cell dysfunction and VSMC reorganization, both of which induce monocyte adherence to and transmigration through the vessel wall. The penetrating monocytes secrete elastolytic enzymes, such as MMPs, cathepsins, and interleukins, which propagate the inflammatory cascade and further destruction of the ECM.

Antioxidant studies also support the link between oxidative stress in the vascular wall and aneurysmal disease. The incidence of AAA formation was decreased in animals treated with the antioxidant, vitamin E, an inhibitor of ROS production (39). In addition, histological investigation showed blunted macrophage infiltration into the media of vitamin E treated animals. This is a very significant finding, suggesting that ROS may signal macrophage recruitment into the aortic wall to propagate aneurysmal changes. The result of the study also suggests that exogenous MMPs from migratory inflammatory cells play a critical role in AAA formation, as vitamin E treatment did not affect the levels of MMP-2 or MMP-9 in the aneurysmal tissue. To date antioxidant treatment has failed to provide inhibition of AAA in human clinical trials (41). The subject group, however, was populated with male smokers which is a high risk group largely predisposed to AAA development.

2.4 Catalase and AAA

The link between ROS induced ECM remodeling and aneurysm formation will be investigated and described in this work from studies involving a transgenic mouse with smooth muscle cell-specific overexpression of the human catalase gene (referred to as SMC-Cat). This mouse model has increased VSMC-specific catalase activity and hence blunted H_2O_2 expression in the aortic media. Experiments in SMC-Cat mice on C57Bl/6 background suggest that SMC-specific H_2O_2 promotes SMC hypertrophy in the setting of angII (42). To date only there is only one report on the role of catalase in AAA formation (34). In this study to study the vasoprotective effects of selective estrogen receptor modulators, a tamoxifen pellet was implanted subcutaneously one week prior to AAA induction via the porcine elastase infusion model of AAA. Aortas from these mice

demonstrated high levels of catalase message and protein. Inhibition of catalase in conjunction with tamoxifen treatment partially recovered the aneurysmal phenotype indicating that catalase has a mitigating role against AAA formation.

By breeding into the SMC-Cat into the apoE$^{-/-}$ background, we have transitioned this transgenic mouse into a better model of atherosclerosis and aneurysm formation. The apoE$^{-/-}$ and SMC-Cat transgenics create a platform on which we attempted to define the fundamental role of ROS as critical mediators of the biomechanical changes of the pre-aneurysmal aorta. To determine whether overexpression of catalase reduced aneurysm formation, SMC-Cat and apoE$^{-/-}$ mice were treated with angII (0.75mg/kg/day) alone, angII plus HF diet, HF diet alone, and LF diet (n=5 in each group). After 8 weeks of treatment AAAs were present in approximately 30% of the HF and HF/angII treated apoE$^{-/-}$ population, but were completely absent in all catalase/ApoE$^{-/-}$ groups as represented by en face dissection (Figures 2.2 and 2.3). The results further demonstrated that ROS production is mechanistically linked to AAA formation.

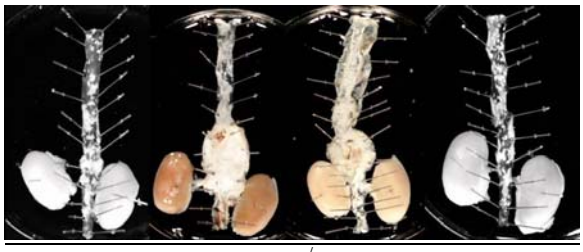

Figure2.4.1. En face dissection of WT apoE$^{-/-}$ without catalase in the setting of HF diet and AngII infusion, illustrating AAA presentation.

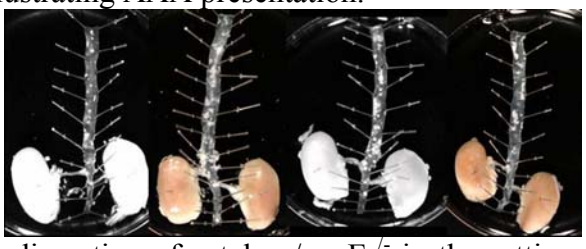

Figure 2.4.2. En face dissection of catalase/apoE-$^{/-}$ in the setting of HF diet and AngII infusion, illustrating the absence of AAA presentation.

Furthermore, genome wide transcription analysis (Affymetrix, Santa Clara, California) of aortic tissue from these same treatment groups suggests that the mechanism of ROS-induced AAA formation is through ECM reorganization and remodeling. Aortic tissue was harvested after only 1 week of treatment to investigate changes that are well within our pre-aneurysmal time scale. The analysis showed that the anti-aneurysmal environment in the angII-treated catalase overexpressing mice promoted a downregulation of matrix-associated genes, as compared to the angII-treated WT. In fact many genes undergoing at least a 50% reduction from WT control were matrix-associated proteins (Table 2.4.1). Such downregulated matrix components were procollagen Col-5a2, -8a1, -9a1, -11a1 and MMP-3, -12, -14. The procollagen gene is responsible for new ECM deposition, which occurs during matrix remodeling in the WT model. Downregulation of MMP-3 suggests its redox sensitivity. MMP-14 downregulation was expected since it activates MMP-2 in small and large aneurysms. In addition, since MMP-2 presence in AAA was not affected by antioxidant administration (39), the microarray results support the role of MMP-14 as the redox sensitive activator of MMP-2. The downregulation of macrophage-specific MMP-12 also supports this study, which found blunted macrophage recruitment in AAA adventitia after vitamin E administration. The striking specificity toward H_2O_2-induced matrix regulation illustrates the synergy between oxidative stress and ECM composition. Moreover, the combination of robustly reduced matrix genes and the complete absence of aneurysm incidence in all SMC-Cat treatment groups strongly suggest that VSMC-generated H_2O_2 is a pivotal molecular signal which induces aneurysm formation by regulating the matrix environment.

Table 2.4.1. Genes downregulated by at least 50% in the VSMC-Cat model in the setting of angII/HF, angII alone, or HF alone as verified by genome wide transcription analysis.

	Gene	Function
ECM Components	Collagen-5a2, -8a1, -9a1, -11a1	Procollagen proteins providing ECM tensile strength
	Fibrillin 2	ECM structural component
	Aggrecan 1, Dermatan sulphate proteoglycan 3	ECM proteoglycans
	Hyaluronan mediated motility receptor	Promotes ECM-associated glycosaminoglycan production
Proteolytic Enzymes	MMP-3, -14	Gelatinase- degrades ECM collagen
	MMP-12	Elastase- degrades elastin fibers
	ADAMTS1	Cleaves aggrecan 1

2.5 Animal Models of AAA Formation

Aneurysm formation has been studied in a variety of mouse models including MMP-3$^{-/-}$ (10), MMP-9$^{-/-}$ (26), tissue inhibitors of MMP-(1,2, and 3)$^{-/-}$ (31), and low density lipoprotein receptor-knockout mice (43). Our research group and others (44) have studied aneurysm formation in either ApoE$^{-/-}$ or C57 mice infused with angII (0.75 to 1.5 mg/kg/day). AngII is the end product of the renal renin-angiotensin system, which contributes to regulation of vascular tone and blood sodium/electrolyte balance. AngII binds its receptor in the vascular wall to promote VSMC contraction, and therefore, is critical in the maintenance of vascular structure (45). The excess angII induces a sustained increase in blood pressure. In addition, unpublished data from our lab has shown that infusion with the lysyl oxidase inhibitor β-aminoproprionitrile (βAPN, 100 mg/kg/day) promotes rapid matrix remodeling and AAA formation. βAPN inhibits the lysyl oxidase family of enzymes. This family of enzymes promotes covalent cross-linking of collagen to elastin, collagen to collagen, and elastin to elastin. Inhibition by βAPN severely weakens the fiber microstructure in the vessel wall, leaving it vulnerable to aneurysmal expansion. Infusion with angII (0.75mg/kg/day), βAPN, and high fat (HF)

diet provides a mouse model in a C57 or ApoE$^{-/-}$ background with nearly 100% occurrence of accelerated aneurysm formation. Though this model differs in time scale compared to pathophysiological aneurysm formation, the short time to aneurysm formation (approximately 2-4 weeks) is very suitable for our AAA investigation. Knowing definitively that our mouse model will develop aneurysms is critical to define the biomechanical changes of early AAA development and progression.

Other chemically-induced models of AAA formation directly induce elastin fiber degradation in the aortic media to promote localized AAA formation. Porcine pancreatic elastase injected via catheter into the abdominal aorta induced local inflammation of the vascular lumen (46). Histological evaluation 14 days after elastase infusion shows aortic dilation with degenerated elastic lamellae in the media and inflammatory infiltrate in the adventitia. Another chemically-induced model of AAA formation is initiated by peri-aortic insult, in contrast to the luminal insult in the elastase model. In this calcium chloride model, the peri-adventitial abdominal aorta is painted with 0.2 to 0.5 mol/L calcium chloride (47). The calcium chloride promotes calcification of the elastin fibers, disrupts the ECM, and induces VSMC apoptosis to initiate and propagate aortic dilation into aneurysm. These models clearly demonstrate that elastin degradation is a pivotal event in the transition from a healthy to an aneurysmal aorta. Accordingly this work seeks in part to investigate the molecular mediators and mechanical ramifications of ROS-mediated elastin degradation in the setting of AAA.

2.6 AAA Biomechanics

AAA are characterized in part by localized remodeling and vessel dilation attributable to degeneration of the elastin and collagen structural proteins in the aortic

wall (8-10). Matrix degeneration is mediated by infiltration of leukocytes, production of inflammatory mediators (e.g., MMPs, cathepsins, and interleukins) and smooth muscle apoptosis. This new milieu effectively changes the structural organization of the vessel and accordingly changes the biomechanical response to hemodynamic forces. AAAs rupture when wall stress exceeds wall strength.

Direct *ex vivo* measurement of mechanical properties of aneurysmal tissue have demonstrated that aneurysmal tissue exhibits reduced tensile stress (6, 48) and increased circumferential stiffness (4, 5). Contrary to original hypotheses that diameter determined rupture potential, remodeling-related increases in wall thickness were not shown to invoke increases in wall strength as ruptured human aneurysmal tissue was shown to be 40% thicker than nonruptured aneurysmal tissue (48). Moreover, growth of intraluminal thrombus, which often develops in established AAA, was shown to impart a wall stress reduction of nearly 30%, while intima-associated atherosclerosis increased local aneurysmal wall stress.

In this regard, reliable and accurate stress analyses of the *in vivo* AAA require suitable 3D constitutive models. Recent biomechanical characterization suggest that AAA rupture is related to the stress in the wall and utilize *in vivo* imaging to reveal significant geometrical and assymetrical remodeling during AAA evolution (49, 50). Recently peak wall stress was demonstrated to be a function of collagen organization with the aneurysmal wall (51). The authors generated three-dimensional computer models of symmetric and asymmetric AAAs in which the maximum diameter and length of the aneurysm were individually controlled. A five parameter exponential type structural strain-energy function was used to model the anisotropic behavior of the AAA

tissue which was determined by the orientation of the collagen fibers. The results suggest that shorter aneurysms are more critical when asymmetries are present. They show a strong influence of the material anisotropy on the magnitude and distribution of the peak stress and suggest that relative aneurysm length and the degree of aneurysmal asymmetry should be considered as criterion for risk of AAA rupture.

Indeed acceptance that diameter is not an isolated indicator of rupture potential has opened the door to a new found appreciation of material anisotropy as a crucial parameter in AAA mechanics. Watton and Na (52) have developed a model of AAA growth that embraces increased collagen anisotropy and elastin fiber breakdown as the major components in a membrane-based theoretical model. Other recent studies also reflect appreciation for elastin and collagen fiber direction and stress modulation though not all in the setting of AAA (53-55). Current AAA biomechanical characterization includes growth as influenced by changes in the matrix structure as well as by mechanics-mediated cellular responses.

2.6.1 Modeling the Mechanical Behavior of Large Arteries

Loss of intact elastin and de novo production of monomeric collagen reduces the elasticity and compliance of the aneurysmal aorta (5, 7). Elasticity, or reversible distensibility, is not typically a quantified metric. However, vessel compliance (reversible distensibility or the change in diameter for a given change in pressure) can be determined experimentally as the slope of a pressure-diameter curve, achieved by recording vessel diameter changes resulting from an applied transmural pressure. Compliance measurements are recorded by fastening the ends of a vessel to cannula and inducing pressure via flow or air to distend the lumen. The resulting diameter change is recorded

and a pressure diameter curve is generated. Optimization of compliance measurements in our experiments is discussed in detail in Chapter 3: Optimization of Isolated Inflation Data Acquisition. Isolated vessel compliance has been evoked repeatedly to characterize vessel stiffness in many species (20, 56, 57).

Compliance is a useful metric to identify remodeling events and characteristics of mechanical behavior. However, as a function of both material and geometry, compliance is not a true material property. That is, the compliance will be different for two vessels of identical material, but of different thickness. The compliance will also be different for two vessels with identical thickness, but different material composition. This is a significant disadvantage as fixed-length compliance testing does not reveal any information about AAA-induced aortic material properties, and indeed, only material properties can be applied to other AAA models or characterization of arterial mechanics. The aorta can be modeled as a uniform cylinder under axial loading and pressure, creating longitudinal stress, σ_z, and circumferential, σ_θ, stress within the wall (Figure 2.6.1 a and b). Figure 2.4a and 2.4b provides schematic description of the acquisition and interpretation of aortic mechanical testing parameters. During fixed-length compliance testing, transmural pressure and outer radius are known and measured, respectively. If wall thickness, t, (or inner radius, r_i) is known, circumferential stress, σ_θ, can be determined by the Law of Laplace, $\sigma_\theta = \frac{\mathrm{Pr}_o}{t}$. Ideally, *t* should be measured in real-time. However, measurement of *t* is often difficult to acquire, depending on the sophistication of the testing apparatus, and therefore, may be reflected by an appropriate approximation.

Biaxial acquisition of parameters increases the level of sophistication by allowing measurement of axial force, *f*, during inflation. With f known we can calculate

longitudinal stress, $\sigma_z = \frac{f}{\pi r^2}$ and strain, $\varepsilon_z = \frac{l - l_o}{l_o}$ (l=length and l_o= unloaded length).

calculation of can be calculated from stress-strain curves. Acquisition of longitudinal force allows development of constitutive models, which relate stresses to strains, to describe AAA-induced changes in aortic material behavior independent of geometry. The material properties of the vessel are then determined through these relationships.

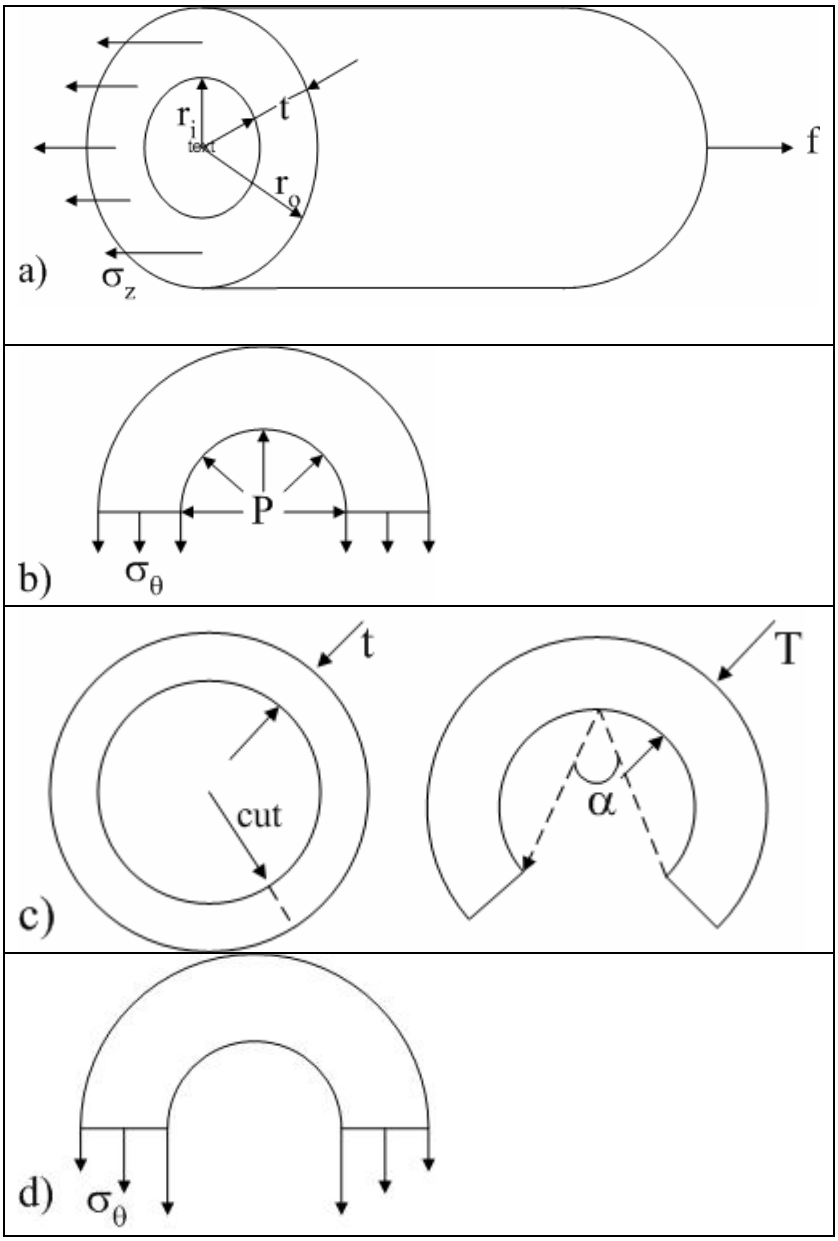

Figure 2.6.1. a)Free-body diagram of an axially loaded artery. b) Free-body diagram of an artery in the loaded configuration with conserved circumferential stress across the wall thickness. c) Free body diagram of an aortic ring in both the loaded (left) and zero-load (right) configuration. d) Diagram of an unloaded artery with non-uniform circumferential stress through the wall thickness. σ_z = mean stress in the longitudinal direction, σ_θ = mean stress in the circumferential direction, f=axial force, P= pressure, r_i= inner radius, r_o=outer radius, and t= loaded thickness, T= zero-load thickness, α= opening angle.

The stress-strain behavior of the passive mechanics of the early aneurysm can be fit into a theoretical framework of normal arterial mechanics. In this framework the early aneurysm is considered pseudoelastic, that is, subject to small strains controlled by the elastic laminae and collagen fibers (58-60). However, the stress-strain relation at late aneurysmal development may change dramatically, requiring a different constitutive framework to describe AAA pathophysiology. Moreover, the material differences between the abdominal and thoracic aorta may also be described by different relations (61). Therefore, in late pathological aneurysmal progression, a different theoretical framework may apply, where the vessel is considered anisotropic and hyperelastic, that is, subject to nonlinear, large strains due to the action of arterial collagen fibers (62).

Biological materials are highly non-linear and experience large strains compared to linear materials. Growth and remodeling events, such as ECM degradation and cell growth, have been correlated with not only mean stresses, but also local stresses in the tissue (63). While 2D constitutive models capture the mean stress-strain relationship, 3-dimensional models can describe these local stress gradients in the vascular wall (Figure 2.6.1d). This stress gradient is called residual stress, or residual strain, and is apparent when a ring segment of an artery at circumference, $C_{unloaded}$, is cut radially and the newly opened sector contracts in length to circumference, C (Figure 2.6.1c)(64). Residual strain is calculated as $\varepsilon = \frac{(C - C_{unloaded})}{C_{unloaded}}$. The balance between compressive forces on the interior of the wall and tensile forces on the exterior is quantified by the opening angle, α, of the radially cut sector. The geometry of the ring is related to α by $\alpha = \pi - \frac{C_o - C_i}{2H}$, where C_o is the outer circumference, C_i is the inner circumference, H is the thickness of

the bisected ring. However, when generating 2D models of very thin arteries, such as the mouse aorta, the vessel wall is often considered homogeneous, that is, the mechanical behavior of the intima, media, and adventitia are considered as one material. Under this assumption, a 2D constitutive model will appropriately describe the aortic behavior, precluding the necessity of advanced 3D models.

Development of constitutive models of arterial behavior has helped to describe phenomenon that are difficult to test directly by experimental means. As an example, the most recent model of aneurysm development includes a term describing both elastin degradation and collagen fibril recruitment upon loading (52). In this thesis we have designed experiments with the ultimate goal to experimentally describe the earliest events of AAA formation. This characterization includes but is not limited to a description of the mechanisms of elastin degradation and collagen turnover. It is critical to understand these major events in AAA development so as to identify the initial molecular and biomechanical determinants, i.e. ROS production, ECM remodeling, and material property variation, involved. Defining these pre-aneurysmal events is essential to move toward clinical intervention and prevention of aneurysmal disease. Indeed two recent studies have presented evidence from animal studies that demonstrated the ability to reverse small aneurysms (18, 65). Both of these studies targeted inhibition of proximal signaling molecules in AAA pathogenesis to prevent elastic laminae degradation and increase de novo biosynthesis of ECM components. With this in mind, this thesis has sought to more clearly define the early molecular and mechanical events in AAA pathogenesis.

Chapter 3
BIOMECHANICAL AND MOLECULAR CHARACTERIZATION OF THE EARLY MURINE ABDOMINAL AORTIC ANEURYSM

3.1 Introduction

An abdominal aortic aneurysm (AAA) is characterized in part as a localized doubling in aortic diameter induced by inflammatory molecular mediators and spatial changes in wall mechanics. AAA rupture accounts for nearly 1-2% of all deaths (1) and occurs when forces acting on the aortic wall exceed the strength of the wall itself (5). Decreases in aortic wall strength reflect changes in microstructure and cellular composition that occur during disease progression. Established AAAs in suitable candidates may be reinforced via endoarterial stent or surgically resected followed by implantation of an aortic graft implant. Small AAAs lack reliable prognosis and are managed primarily by close monitoring of growth rate. In light of exciting new studies unveiling the potential for reversal of early aneurysmal growth (18, 65) it is critically important to find methods to detect AAA at the earliest growth stages possible and to determine their mechanical stability. Detection is a challenge in aneurysmal disease, as AAA are typically asymptomatic and usually present in the clinic as large, established dilations of the aorta. Development of effective subclinical detection methods is critically dependent upon thorough characterization of the natural course of aneurysm development. Our investigation in controlled murine models of aneurysm formation attempts to fill this gap from both a biomechanical and histological perspective. *Ex vivo* biomechanical testing was used to test the hypothesis that early changes in aortic mechanics could be detected before overt aneurysmal dilation.

3.2 Methods

To determine the changes in aortic mechanics during AAA, aortas from control and treated mice were isolated in a vessel chamber and subject to transmural pressure loading at the *in vivo* stretch. These measurements were subsequently validated with *in vivo* methodologies. Histological analysis was used to investigate the molecular mediators and matrix events occurring in early aneurysm formation.

3.2.1 Animals

Male C57Bl/6 and apoliprotein E deficient ($apoE^{-/-}$) mice were purchased from the Jackson Laboratory (Bar Harbor, ME) and used in experiments at 15-17 weeks of age. Mice were allowed free access to standard chow and water. All protocols were approved by the Institutional Care and Use Committee at Emory University.

3.2.2 Models of Aneurysm Formation

To achieve a highly reproducible "accelerated" model of suprarenal AAA development, C57Bl/6 mice were fed an atherogenic diet (high fat, HF) and infused with angII (0.75mg/kg/day) and βAPN (100 mg/kg/day) via subcutaneous osmotic minipumps (Alzet). Wild type controls were fed standard diet (low fat, LF) diet only. A more physiologic model of AAA lacking βAPN was generated in C57Bl/6 and $apoE^{-/-}$ mice fed HF diet and infused with angII only.

3.2.3 Wire Myography

At the conclusion of the experiment, animals were euthanized via carbon dioxide asphyxiation. Following euthanasia, 4 WT C57Bl/6 mice and 4 C57Bl/6 treated via the accelerated model for 14 days were perfused via left ventricular puncture with 9% normal saline. The aorta was then freed from fat and connective tissue and cut into 2 mm thick rings. Rings were then grouped to obtain samples from the arch, thoracic, supra-renal,

and infra-renal aortic regions. Myogenic tone was removed by adding 10 μM sodium nitroprusside, a nitric oxide donor, to the Dulbecco's Modified Eagles Medium (DMEM) perfusate. The rings were positioned in the myograph by sliding two thin metal wires through the lumen and fastening the wire ends to the myograph "feet." For data acquisition, the aortic ring was deformed by separating the feet with a stage micrometer. The resistive force generated within the ring was recorded via a force transducer.

3.2.4 Vessel Isolation and Mechanical Testing

Vessel isolation and mechanical testing were performed in bothC57Bl/6 and apoE$^{-/-}$ mice. Mice were euthanized by carbon dioxide asphyxiation. The thoracic cavity was opened and the apex of the heart exposed. The left ventricle was punctured and the animal perfused with 0.9% saline solution for four minutes. Prior to dissection, the *in vivo* aortic length was measured with digital calipers. All arterial branches were tied off to obtain a leak-free aorta for the perfusion setup. The fatty tissue surrounding the aorta was removed carefully, leaving the intercostals, celiac trunk, mesenteric artery, and renal arteries attached. After fat removal, all arteries and intercostals were tied off with nylon filament, fastening each at least 1 mm away from the surface of the aorta. This distance

prevented the tie from interfering with aortic expansion under the pressurization protocol.

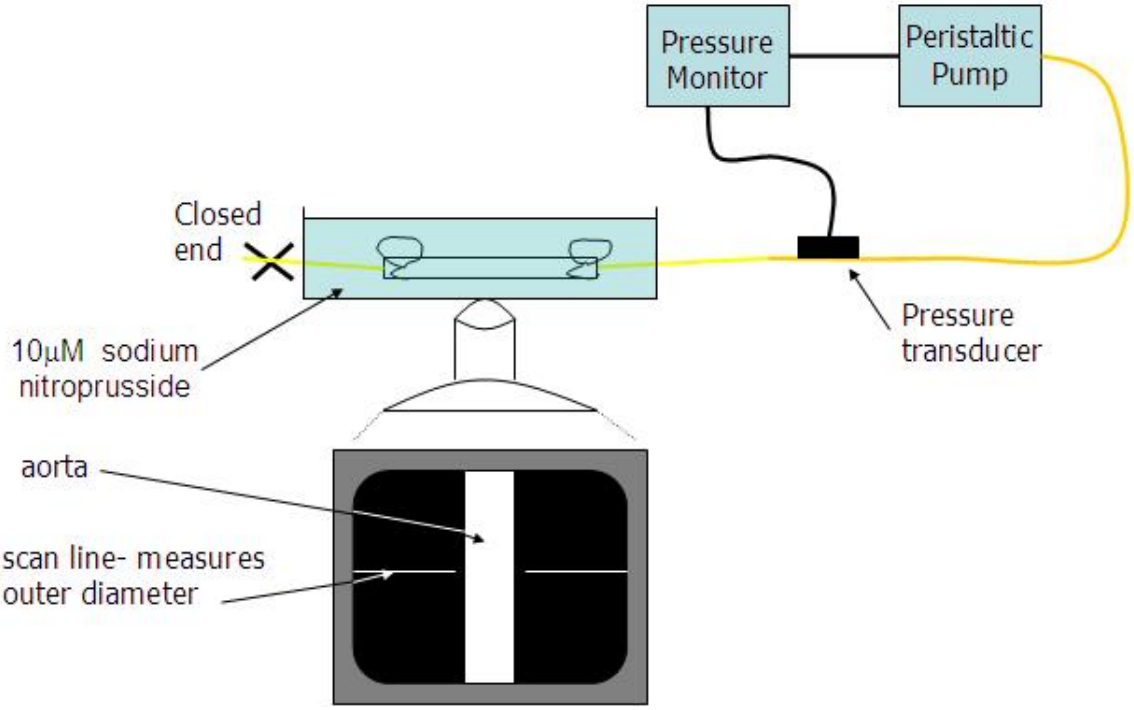

Figure 3.1. Isolated vessels were cannulated on 200μm glass pipettes and bathed continuously in 37˚ DMEM containing 10μM sodium nitroprusside. A pressure transducer was connected to the proximal end and the fluid was introduced from this end. A pressure monitor and peristaltic pump completed the pressure regulation system. The chamber was placed over an inverted scope and displayed on a monitor. A video dimension analyzer recorded real-time diameter.

The isolated perfusion set-up is shown in Figure 3.1. The aorta was cannulated with 200 μm diameter glass micropipettes in the vessel isolation chamber and stretched to the *in vivo* length using the micropipette adjusters. The in-flow micropipette was attached to a peristaltic pump, the source of the perfusion fluid. The outflow side of the chamber was closed with a stop cock for the blind-sac/pressurization experiments. The cannulated aortic segments were continuously bathed at 37°C with DMEM solution at pH 7.4$\pm$ 0.05. Ten μM sodium nitroprusside was added to both the bath and perfusate to prevent smooth muscle cell contraction and isolate passive elastic vessel mechanics..

After cannulation the vessel isolation chamber was mounted on the stage of a Nikon DIAPHOT 200 inverted microscope and allowed to equilibrate for 30 minutes to control for vessel handling during preparation. Real time video of the aorta was obtained with a SIT 66 camera (Dage-MIT, Inc., Michigan City, IN). A video dimension analyzer (LSI) was used to optically measure the outer diameter of the vessel by means of a video scan line that detected the optical contrast between the vessel wall and background.

3.2.5 Magnetic Resonance Angiography

To validate our experimental pressure-diameter (P-D) data, angiograms of the abdominal aorta were acquired for *in vivo* estimates of vascular compliance. Image acquisition was optimized using the 4.7 Tesla Varian Anova Small Animal Imaging & Spectroscopy system. Prior to image acquisition, the mice were anesthetized with 2.5% inhaled isoflurane and at 1% isoflurane by nose cone thereafter. The mice were restrained in the supine position on a heated bed and centered inside the magnet. Image acquisition was gated by electrocardiogram so that each image was obtained at the same point in the cardiac cycle. Two dimensional time of flight cine-MR angiography provided multiple images of aortic lumen diameter change within the cardiac cycle at each slice.

3.2.6 Ultrasound Imaging

Additional *in vivo* verification was performed via ultrasound imaging of the aorta using the VisualSonics™ Vivo 770 (Toronto, Ontario, Canada) high resolution *in vivo* micro imaging system. The accelerated model was studied longitudinally at baseline, 6, and 12 days after angII and βAPN infusion and HF diet. Mice were anesthetized with 3% isoflurane and maintained at 1%. Vital signs were monitored through the temperature

controlled Vevo™ Mouse Handling Table, which includes embedded EKG and respiration monitoring. Images were acquired with the 707B mouse RMV (Real-time microvisualization) scanhead. Scout images of the suprarenal aorta were acquired in B-mode with scanhead perpendicular to the aortic axis. When possible the scanhead was positioned parallel to the axis to capture the longitudinal axis. Images of aortic diameter were captured in M-mode. Diameter was measured in the Vevo™ system software.

3.2.7 Histological Analysis

After inflation, aortic samples were fixed with formalin and cut into two segments for thoracic and suprarenal division. Samples were embedded in paraffin wax and sectioned at 5 microns. Sections were stained with hemotoxylin and eosin for aortic morphology and Verhoff's Van Geison Elastic stain (Sigma, St. Louis, MO) for elastic laminae and adventitial collagen distinction. Where applicable, aortic inner diameters were calculated using NIH Image J software (Bethesda, MD).

3.2.8 Statistical Analysis

All data are presented as Mean +- SEM. Statistical analyses were performed using GraphPad™ Prism software. ANOVA was used to examine the effect of aneurysmal treatment time on aortic compliance and Bonferonni post tests were used for post hoc analyses. $P<0.05$ was considered significant.

3.3 Results

3.3.1 Aortic rings demonstrate stiffening during aneurysm progression. Initial experiments to determine pre-aneurysmal mechanical behavior utilized a wire myograph to measure the force-deformation behavior of aortic rings. Figure 3.1.1 shows that the resistive force against deformation decreased sequentially down the length of the aorta.

Figure 3.1.2 shows that aortas from mice treated with HF/angII/βAPN have increased stiffness compared to WT in all aortic regions except the infra-renal. At deformations greater than 40 μm the thoracic and suprarenal comparisons are statistically different from control (Figure 3.1.2 B,C), while a trend toward increased stiffness by aneurysmal rings was shown in the arch comparison (Figure 3.1.2A). Most notable is the lack of any biomechanical separation between WT and aneurysmal infra-renal aorta (Figure 3.1.2D). Because mice present with aneurysms in the arch, thoracic, and suprarenal aortic regions, but never in the infra-renal region, this lack of significance was expected and supports the link between alteration of aortic mechanical properties and the spatial tendency for aneurysm formation.

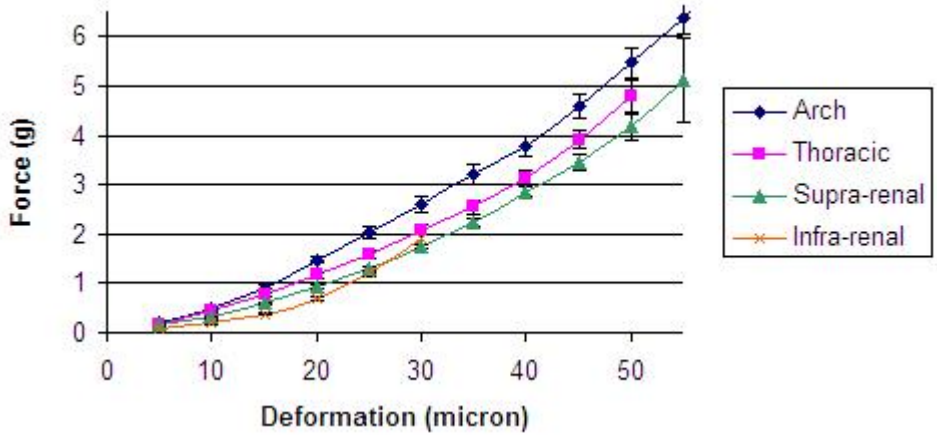

Figure 3.1.1 Baseline force versus deformation behavior of aortic rings from the arch, thoracic aorta, supra-renal aorta, and infra-renal aorta. All curves exhibit an initial phase of low stiffness followed by a linear increasing region of increasing force. The arch produces the greatest force when deformed and the infrarenal produces the least. Infrarenal rings reached a maximum deformation of 25 micron before destruction of tissue. Analysis by ANOVA demonstrates that aortic region significantly effects its stiffness, $P<0.001$.

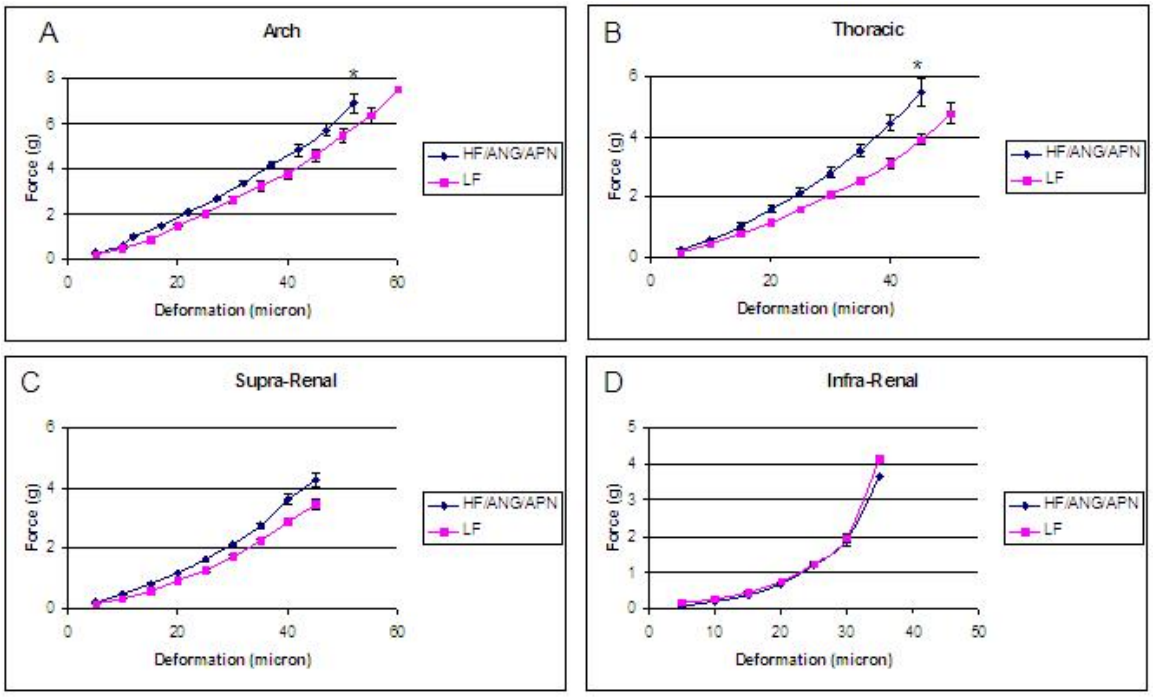

Figure 3.1.2. Force versus deformation curves from aortic rings of control C57 mice on low fat diet (pink squares) and ANGII/β-APN treated C57 mice on a high fat diet (blue diamonds). A) Aortic arch, B) Thoracic aorta, C) Suprarenal abdominal aorta, D) Infrarenal abdominal aorta. The stiffness decreased from the arch down to the infra-renal segment. N=5 at each data point. *=$p<0.05$.

Though these data support the expected mechanical differences between healthy and early aneurysmal aortas, as well as showing the spatial mechanical variation along the aortic length, the set-up and experimentation with the wire myograph may have introduced unwanted artifact into the data. First, cutting the aorta into rings damages the integrity of the underlying microstructure. Second, the vessel rings are too small in diameter (less than 1mm) to neglect the vessel damage that occurs at the wire/vessel ring interface. Because of the limitations imposed by aortic ring testing, all subsequent experiments utilized an isolated vessel perfusion system, which provided a more thorough characterization of aortic mechanical properties. This system bypasses the problems encountered with the ring myograph by allowing application of user defined transmural pressures to intact, whole aortas.

3.3.2 Mechanical testing by isolated vessel perfusion

3.3.2.1 Experimental Design and Aortic Preparation

Ex vivo blind-sac experiments were performed to study the compliance response of the aorta. Based on the wire myography results showing that the aortic wall in early aneurysm disease is stiffer than healthy tissue, we expected that aortic compliance in our aneurysmal models would decrease. Aneurysm pathogenesis was induced in either C57Bl/6 or apoE$^{-/-}$ mice (background strain will be indicated when necessary). The longitudinal time course investigated included time points of 3, 6, 9 and 12 days to ensure a thorough investigation of the earliest aneurysmal changes to aortic microstructure. We also investigated this model without βAPN. This model promoted less aggressive disease to allow a wider window for capturing cardiovascular events, such as medial hypertrophy, elastin degradation, and vessel dilation.

3.3.2.2 Optimization of Isolated Pressure versus Diameter Data Acquisition

Compliance changes were investigated just above the celiac artery, the location where murine aneurysms develop. We first demonstrated that reproducible pressure versus diameter (P-D) curves could be obtained. Transmural pressure was applied in a linear ramp increasing from 0 to 130mmHg and decreasing back to 0 mmHg (Figure 3.2.1, left). Optimization of the perfusion set up revealed that subjecting the aortas to 120 second pressure ramps (60 seconds up, 60 seconds down) created the most reproducible pressure-diameter curves (Figure 3.2.2).

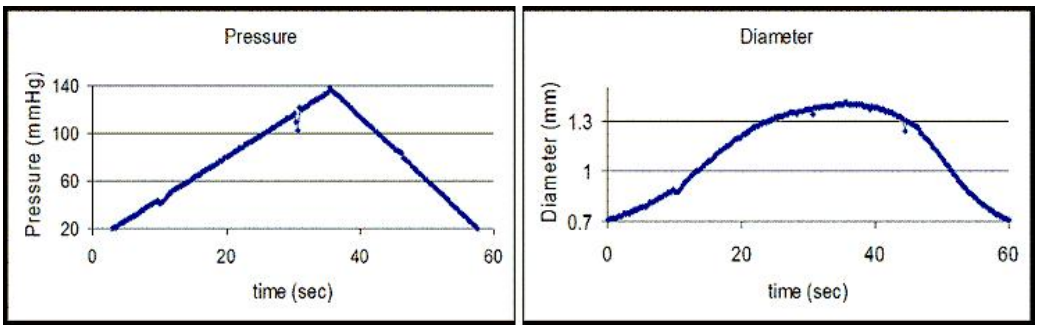

Figure 3.2.1. Representative linear transmural pressure ramp and resulting biphasic diameter response. This is the typical raw data obtained in each isolated vessel test.

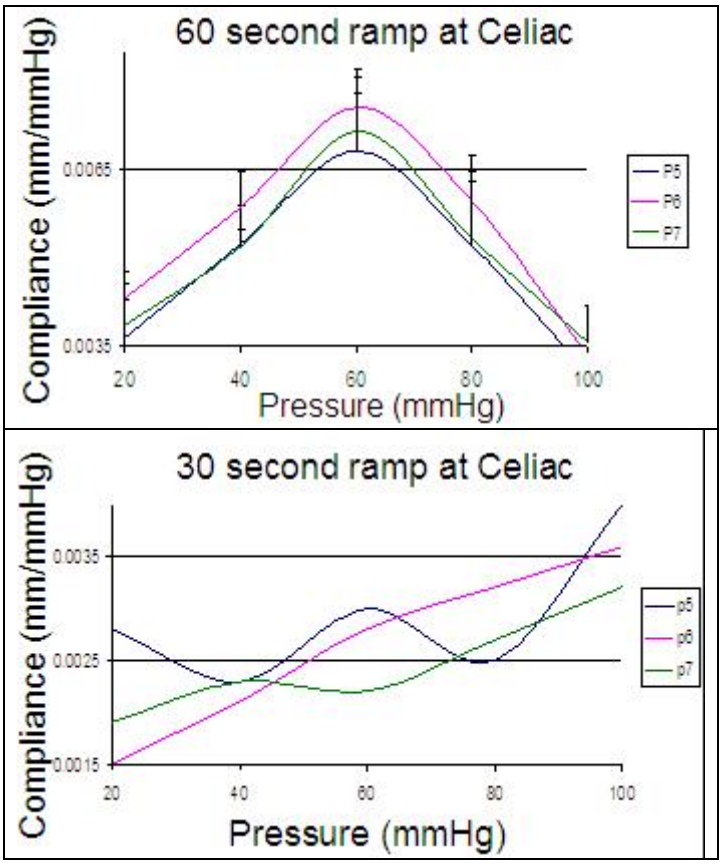

Figure 3.2.2. The first step in optimizing aortic testing was to determine the pressurization protocol. The pressure was increased linearly at different trial rate. The top panel illustrates bell-shape compliance versus pressure response from 3 sequential ramps after increasing pressure at 2mmHg/second. The bottom panel illustrates noisy compliance versus pressure data obtained from 3 sequential ramps after applying transmural pressure at 4 mmHg/second.

To determine the number of preconditioning ramps, aortas were subject to 20 consecutive pressure ramps. These tests showed that ramps 5 through 12 created the most reproducible curves and compliance values (Figure 3.2.3).

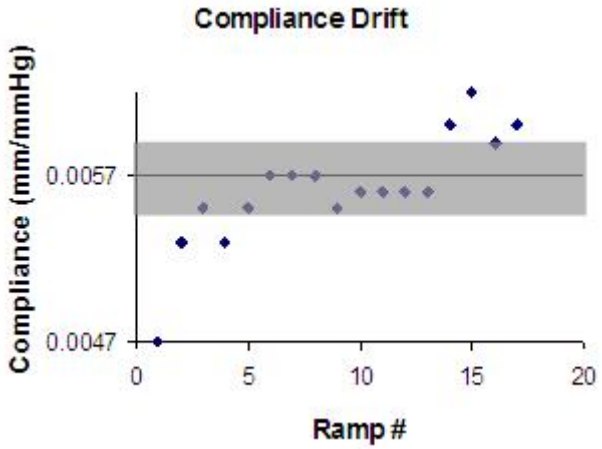

Figure 3.2.3. To determine the number of preconditioning cycles need before data acquisition vessels were subject to 20 sequential 2mmHg/second pressure ramps. Maximum compliance of each ramp was calculated and plotted against ramp number. Ramps 5 through 13 demonstrated the range within which reproducible compliances measurements were obtained.

Therefore, the protocol for data acquisition was defined as 4 preconditioning ramps followed by a maximum of 7 consecutive ramps for data recording.

P-D curves were generated from the raw data. The P-D curves obtained for all control vessels were biphasic and include a region of limited deformation under low increasing pressure, a linear increasing region, and a flat deformation plateau at peak pressure (Figure 3.2.4). Local compliance was then calculated at 20mmHg increments to generate pressure-dependent compliance versus pressure curves for each sample. To obtain local compliance, a linear trend line was applied to the pressure-diameter curves 10 mmHg above and below the indicated pressure, i.e. 20mmHg ± 10mmHg. Conversion of the raw data into pressure-dependent compliance provided a measure of local compliance behavior at increasing transmural pressures (Figure 3.2.5). Compliance

was minimal at low pressure 20mmHg and peak pressure 100 mmHg and was maximal at midrange pressure 60 mmHg.

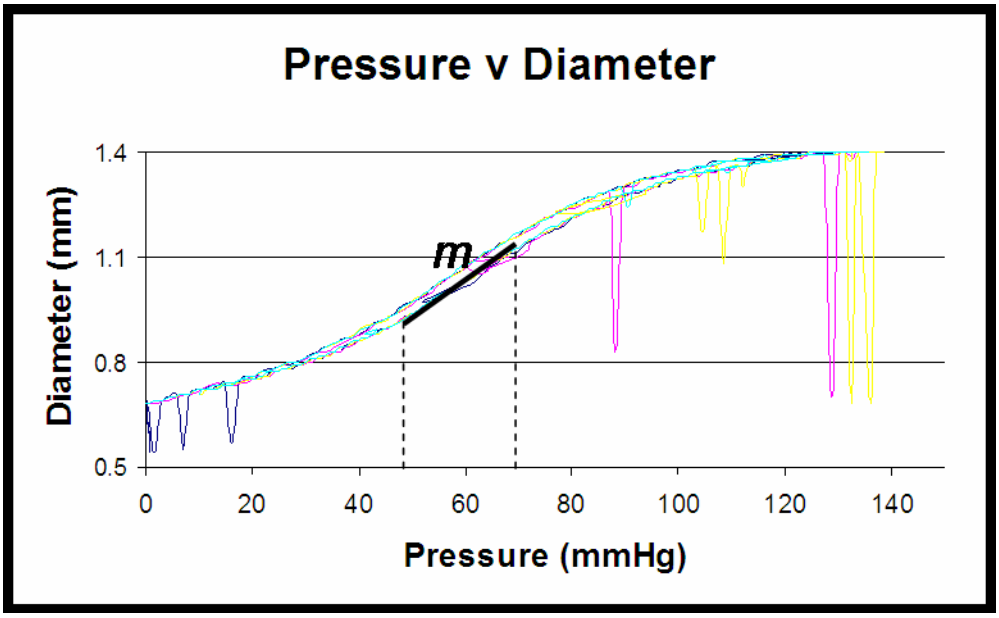

Figure 3.2.4. Typical pressure versus diameter (P-D) response acquired during isolated vessel mechanical testing. The diameter response to increasing pressure is biphasic demonstrating a limited increase at low pressure, a linear increasing region at midrange pressure, and stiffening at high pressure. Local diameter compliance ($\Delta d/\Delta p$), m, is the first derivative of the P-D curve and was calculated at 20mmHg increments.

3.3.2.3 Compliance mechanics of C57/angII/HF model conserved at all time points. Compliance mechanics in the accelerated model were unchanged until 12 day after treatment, while axial mechanics were altered at 6 days: Overall our results demonstrated that circumferential mechanics in the C57/angII/HF mode remained unchanged within the timeframe investigated, while circumferential changes in the accelerated model (C57, angII, βAPN, HF diet) were detected at 12 days. Vessels were extended to the *in vivo* length during inflation. Axial *in vivo* pre-stretch was unchanged in C57/angII/HF from 0 to 12 days (Table 3.2.1). However, axial *in vivo* pre-stretch was significantly reduced by 6 days in the accelerated model providing immediate evidence of

an altered axial environment as a result of AAA progression. The *ex vivo* stretch was adjusted accordingly.

Table 3.2.1. *In vivo* pre-stretch, or axial stretch ratio, of aortas from the physiologic and accelerated models of AAA formation. Upon excision aortic length decreased in all groups. No significant stretch occurred as result of treatment in the physiologic model. Pre-stretch increased by 10% compared to control after 6 days of treatment in the accelerated model. (*P<0.05, In angII/HF model: control v 6 day, P=0.095 and control v 12 day, P=0.111, Mann-Whitney test).

	Control	6 days	12 days
C57+ angII.HF	1.45 ± 0.038	1.38 ± 0.04	1.37 ± 0.06
Accelerated Model C57+ angII/βAPN/HF	1.45 ± 0.038	1.33 ± 0.034*	1.32 ± 0.025*

Table 3.2.2. Baseline maximum compliance of untreated C57Bl/6 and apoE$^{-/-}$ mice; P=NS.

	Maximum Compliance (μm/mmHg)
C57Bl/6 control	9.29 ± 0.85
apoE$^{-/-}$ control	9.15 ±1.86

Aortic mechanical compliance was first measured in LF control aortas. Maximum compliance in C57 and apoE$^{-/-}$ controls (Table 3.2.2) was determined to be 9.29 ± 0.85 μm/mmHg and 9.15 ±1.86 μm/mmHg, respectively, and occurred at 60mmHg transmural pressure in each strain. These values were not significantly different from each other and correspond with published area compliance measurements in male C57Bl/6 mice (66). Local compliance variation with transmural pressure is shown in Figure 3.2.5. Overall compliance behavior was similar between the 2 strains except for a significant compliance reduction in the apoE$^{-/-}$ mice occurring at 80 mmHg.

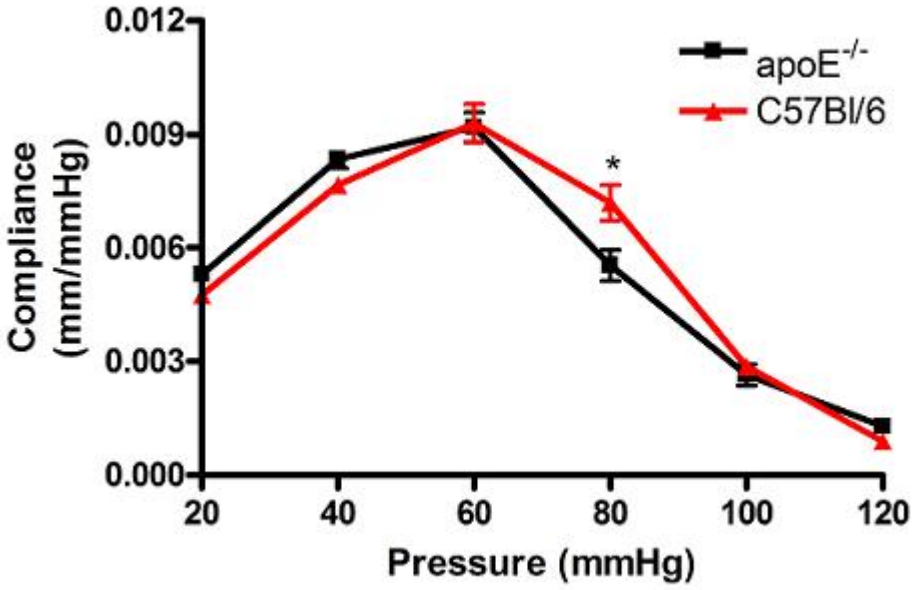

Figure 3.2.5. Local compliance versus pressure curve showing apoE$^{-/-}$ and C57Bl/6 wild type. This is a representation of the p-d data, but displays the slope (local compliance) of the p-d at 20mmHg increments. Bell-shape behavior indicated that both mouse models demonstrate minimum compliance at low and high pressure, and maximum compliance at midrange pressure. (*P<0.05, Bonferroni post tests).

We next investigated the mechanics of the accelerated model (C57Bl/6, angII/βAPN/HF) at time points of 3, 6, 9, and 12 days. Analysis of the longitudinal P-D relationships did not reveal any significant differences relative to the controls (Figure 3.2.6, 6 and 12 day time points shown). Conversion of the P-D data into pressure-dependent compliance, however, revealed significant variation in overall circumferential compliance between the C57 control and accelerated model at 12 days after treatment (Figure 3.2.7, black versus pink line).

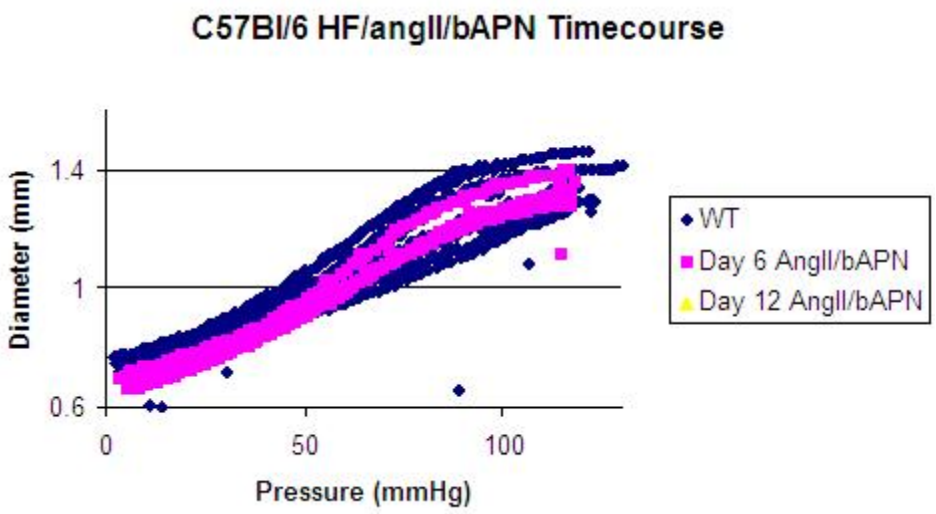

Figure 3.2.6. Raw pressure versus diameter response of the accelerated model of AAA (angII/βAPNHF) at 0, 6, and 12 days. The data exhibits a large amount of scatter, but still retains a biphasic shape. The control data exhibits more scatter compared to treatment groups.

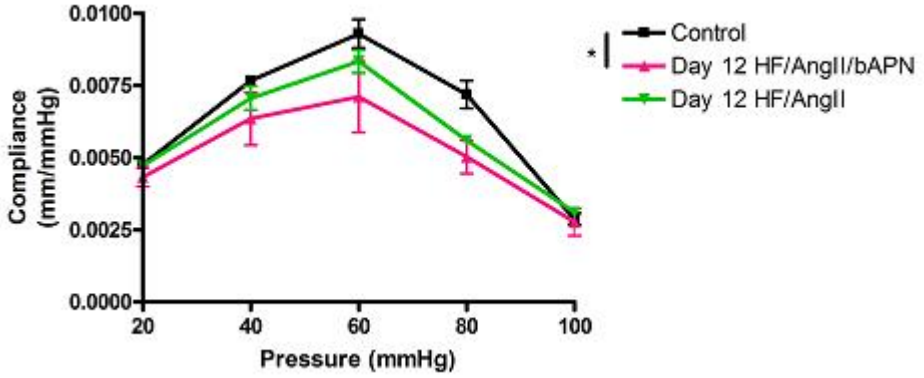

Figure 3.2.7. Compliance versus pressure response at 0 and 12 days treatment in the accelerated model of AAA (angII, βAPN, and HF diet, pink line) and C57/angII/HF diet (green line). All groups exhibit bell-shaped compliance response. 12 day accelerated group showed significant deviation from control due to treatment ($P<0.05$, ANOVA).

Also tested was the inflation behavior of the C57/angII/HF model. The compliance response in this less aggressive model of AAA formation and did not vary

from control in either raw P-D data (Figure 3.2.9) or pressure-dependent compliance at any time point investigated (Figure 3.2.7 and Figure 3.2.8).

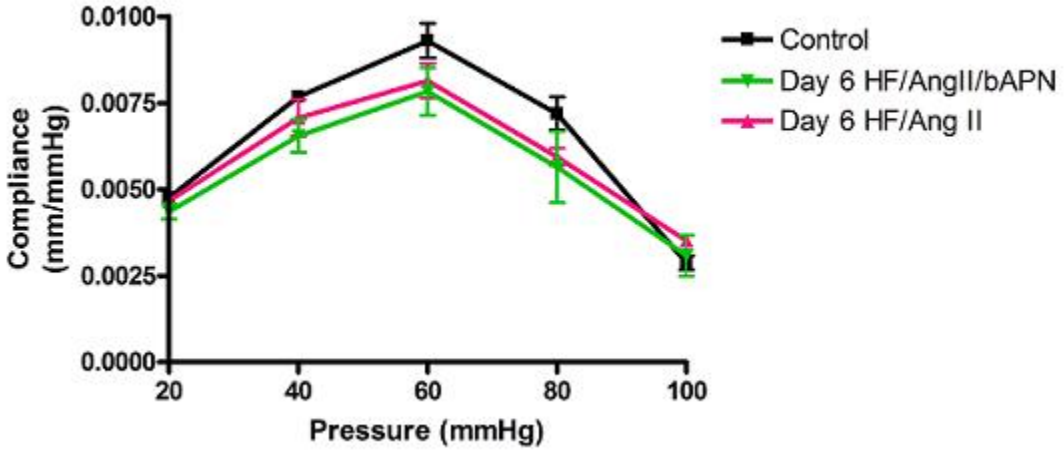

Figure 3.2.8. Compliance versus pressure response at 0 and 6 days treatment with the accelerated model of AAA (angII, βAPN, and HF diet, pink line) and C57/angII/HF diet (green line). All groups exhibit bell-shaped compliance response. No variance between treatment groups and control were detected (P=NS, ANOVA).

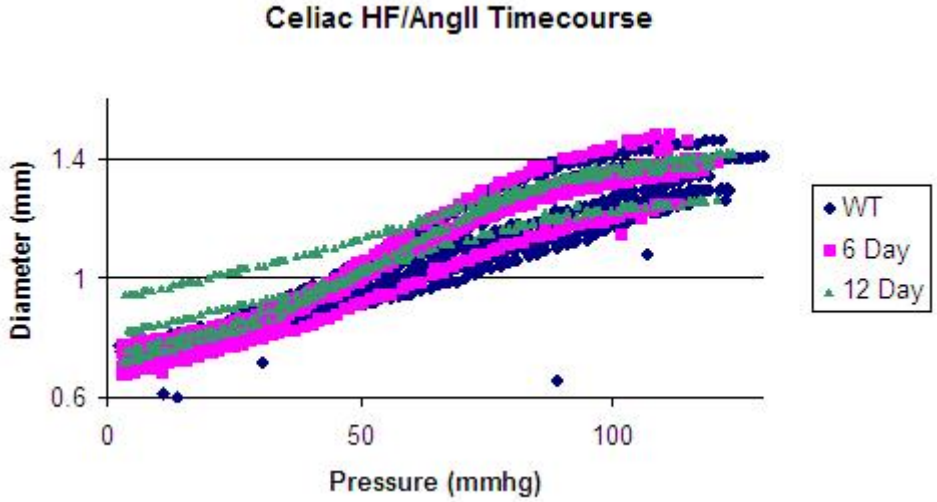

Figure 3.2.9. Raw pressure versus diameter response of the C57/angII/HF (16 week old mice treated with angII and HF diet) at 0, 6, and 12 days. The data exhibits a large amount of scatter, but still retains a biphasic shape. The control data exhibits more scatter compared to treatment groups.

3.3.2.4 Compliance mechanics are conserved in apoE$^{-/-}$ mice treated with angII and HF diet

To determine whether its inherent basal inflammatory state would exacerbate manifestation of mechanical changes, we also tested the circumferential mechanics of apoE$^{-/-}$ mice treated with angII and HF. Significant circumferential compliance changes were not detected in apoE$^{-/-}$ HF/angII mice compared to control at any time point up to 21 days (Figure 3.3.1). In fact, this longitudinal study showed better conservation of normal vascular mechanics than that which was seen in the C57/angII/HF or accelerated model.

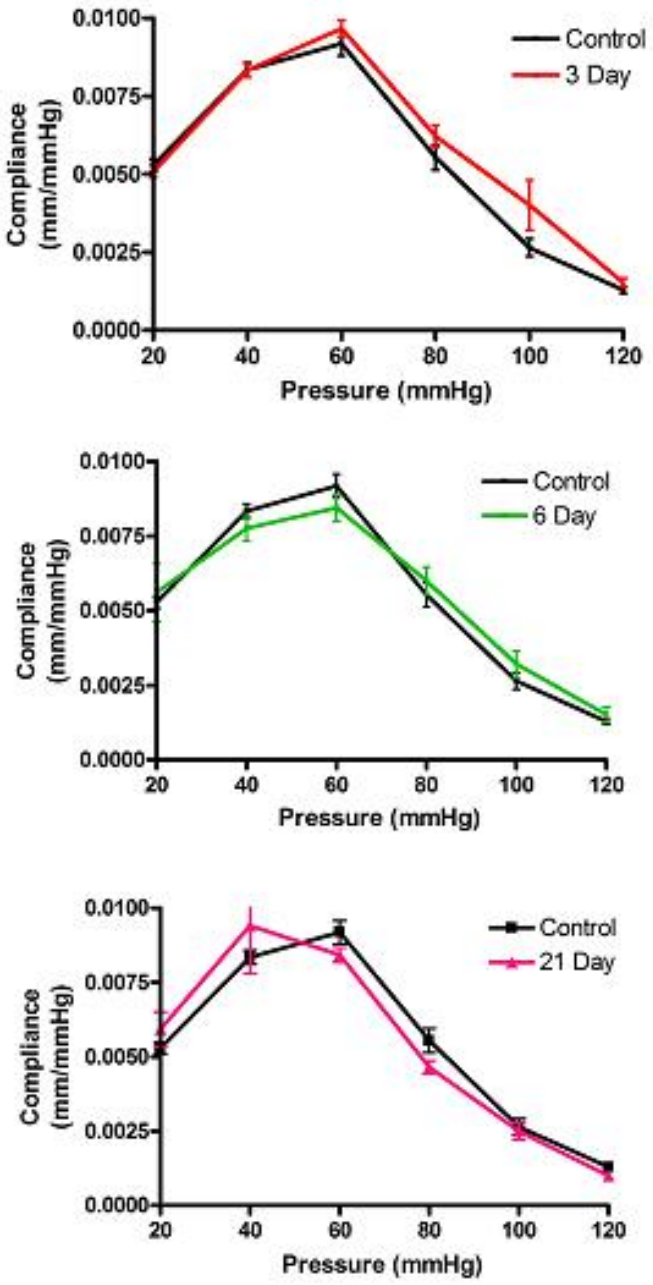

Figure 3.3.1. Compliance versus pressure behavior at 3, 6, and 21 days in the model of physiologic AAA formation in an apoE$^{-/-}$ background (16 weeks old mice with angII treatment and HF diet). The curve exhibited bell shape compliance behavior with pressure loading. Late time points show well conserved mechanical behavior at up to 21 days of treatment. No significant changes were detected during the longitudinal study (P=NS, ANOVA).

Taken together the results support the hypothesis that circumferential mechanics of early aneurysmal disease can be detected by an *ex vivo* isolated aorta perfusion system. However, the original expectation was that we would be able to detect mechanical changes in both models of AAA formation and at time points much earlier than 12 days. Because mechanical changes were detected only in the most aggressive model of AAA formation, we undertook validation of these results with *in vivo* measurements as well as a more detailed analysis of early molecular and microstructural events in AAA formation.

3.3.3 In Vivo Validation of Mechanical Testing

3.3.3.1 In vivo Validation: MRI

MR imaging required intensive optimization as these were the pilot studies for imaging the abdominal aorta. Scout images (Figure 3.3.2) were initially acquired to locate the upper portion of the right kidney at the level of the celiac artery. This location served as the center point for axial slice series of 21 images acquired to capture lumen diameter along the aortic length. The aorta, vena cava, and kidneys were resolved with spatial resolution of 256 x 128 pixels, corresponding to a field of view of 8cm x 4cm, and 1mm slice thickness (Figure 3.3.2). A subset of the cine MR angiograms encompassing an established aneurysm is shown in Figure 3.3.3. Panel 1 is superior to the AAA and panel 6 is inferior. Panels 3 and 4 display the enlarged lumen of the AAA as well as the mural thrombus (dark area surrounding the lumen, indicated by arrow), which is characteristic of murine aneurysms.

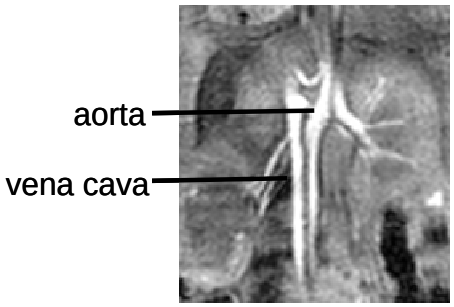

Figure 3.3.2. Angiogram showing resolution between aorta and inferior vena cava in mouse at the level of the renal arteries. Resolution= 256 x 128 pixels. Slice thickness=1mm.

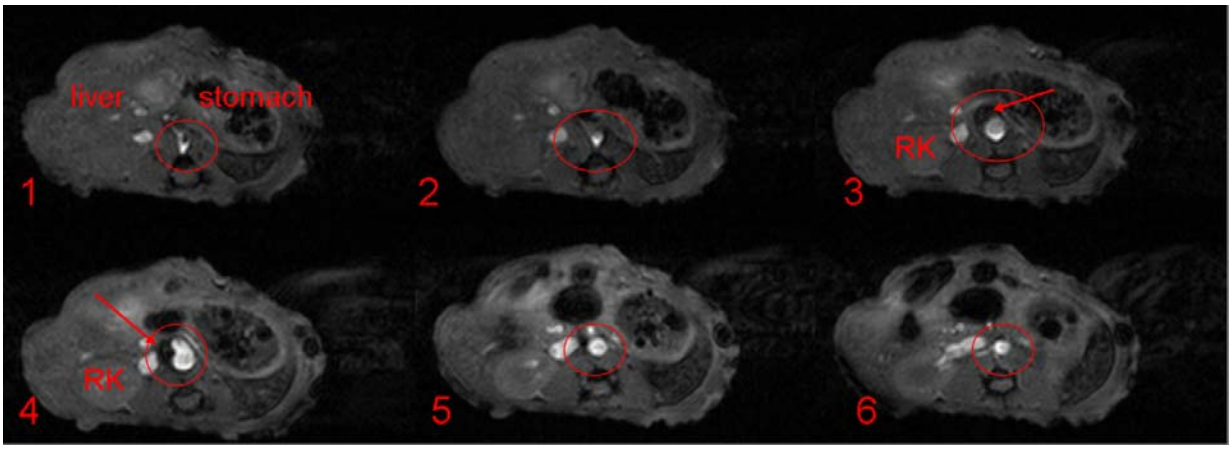

Figure 3.3.3. Consecutive axial MRA images of murine AAA. Images in panels 1 and 2 show the aortic lumen superior to AAA, while panels 5 and 6 show the inferior lumen. The slice thickness of each image is 1 mm. Resolution is 256 x 128 pixels. The red circle encompasses the aortic lumen and the arrows in panels 3 and 4 indicate the AAA mural thrombus. Legend: RK= right kidney

The limitation of MR imaging is that transmural pressure is unattainable and therefore must be arbitrarily applied based on normal systolic and diastolic blood pressure. To validate the compliance measurements acquired in the *ex vivo* inflation it was assumed that maximum lumen diameter occurred at systolic blood pressure (120mmHg) and the minimum diameter occurred at diastolic blood pressure (80mmHg), providing a pulse pressure, ΔP, of 40 mmHg. Therefore physiologic compliance was calculated as $\frac{D_{120mmHg} - D_{80mmHg}}{\Delta P}$. In healthy vessels, *in vivo* and *ex vivo* compliance

measurements were statistically comparable (Table 3.3.1) therefore supporting the experimentally acquired results.

Table 3.3.1. Comparison of physiologic aortic compliance measured by *ex vivo* inflation and *in vivo* MRI. Physiologic compliance measured by $\frac{D_{120mmHg} - D_{80mmHg}}{\Delta P}$, where ΔP =40mmHg (P=0.09 compared to *in vivo* control, Mann-Whitney test).

	Compliance (μm/mmHg)
Ex vivo (Inflation)	3.7 ± 1.3
In vivo (MRI)	6.5 ± 2.7

Black blood imaging was attempted in addition to angiography in effort to obtain aortic wall thickness. Trial scans in a 9.4T horizontal Bruker magnet (20 cm bore) equipped with a Bruker AVANCE console (Bruker Biospin Inc., Germany) and a set of gradient coils achieved in-plane resolution 98 × 78 μm^2 with slice thickness of 781 μm (Figure 3.3.4). This resolved the aorta better than the Varian system, but was still insufficient to accurately resolve the aortic wall. Therefore, the protocol attempted here does not provide a suitable method to determine wall thickness. Given that murine aortic thickness less than the resolution boundary, determining wall thickness with MRI is most likely unfeasible. However, MRI acquisition of diameter compliance is an excellent method for validating experimentally acquired mechanical data.

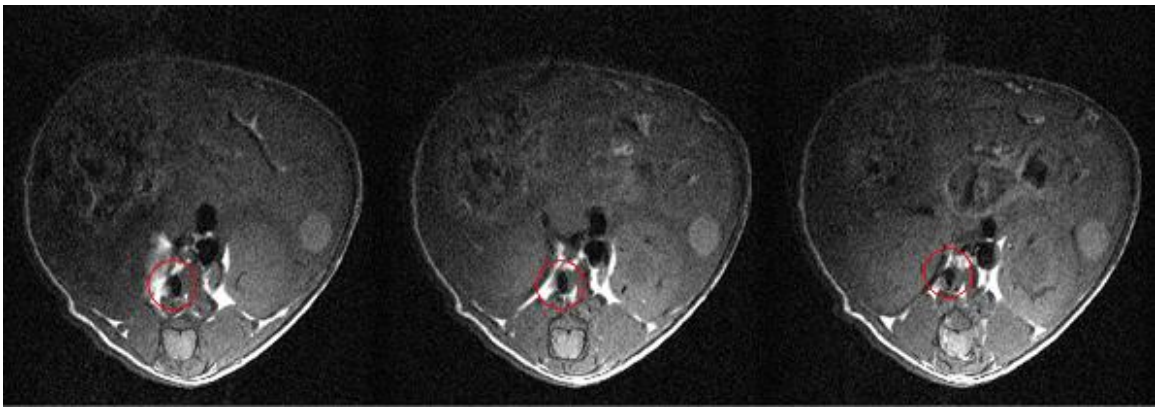

Figure 3.3.4. Black blood or spin echo MR images of the abdominal aorta. Aorta is indicated by red circle. Resolution 98 x 78 x 781 mm/pixel.

Although proper validation was achieved with MRI, we found that the methodology limited sample size because of the data acquisition time. Anesthetic delivery to final image acquisition often took 2-3 hours and processing of the data into workable image files took additional time. Therefore while MRI is an appropriate method to obtain high resolution of aortic geometry for modeling purposely, we also used Doppler ultrasound to acquire relatively quick (less than 45 minutes from aesthesia to compliance result) measurement of *in vivo* aortic compliance.

3.3.3.2 *In vivo* Validation of Inflation Testing: Ultrasound

Ex vivo compliance measurements were further validated with ultrasound Doppler imaging. Figure 3.3.5 provides an M-mode image of the abdominal aortic wall. The top trace reflects free compliant movement of the anterior wall, while the bottom trace reflects restricted movement indicative of posterior tethering to the vertebral column. Respiration and EKG monitoring allowed capture of all inner diameter measurements at exhalation and early systole. Physiologic compliance behavior from 0 to 12 days treatment of the accelerated model (C57, HF/angII/βAPN) is shown in Table 3.3.2. Baseline compliance measurement via ultrasound was statistically comparable to the *ex vivo* measurement of physiologic compliance which calculated as $\frac{D_{120mmHg} - D_{80mmHg}}{\Delta P}$.

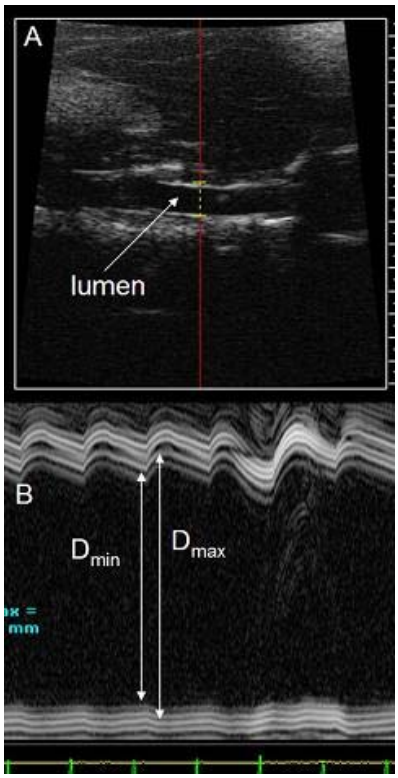

Figure 3.3.5. A) B-mode acquisition of the abdominal aortic lumen in the longitudinal axis. B) M-mode of the movement of the anterior (top) and posterior (bottom) aortic wall at the location indicated in A. D_{max} and D_{min} are measured as shown.

Table 3.3.2. Physiologic compliance of the accelerated model after 6 and 12 days of treatment measured by *ex vivo* inflation and *in vivo* ultrasound. Physiologic compliance was measured as described in Table 2. (P=0.39 in 6 day *ex vivo* versus *in vivo*, P=0.18 in 12day *ex vivo* versus *in vivo*, Mann-Whitney test).

	Maximum Compliance (μm/mmHg)		
	Baseline	6 day	12 day
Ex vivo (Inflation)	3.7 ± 1.3	3.1 ± 1.3	3.3 ± 0.74
In vivo (Ultrasound)	5.9 ± 2.2	2.6 ± 0.88	2.6 ± 0.63

Validation of our *ex vivo* mechanical results demonstrated that in the physiologic pressure range our *ex vivo* compliance results between 0 and 12 days do not differ significantly. This is critical result, suggesting that although overall compliance behavior may change

upon treatment with angII/βAPN and HF, mechanics within the physiologic range are conserved.

3.3.4 Microstructural Analysis of Models of AAA Formation

3.3.4.1 Incidence of AAA formation in murine models

Our objective was to determine whether we could detect mechanical changes before deleterious molecular events occurred. Therefore the next component of our study was histological investigation of AAA formation. Early time points were selected to capture these events and therefore observation of aortic dilation and established AAA outcomes were expected to be rare. Table 3.4.1 shows the observed outcome of aneurysmal and dissection events in our models of AAA. Our results corroborate published results of increased incidence of dissection in the physiologic models. The incidence of dissection on C57 background was higher than that seen in the mice on an apoE$^{-/-}$ background (12% versus 8%, respectively). As expected, aneurysmal outcome predominated in the accelerated model with low occurrence of dissection (10% versus 3%, respectively).

Table 3.4.1. Incidence of AAA and dissection in murine models studied longitudinally until date of aortic harvest. Animals on C57Bl/6 background were harvested at a maximum of 15 days. Animals on apoE$^{-/-}$ background were harvested at a maximum of 21 days.

	Outcome	Overall	By 12 days	By 15 days
C57 HF/angII	AAA Dissection	12% 12%	1% 12%	-NA- -NA-
C57 HF/angII/βAPN	AAA Dissection	10% 3%	6% 2%	10% 3%
apoE$^{-/-}$ HF/angII	AAA Dissection	15% 8.5%	6% 8%	13% 10%

3.3.4.2 Microstructure of Established Aneurysms

Gross morphology of a healthy murine aorta includes a translucent artery that tapers from the thoracic to infrarenal aorta (Figure 3.4.1). Large, established AAAs can present with thrombus in the suprarenal aorta (Figure 3.4.2). The established AAA completely encompassed the celiac and superior mesenteric arteries.

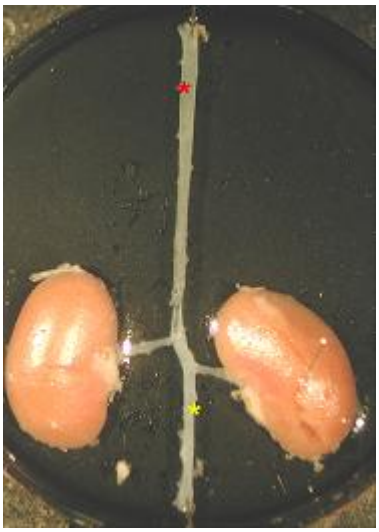

Figure 3.4.1. Representative image of a healthy aorta. The vessel has a natural taper from the upper thoracic (red*) to infra-renal aorta (yellow *).

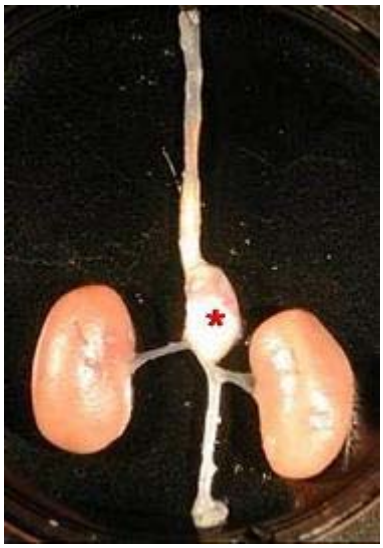

Figure 3.4.2**.** Representative image of an established AAA located in the suprarenal aorta. Red* indicates dilated region.

Representative images of healthy aortic microstructure are shown in Figure 3.4.3. The images show that the aortic wall was composed of 3-4 intact elastic laminae forming concentric rings about the lumen. A very thin adventitia surrounded the elastic laminae and this layer was relatively free of inflammatory cell infiltration as shown by H&E stain (Figure 3.4.4). These images also illustrated the variability in aortic diameter typically observed among samples. The diameter of the first sample was greater than 1mm, while the diameter of the second sample was less than 1mm. Average inner diameter of healthy aorta is generally considered 1mm.

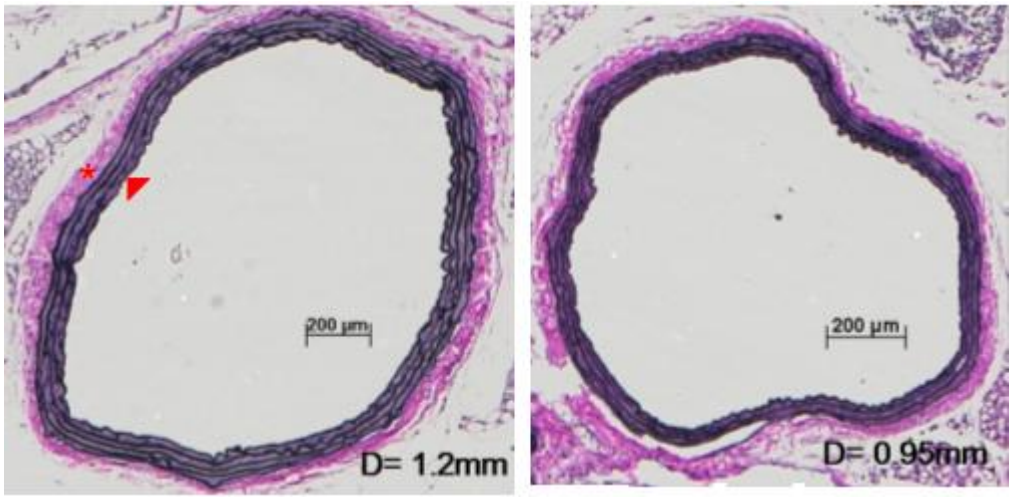

Figure 3.4.3. Representative images of healthy aortic microstructures of individual samples stained with Verhoff's van Geison Elastic stain. The samples show 4-5 concentric elastic laminae surrounded by a thin adventita. Inner diameter of each is indicated. (*=adventitia, arrowhead=inner elastic lamina).

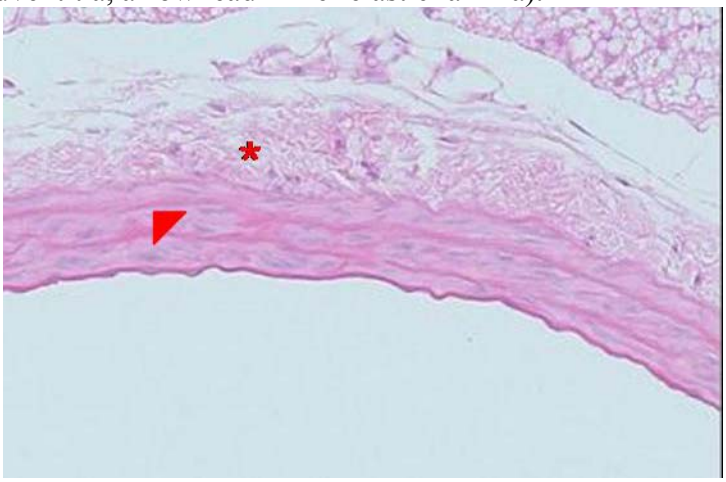

Figure 3.4.4. Cross section of the healthy aortic microstructure showing acellular adventitia by H&E staining. (*=adventitia, arrowhead=inner elastic lamina).

We found that the aortic microstructure of the aorta of large, established AAAs (Figure 3.4.5) was distinctly different from that of normal aortas. Aortic lamellar organization was completely abolished in fully developed aneurysms. Notably, there was focal separation of the elastic laminae, leaving the lumen tethered together by adventitial connective tissue. The adventitia appeared unevenly remodeled and abundant in collagen, particularly in the area adjacent to the separated elastic laminae. Moreover,

cellular infiltration was increased throughout the aneurysmal aortic wall, as well as, throughout the periadventitial fat.

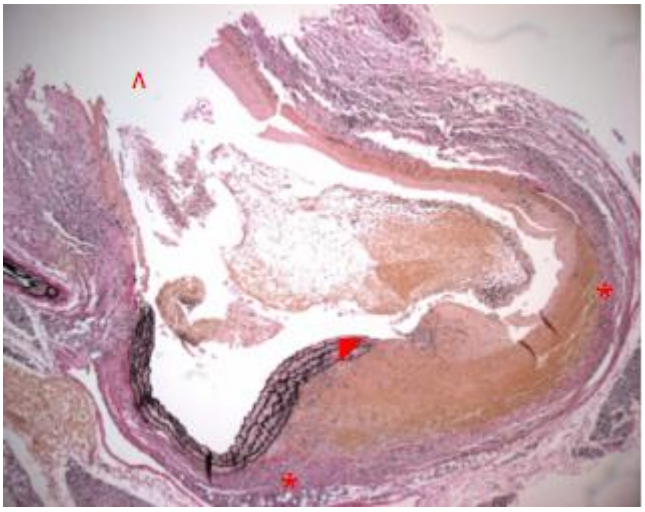

Figure 3.4.5. Representative image of the microstructure of a large, established AAA stained by Verhoff's van Geison stain. There is a focal separation of the elastic laminae which is tethered together by the adventitia**.**

3.3.4.3 Microstructure of Small AAA

Analysis of the microstructure of small aortic dilations in the C57/angII/HF model revealed an intermediate stage in AAA development. Histological investigation of the aortic wall revealed biological remodeling and cellular infiltration. Figure 3.4.6 provides an illustration of the small AAA observed. This sample demonstrated two regions of aortic dilation, one between the superior mesenteric artery and celiac artery, and the second one slightly proximal, in the suprarenal region. The affected areas appeared opaque compared to the remainder of the aorta.

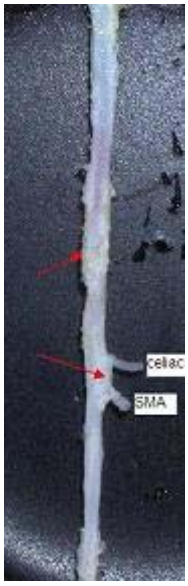

Figure 3.4.6. Representative en face image of early aneurysmal dilation. Red arrows indicate areas of aortic dilation. The branching arteries shown are the celiac and superior mesenteric artery (SMA).

The microstructure of two early stage AAAs in shown in Figure 3.4.7 and demonstrated increased collagen deposition and preferential thickening of the adventitia compared to control. Both the inner and outer diameters were enlarged, which demonstrated outward remodeling. In addition, there is dramatic infiltration of inflammatory cells into the adventitia confirming an upregulated inflammatory response definitive of AAA progression.

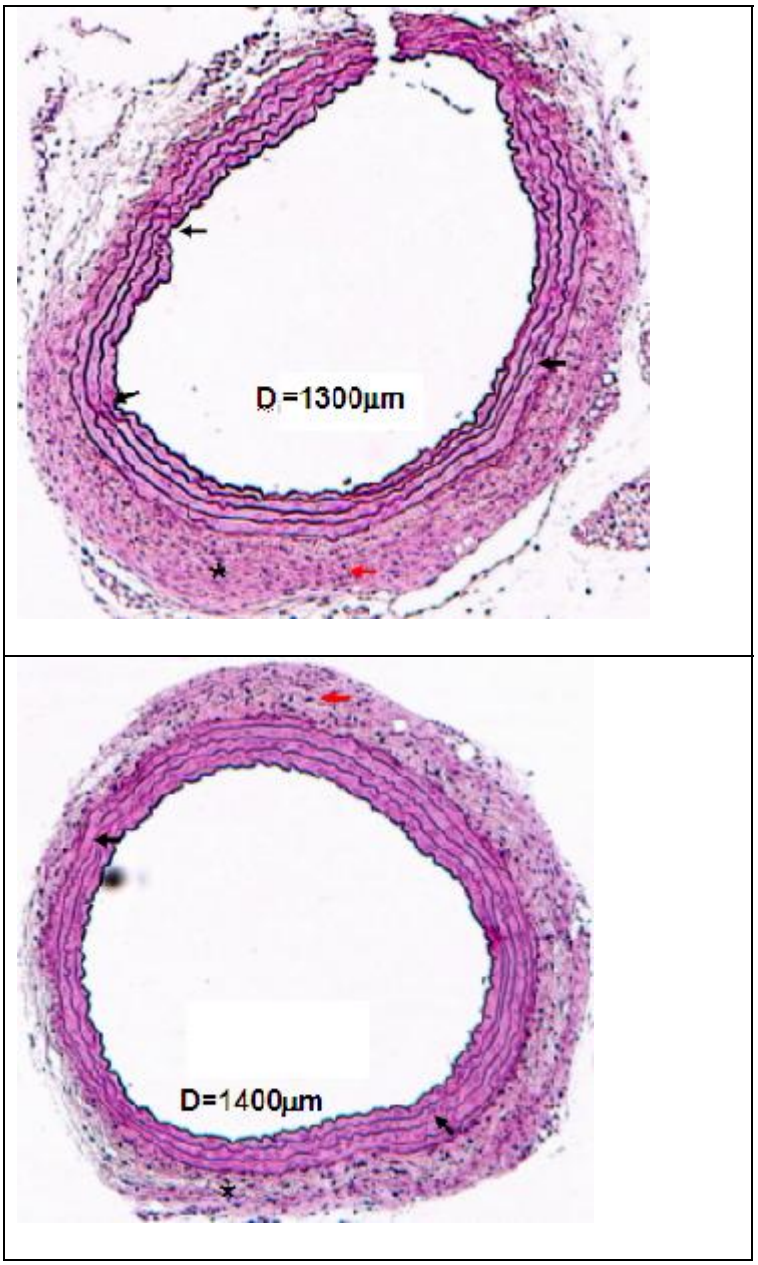

Figure 3.4.7. Representative images of small AAA resulting from the C57/angII/HF model of AAA. The adventitia appears preferentially thickened on one side and there is minimal elastin fragmentation. Inflammatory cells are high in number in the adventitia. The adventitia is indicated by *, breaks in elastin fibers are indicated by black arrowheads, inflammatory cell is indicated by red arrow.

3.3.4.4 Microstructure of the Pre-Aneurysm

To capture the earliest pathogenic events, the time course that we focused upon was adjusted to encompass the first few days of AAA induction. The first appearance of disease was observed at 3 days after treatment in the C57/HF/angII model. As shown in Figure 3.4.8top macrophage infiltrates were observed in the adventitia at 3 days indicating an initial inflammatory response in the aortic wall.

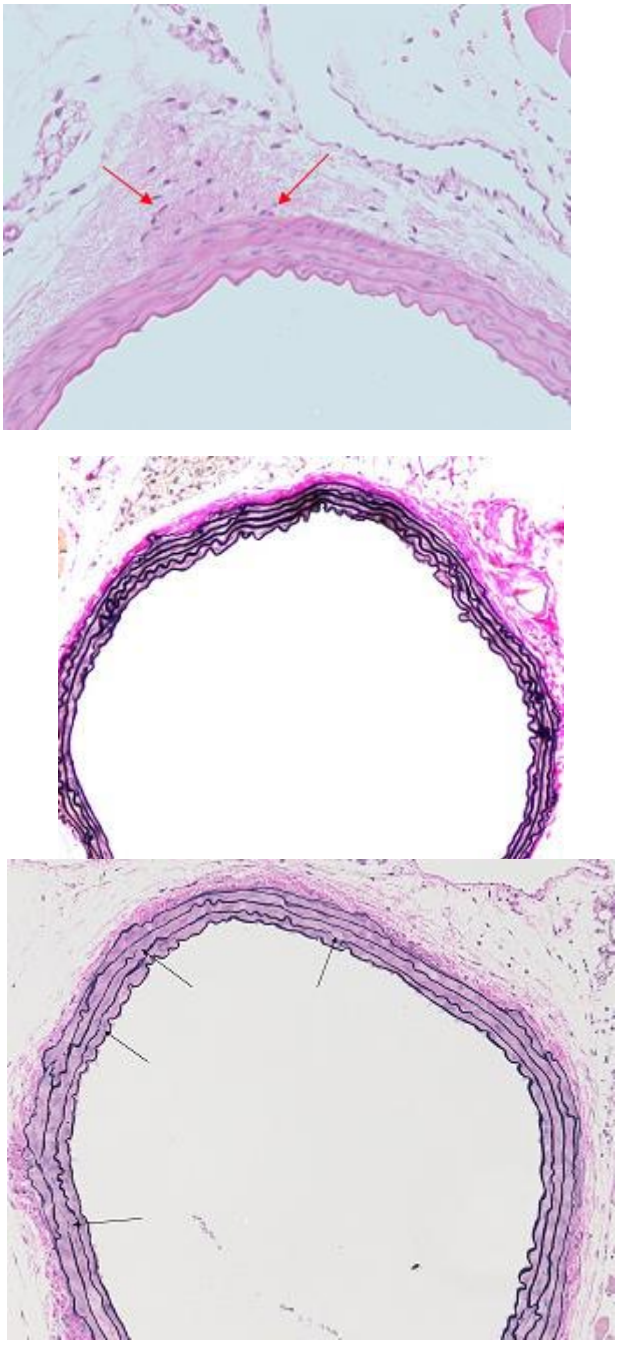

Figure 3.4.8. Top) H&E stained image of C57/angII/HF model of AAA after 3 days. Red arrows point to inflammatory cells in the adventitia. Middle) Representative Verhoff van Geison stained image of the C57/angII/HF model of AAA after 6 days. There no detectable breaks in the elastic laminae Bottom) Verhoff van Geison stained image of physiologic model on the C57Bl/6 background after 9 days. Black arrows indicate punctate snaps in the elastic laminae.

Elastin breaks were rarely seen in the C57/angII/HF model by 6 days (Figure 3.4.8mid), but were frequently observed by 9 days (Figure 3.4.8, lower panel), likely attributable to matrix degrading factors in the aortic wall at this time point. As expected, however, elastin fragmentation was observed earlier (by 6 days) in the accelerated model (Figure 3.4.9, B-E). Most notable is the lack of appreciable adventitial thickening in either model of AAA. Indeed the representative images of the 12 day accelerated model suggest that the adventitia became thinner as disease progresses. This observation leads us to speculate that dilation-associated collagen deposition, as seen in the small AAAs in Figure 3.4.7, may be a rapid event in AAA pathogenesis. Summary of matrix changes in the "pre-aneurysm" therefore include inflammatory cell presence as early as 3 days, gradual increases in elastin fragmentation, and uneven remodeling of the adventitia.

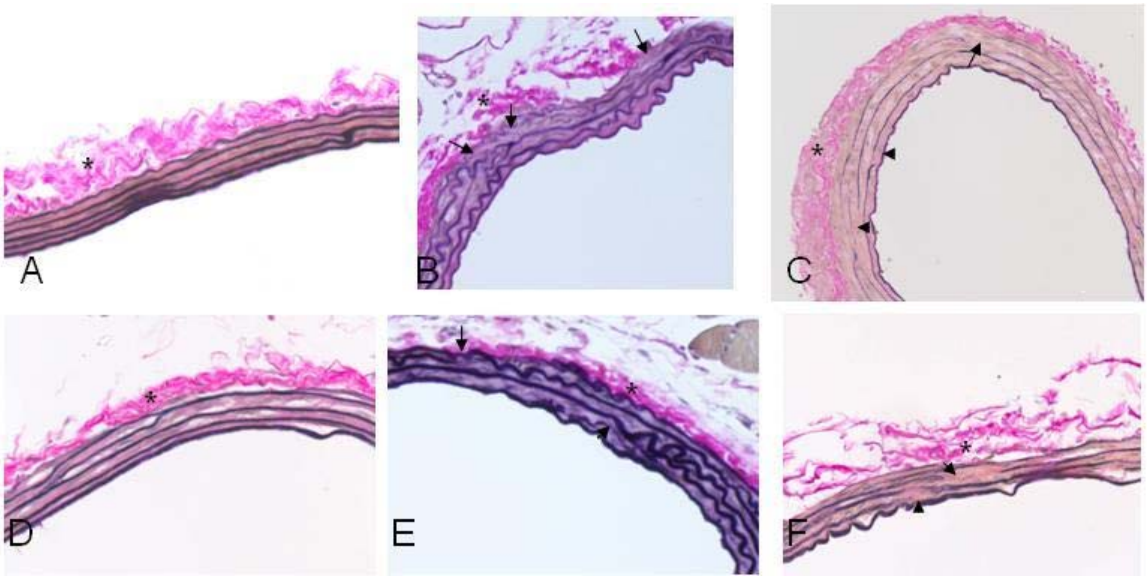

Figure 3.4.9. Representative Verhoff Van Geison Elastic staining of aortic cross section of the accelerated model of AAA formation at 0(A-D), 6 (B-E), and 12 (C-F) days. Control images show a thin adventitia with intact elastic laminae. 6 day images show increase elastin breaks within the media and no appreciable adventitia change. 12 day images show further elastin fragmentation and areas of both adventitial thickening and thinning. (*=adventitia, arrows=elastin breaks).

3.4 Discussion

We originally hypothesized that in the pathogenesis of AAA, mechanical events precede molecular events. We proposed that this would provide the ability to detect aneurysms *before* adverse biological changes affected the aortic wall. However, histological analysis demonstrated that molecular events were indeed the first indication of the degradation of the aortic microstructure. Because significant mechanical stiffening was detected only at late time points in our most aggressive model, we posed a new hypothesis that molecular remodeling compensates for mechanical changes step-by-step, minimizing the window in which these changes can be detected before aneurysmal dilation ensues. Overall our results support 2 main conclusions:

1) that clinical imaging modalities may not have the capacity to detect aneurysmal progression before harmful molecular events occur, and

2) in the setting of AAA progression, vascular cells maintain physiologic circumferential compliance at the risk of deleterious augmentation of their local matrix environment.

At the onset of this project, we expected that changes in matrix structure, particularly in elastin fragmentation and collagen resorption/degradation, would eventually lead to aortic stiffening. Indeed measurement of aortic stiffening during aneurysm development in our studies is corroborated by published work (4, 5, 48, 51, 52, 67, 68). However, we believed the mechanical ramifications of this matrix remodeling would reveal themselves much earlier. Thus, we consider that in the setting of aneurysmal disease, the vessel maintains its homeostatic mechanical state while at the same time undergoing irreversible ECM degradation. Indeed, despite significant variance in overall compliance behavior in the accelerated model, compliance within the

physiologic range was unchanged. *In vivo* measurement by Doppler ultrasound confirmed this *ex vivo* result. Since remodeling without growth would have altered the compliance of the vessel, we can assume that maintenance of aortic compliance was mediated by significant vascular growth and remodeling. Therefore we can hypothesize that, in the setting of AAA development, vascular cells have a strong tendency to restore their intrinsic homeostatic state, which can lead to irreversible ECM remodeling.

Indeed vascular adaptation to restore homeostasis has been shown in many settings. Most recent demonstrations have been in isolated vessel culture in which arteries extended beyond their *in vivo* length remodel back to their *in vivo* length (69, 70). Vascular adaptation has also been demonstrated in the setting of hypertension, in which aortas were shown to maintain compliance and stress-strain relationship despite altered hemodynamic pressure (71). To our knowledge the studies presented here provide the first evidence of vascular adaptation in the setting of early aneurysmal remodeling.

Our data also provide evidence for the independent augmentation of axial and circumferential mechanics. Despite delayed manifestation of overall circumferential behavior at 12 days in the accelerated model, altered axial stretch ratio was detected by 6 days. Changes in axial stretch were likely an effect of elastin fragmentation, which was also observed in this model by 6 days. Elastin has been demonstrated as the tensile component of the aorta that bears axial load (11). Thus the results demonstrate a direct association between elastin degradation and altered axial force. Moreover, altered axial behavior reflects the major limitation of our mechanical testing system, which cannot measure axial force during pressurization. Therefore it is possible that early molecular events were accompanied by altered mechanics that were not detected in our system.

Thus, although our results suggest that alterations in circumferential mechanical behavior are significantly delayed in the origins of AAA formation, we cannot dismiss the role and effects of changes in axial mechanics, which may play a major role in early AAA development.

As lysyl oxidase inhibition was the "accelerating" component of the accelerated model of AAA, it is possible that lack of lysyl oxidase may have mechanistically affected the axial mechanics as well. Lysyl oxidase activity is represented by the gene products of five family members including LOX, LOXL1, LOXL2, LOXL3 and LOXL4. These enzymes function by oxidatively deaminating lysine residues in proteins. The products then autocatalytically combine with other lysines or deaminated lysines to form covalent cross-links. Lysyl oxidase activity therefore plays a key role in the formation of insoluble aggregates of matrix protein that are less susceptible to proteolytic degradation and thus more stable against disease. We hypothesize that in the accelerated model of AAA, inhibiting lysyl oxidase may have blunted mechanisms of ECM synthesis which counterbalance ECM degradation, therefore precipitating mechanical changes.

Finally we must address the possibility that altered circumferential compliance in the physiological range did occur at earlier time points, but that the effects were masked by the overall behavior of the whole aorta. Spatial development of mechanical gradients within the vasculature is well established. Evaluation of the variation of mechanical properties has been performed in both C57Bl/6 (66) and apoE$^{-/-}$ mice (72). Both reports demonstrate tight regulation of aortic mechanical properties within distances of a few millimeters. One distinction not addressed in our study is the variation in axial stretch ratio along the aortic length. Guo and Kassab (66) demonstrate that the overall stretch

ratio of the C57Bl/6 mouse is approximately λ=1.4, but that the stretch within the suprarenal abdominal aorta is λ=1.2. Therefore we can assume that aortas in our studies may have been overstretched relative to the *in vivo* configuration, which may have prevented extraction of physiologic mechanics. Recalling our argument of the benefit of isolated vessel inflation over aortic ring testing, we must now appreciate the utility of the two methods. Aortic ring studies provide spatial sensitivity representative of circumferential mechanics and blunt the axial contribution. Vessel inflation detects the response of the aorta in its physiologic-like state and limits spatial sensitivity. Indeed a thorough characterization of our models of AAA formation deserves attention to both the axial and circumferential manifestation of mechanical properties.

In summary the studies performed in this work help to better understand both clinical management and mechanical characterization of AAA. To our knowledge the studies presented here provide the first mechanistic discussion of early aneurysmal remodeling. They suggest that subclinical detection of early aneurysmal disease may not be possible with current noninvasive imaging methodologies and demonstrate that vascular cell mechanosensitivity promotes a strong tendency to restore mechanical homeostasis, even if irreversible ECM remodeling occurs. Our results therefore merit further study of the vascular response to disease progression as it is clear that cellular function is finely tuned to mechanical state.

CHAPTER 4

H_2O_2 IS MECHANISTICALLY LINKED TO AAA BIOMECHANICAL REMODELING

4.1 Introduction

Abdominal aortic aneurysm formation has been established as an inflammatory disease (73) that affects the normal matrix organization of the aortic wall (11). It is clear that aneurysm formation proceeds from localized remodeling and vessel dilation attributable to degeneration of the elastin and deposition of collagen structural proteins within the aortic wall (8-11). Reactive oxygen species (ROS) have been detected at all stages of aneurysm development (36, 38, 39) and have been established as mediators of ECM degradation by upregulating MMP activity via the NAD(P)H oxidase (13, 40).

Physiologic aortic mechanical behavior is clearly linked to the material composition of the aortic wall. *In vivo* aortic pre-stretch, also called homeostatic stress, define as the ratio of the *in vivo* length, L, to the *ex vivo* length, L_o, can indicate the magnitude of axial tension experienced *in vivo* or it may alternatively reflect aortic material density. Compliance measurements which reflect the capacity of the vessel to expand under pressure are intimately controlled by material composition and geometry, as a thin-walled vessel expands beyond a thick-walled vessel. Furthermore, bisection of an excised aortic ring creates an open aortic sector that provides insight into the residual stress gradient across the vessel thickness. The angle of the sector corresponds tightly to the matrix and cellular composition within the aortic wall. In this study we have attempted to interpret these mechanical metrics and determine the biological mediators that direct aortic wall mechanics in the setting of AAA.

Matrix degeneration is mediated by infiltration of leukocytes, production of inflammatory mediators, and smooth muscle cell apoptosis. Degeneration of insoluble elastic laminae and collagen fibers reduces the compliance and tensile strength of aneurysmal aortas as demonstrated in Chapter 3 and in the literature (5, 7, 11), underscoring the need to determine the initial molecular and biomechanical determinants involved in early aneurysm development. (i.e. ROS production, ECM remodeling, MMP activity, etc.). Total inhibition of MMP activity (74) and animal models deficient in MMP family members (29, 30) and TIMP inhibitors (10, 31) suggest that MMP-2 and -9 activity is necessary for early matrix degeneration in the setting of aneurysm. However, AAA formation may ultimately require other elastolytic enzymes to fully induce aortic expansion. The concept that elastolysis is necessary, but not sufficient to enhance AAA progression, supports our belief that other factors, such as spatial location along the aorta and altered mechanical properties, must complete the cascade. Thus, a state of active vascular wall remodeling and aneurysmal expansion is induced.

Oxidative stress in vascular walls has been strongly linked to ECM degeneration (36, 38, 39) by upregulating MMP activity via the NAD(P)H oxidase (13, 40). Oxidative disturbance of the ECM promotes endothelial cell dysfunction, SMC reorganization, and myofibroblast transformation, all of which facilitate monocyte adherence to and transmigration through the vessel wall. Antioxidant studies support the link between oxidative stress and aneurysmal disease (39) and point to MMP-2 and MMP-9 activity via ROS-induced macrophage recruitment into the aortic wall. Catalase is an antioxidant enzyme that metabolizes hydrogen peroxide (H_2O_2) into water and molecular oxygen. We were strongly motivated by the observation that transgenic apoE$^{-/-}$ mice with VSMC-

specific overexpression of the human catalase gene (Cat) (42) were completely protected from AAA formation when treated with angII for 28 days, as compared to apoE$^{-/-}$ WT mice. Therefore we utilized this transgenic model and the WT control to investigate H_2O_2-mediated alteration of the aortic ECM in the setting of angII. The working hypothesis for this study was that oxidative stress generated by H_2O_2 is mechanistically linked to the biomechanical remodeling involved in AAA formation by directing matrix remodeling. To test this hypothesis we measured both pressure versus diameter behavior and spatial residual strain, as well as characterized morphology and matrix changes in the aortas of our transgenic model in the setting of angII. The results show that altered aortic biomechanics and tendency toward AAA formation are directly linked to endogenous H_2O_2 within the aortic media.

4.2 Animals

The effect of angII treatment on aortic vascular hypertrophy in our model of VSMC-specific H_2O_2 scavenging was previously characterized in our laboratory (42). H_2O_2 levels in the aortas of WT and catalase transgenic mice were similarly low at baseline. However upon angII infusion H_2O_2 was significantly upregulated in WT. This increase was blunted in the catalase transgenic mice. Treatment with angII induced similar increases in blood pressure between the groups. After 14 days of angII treatment WT mice demonstrated significant vascular hypertrophy compared to the catalase transgenic. Overall the characterization showed that VSMC-derived H_2O_2 plays an important role in angII-mediated vascular hypertrophy.

4.3 Methods

4.3.1 Aortic Preparation and Isolated Vessel Perfusion Set-up

After euthanasia, the thoracic cavity was opened and the vasculature perfused with 10mL 0.9% saline via left ventricular puncture. Prior to dissection, the *in vivo* length was measured with digital calipers. The aorta was then excised and cleaned of connective tissue taking care not to disturb the intercostal arteries, superior mesenteric artery, celiac trunk, or renal arteries. The *ex vivo* length was then measured to obtain the axial stretch ratio ($L_{in\ vivo}$ /$L_{ex\ vivo}$). All intercostal arteries were tied off with nylon filament, fastening each at least 1 mm away from the surface of the aorta. Aortas were cannulated onto 200 μm diameter glass micropipettes in a vessel isolation chamber and stretched to the *in vivo* length. The cannulated aorta was continuously bathed with Dulbecco's Modified Eagle's Medium (Sigma-Aldrich, St. Louis, MO) with HEPES buffer at pH 7.4$\pm$ 0.05 containing 10 μM sodium nitroprusside and maintained at 37°C. After cannulation and 20 minutes of equilibration, mechanical testing via induction of transmural pressure was performed as described in Chapter 3.

4.3.2 Measurement of Aortic Opening Angle

The vasculature of euthanized mice was perfused with a 7% gelatin solution dissolved in PBS. After perfusion the aorta was exposed and cold PBS and ice chips poured over to fix the gelatin. Periadventitial fat and connective tissue was dissected away and the aorta removed. One millimeter thick rings were cut with a scalpel from the suprarenal and thoracic aortic regions. The rings were placed in cold PBS and bisected. After bisection the gelatin was removed and the ring equilibrated at room temperature for 30 minutes. Opening angle measurements were obtained from images acquired with a QImaging Micro Publisher 3.3 RTV camera attached to an Olympus SZ61 dissecting scope and analyzed with Image J software (NIH, Bethesda, MD).

4.3.3 Measurement of Total Aortic Collagen Content

Total aortic collagen per dry weight was measured by hydroxyproline (HP) assay as described by Woessner (75). Briefly, aortic tissue freed from fat was weighed, dehydrated in a speed vacuum for 2.5 hours and the dry weight recorded. The dry tissue was then homogenized and digested in 500 μL 0.25M sodium phosphate buffer with 0.0125g protease K/g wet weight. The homogenized tissue was hydrolyzed into amino acid components in 6N HCl at 120˚C for 14 hours. 50 μL of each sample and hydroxyproline standards were oxidized with Chloramine-T (Sigma, St. Lous, MO). Oxidation was terminated with perchloric acid solution. A colormetric reaction was performed with p-dimethylaminobenzaldehyde at 60˚C and the plate was read at 540 nm. Total collagen content per dry weight was calculated on the assumption that collagen is 13% hydroxyproline.

4.3.4 Gelatin Zymography

Aortic tissue was quickly dissected of fat and connective tissue and snap frozen in liquid nitrogen. The tissue was homogenized on ice in 120uL of buffer (50mM Tris-HCl, 150mM NaCl, 10mM CaCl2, 0.05% Brij35). The 10g supernatant was obtained after 10 minutes of centrifugation at 4˚C. Protein concentration was quantified via Bradford/Lowry protein assay run in parallel with a BSA standard curve. An MMP-2/MMP-9 positive control (Chemicon, Billerica, MA) was run in parallel with 15-19 μg of protein on a 10% acrylamide gel loaded with 1% gelatin under non-reducing conditions for 2 hours. Protein renaturing occurred during gel wash (2 times, 15 minutes each) in 2.5% Triton-X at room temperature followed by enzyme activation in 50mM Tris-HCl pH 7.6 (15mM NaCl, 10mM $CaCl_2$) for 30 minutes. The gel was then

transferred to fresh activation buffer and incubated at 37˚C for 14-16 hours. MMP activity was imaged as clear bands on a blue background after staining with 3% Commassie Blue. MMP activity was quantified by densitometry using the Gel Analysis toolbox in the NIH Image J software package. MMP-specific inhibition with 20mM EDTA added to the activation buffer confirmed the elastolytic specificity to MMP-2 and MMP-9.

4.3.5 Histological Analysis

After mechanical testing, aortic segments were bisected into suprarenal and thoracic sections and embedded in paraffin blocks for sectioning. Rings used for opening angle measurement were snap frozen in Optimal Cutting Temperature (OCT) medium. 5 μm sections were cut for either paraffin or OCT/frozen blocks with subsequent staining with Verhoff van Geison Elastic stain (Sigma-Aldrich, St. Louis, MO) or with Picro-sirius Red (76). Sections stained with picro-sirius red were imaged under plane polarized light to exploit the birefringence of sirius red stained collagen fibers. The birefringence is mostly conferred by alignment of collagen Type I fibers. Picro-sirius red stain under polarized light is an established method to measure the level of Types I and III collagen within the tissue section (76), wherein Type I appears red to orange and Type III appears green to yellow. Both paraffin and frozen sections were analyzed to count and measure elastin fragmentation, which was expressed as the number of elastin break per media area. Medial area was measured as the area in between the inner and outer elastic laminae. Medial and adventitial thickness was measured only in frozen sections of open aortic sectors. These samples were frozen in the zero-stress state and therefore provide

measurement of thickness unaffected by mechanical loading. Area and thickness measurements were made using Image J software (Bethesda, MD).

4.3.6 Gene expression analysis using quantitative real-time PCR

The relative expression of Col1a1, Col3a1, Col5a1. elastin, and fibronectin mRNA was determined by RT-PCR. RNA was extracted from snap frozen aortic tissue using the RNeasy mini kit (Qiagen, UK) according to protocol and quantified using a spectrophotometer at 260nm. cDNA was prepared from aortic RNA using Superscript II reverse transcriptase according to established protocol (Qaigen, UK). cDNA was purified using Qiagen PCR purification minispin columns. RT-PCR was performed using SYBR Green intercalating dye on a capillary Lightcycler (Roche Labs). All gene products were standardized against the housekeeping gene 18S (forward 5'-GAA CGT CTG CCC TAT CAA CT-'3 and reverse 5'-CCA AGA TCC AAC TAC GAG CT-'3). Oligonucleotide primers designed in IDT PrimerQuest software were fibronectin [forward (5'-GCC TCA ATC CAA ATG CCT CTA C-'3), reverse (5' GCC CAC AGT CAC AAC CTC TTC-'3)], collagen Type 5α1 [forward (5'-ATC AAG GTC TCC CAT GAT GGC TGT-'3), reverse (5'-TTC AGC TTC CTT CCC ACC TCA CAA-'3)], and elastin [forward (5'-TAA AGC AGC CAA GTA TGG TGC TGG-'3), reverse (5'-TTA GCA GCC TTA GCA GCA GCC TTT -'3)]. Fifteen μL total volume reaction mixtures included 2.5 mM $MgCl^{+2}$, 0.2 mM dNTP, 0.47μM (each) primer, and 0.07 U/ml platinum *Taq* DNA polymerase. Oligonucleotide primers for procollagenα1(I) and procollagenα1(III) were purchased from Qaigen (Quantitect Primer Assays, Qaigen, UK), run according the QuantiTect SYBR Green 2-step RT–PCR kit protocol, and the product size was verified on an agarose gel. Standards for each gene product were made

by amplifying the product and calculating the copy number based on the concentration and amplicon length. Transcript concentration in the template cDNA was quantified against a linear standard curve.

4.3.7 Statistical Analysis

All data are presented as Mean ± SD. Statistical analyses were performed using GraphPad™ Prism software. The pressure-diameter data were analyzed by ANOVA to examine the effect of mouse strain on aortic compliance and Bonferonni post tests were used for post hoc analyses. All other analyzes between groups was performed with Mann-Whitney test. $P<0.05$ was considered significant.

4.4 Results

4.4.1 Circumferential mechanical behavior of aortas from SMC-Cat mice is altered from WT

To determine whether protection from aneurysm formation is attributable to endogenous differences in aortic mechanical responses, aortas from WT and SMC-Cat mice were isolated in a vessel chamber and inflated for measurement of the aortic diameter response under applied transmural pressure. Vessels were extended to their *in vivo* length during inflation and thus the *in vivo* pre-stretch was measured upon excision. SMC-Cat aorta demonstrated reduced *in vivo* pre-stretch compared to WT (Figure 4.4.1) providing immediate evidence of an altered axial environment (either in tension or material composition) between the groups. The *ex vivo* stretch was adjusted accordingly.

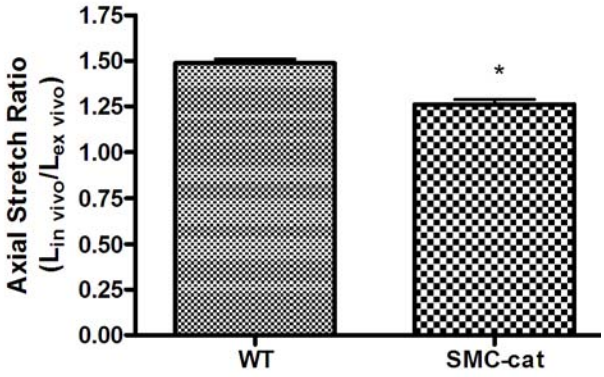

Figure 4.4.1. *In vivo* pre-stretch, or axial stretch ratio, of WT and SMC-Cat aorta. Upon excision, aortic length decreased in both groups. WT aorta shortened 20% more then SMC-Cat aorta. (*P<0.05; WT n=10, SMC-Cat n=6, Mann-Whitney test).

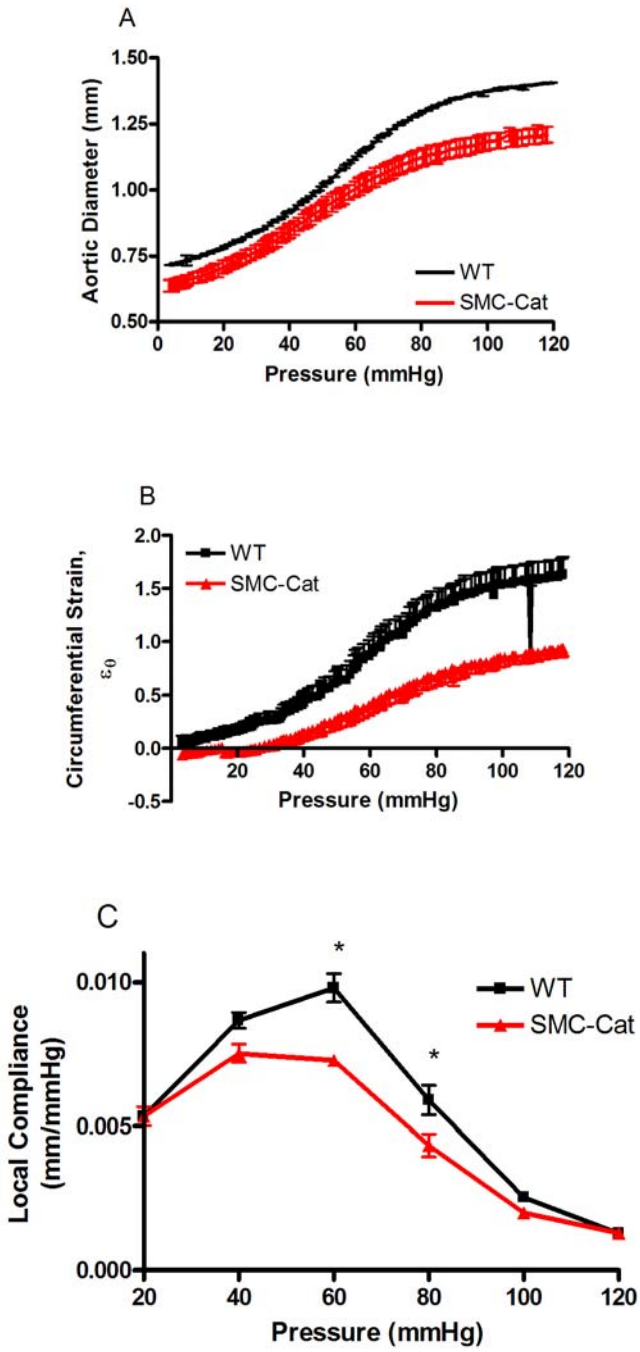

Figure 4.4.2. Mechanical behavior of WT versus SMC-Cat aortas at baseline. A) Pressure versus diameter and B) Pressure versus Circumferential strain, $\varepsilon_\theta = (\lambda_\theta^2 - 1)/2$, where $\lambda_\theta^2 = D/D_o$, response demonstrating bisphasic behavior, including limited diameter increase at low pressure, a linear increasing response at midrange pressure, and a diameter plateau at high pressure. SMC-Cat aorta are smaller in diameter at all pressures than WT. B) Local compliance versus pressure behavior of WT versus SMC-Cat. Both groups demonstrate bell-shaped behavior and significantly diverge in compliance between 60 and 80 mmHg (*P<0.05, WT n=5 for P-D curve, WT n=3 for P- ε_θ curve, SMC-Cat n=5, ANOVA and Bonferroni's posthoc analysis).

The P-D data (Figure 4.4.2A) and pressure versus circumferential strain (P-ε_θ) data (Figure 4.4.2B) of both groups exhibited biphasic behavior, which demonstrated reduced expansion at low pressure and stiffening at high pressure. The significant downward shift of the SMC-Cat P-D and *P*-ε_θ curve from WT indicated that SMC-Cat aorta were smaller in diameter than WT. The marked feature at low physiologic blood pressure near 60-70 mmHg was the sharp increase in WT diameter response to pressure compared to SMC-Cat. Conversion of the P-D data into pressure-dependent compliance confirmed that this difference in slope represented a true difference in the circumferential response of the SMC-Cat group compared to WT at *in vivo* stretch (Figure 4.4.2C). This interpretation of the data exhibited bell-shaped behavior with maximum compliance at mid-range pressures and minimum compliance at low and high pressure. The maximum pressure limit in our system was 120mmHg. Peak compliance magnitudes at 60 mmHg and 80 mmHg in the SMC-Cat group were significantly reduced from WT (10±1.0 versus 7.0±0.50 mm/mmHg and 6.0±1.0 versus 4.0±0.9 mm/mmHg, respectively; $P<0.05$), while at 120mmHg compliance in both groups decreased to the same minimum (1.2±0.17 mm/mmHg in SMC-Cat and 1.2±0.33 mm/mmHg in WT; P=NS). Therefore, aortic compliance in the physiological range, taken as pulse pressure of 40mmHg, was significantly reduced in the SMC-Cat group (2.25±0.27 mm/mmHg versus 2.92±0.45 mm/mmHg in WT; $P<0.05$). Thus, as measured by fixed extension aortic inflation, physiologic circumferential behavior of SMC-Cat aorta indicates that these aortas are significantly less distensible than WT and may impart mechanical protection against aneurysm development. Further interpretation of these data subsequently included evaluation of the material composition of the aortas in both groups.

4.4.2 Collagen content is greater in SMC-Cat aorta compared to WT

Motivated by the significant *in vivo* axial pre-stretch and circumferential mechanical differences between the two groups, measurement of total aortic collagen content was performed to examine the matrix material composition of the aortic wall in each group. Total collagen content per dry weight of aorta (Figure 4.4.3A) was quantitatively determined via HP assay of hydrolyzed aortic homogenates. Collagen content in the SMC-Cat group was increased by 1.5 fold over the WT group indicating an endogenous increase in collagen density in the SMC-Cat aortic wall compared to WT. These results suggest that the differences detected in circumferential mechanics may be directed by preferential collagen accumulation within the aortic wall of the SMC-Cat aortas over that of WT. Indeed Picro-Sirius Red staining imaged under polarized light (Figure 4.4.3B) confirmed an increase in Type I collagen fiber abundance in the SMC-Cat group. Collagen deposition in the WT aortic cross sections revealed increased green illumination indicating abundance of smaller Type III collagen fibrils in the WT adventitia. Thus the increase in collagen in the SMC-Cat aorta as detected by HP content/dry weight appeared to be isolated to the adventitial tunica. This specific accumulation of Type I collagen suggests 1) that the matrix environment of the adventitia partially directs the aortic mechanical response, at least at early time points before angII infusion and 2) that abundant adventitial collagen and the associated decrease in physiologic compliance (Figure 4.4.2C) impart protection against aneurysmal dilation.

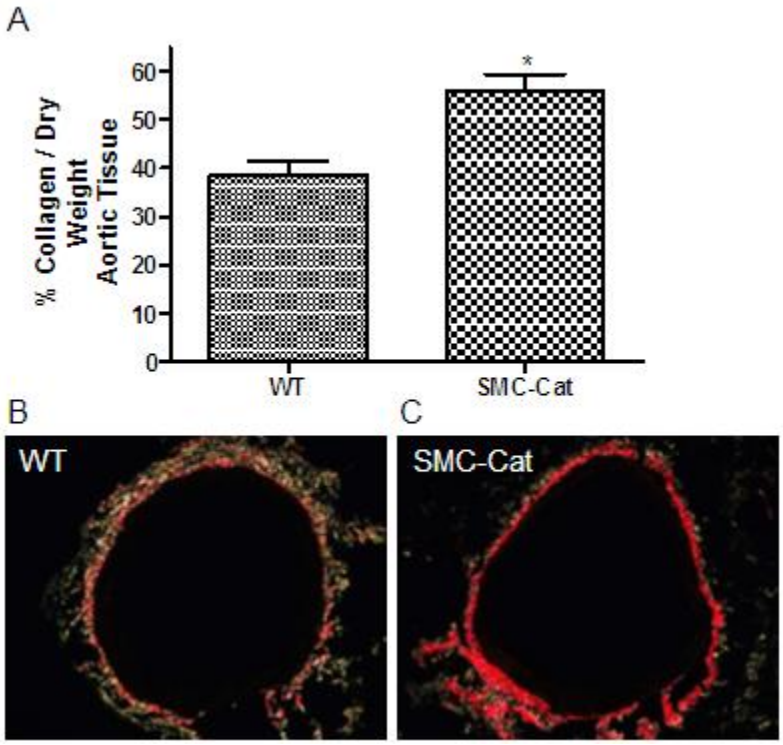

Figure 4.4.3. A) Total collagen content per aortic dry weight is increased by 41% in SMC-Cat (n=3) compared to WT (n=5); *=P<0.05. B) Aortic wall stained with Picro Sirius Red and imaged under polarized light. Only the collagenous adventitia is detected. WT image shows red and green illumination indicating presence of respective Type I and Type III collagen. SMC-Cat image shows intense red illumination indicating abundant Type I collagen presence.

4.4.3 Catalase mediated H_2O_2 scavenging blunts increases in aortic ring opening angle compared to WT

Thus far we have investigated only the baseline mechanical differences of WT and SMC-Cat aorta. To determine if catalase-mediated scavenging of VSMC-produced H_2O_2 imparts protection against aneurysmal growth by modulating vessel remodeling during disease progression, SMC-Cat and WT animals were treated with angII and HF diet for 7 days. This time point captures the earliest stages of aneurysm formation and was expected to illuminate whether early AAA mechanics are dominated by medial or adventitial remodeling. Moreover, H_2O_2 scavenging by catalase is activated in this model only in the setting of angII and HF diet (42). Assay for total collagen content in these

groups demonstrated a reduction of total collagen content in both angII stimulated groups to the same minimum (Figure 4.4.4). This result indicated that the abundant collagen in the SMC-Cat aorta underwent rapid angII-mediated proteolysis by the 7 day time point.

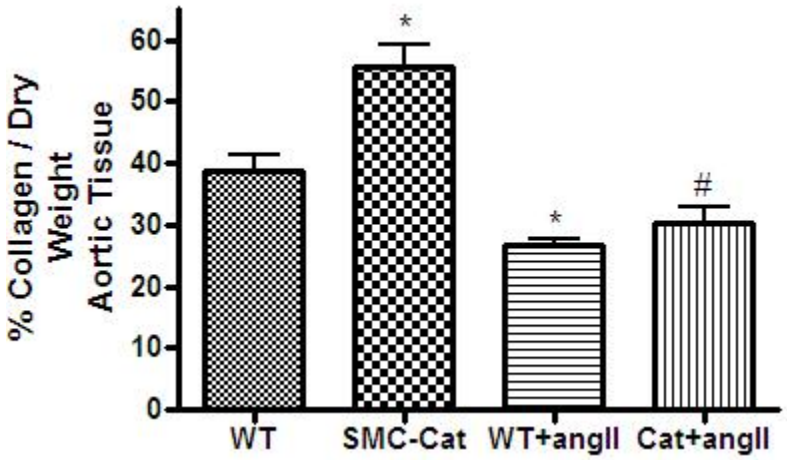

Figure 4.4.4. Total collagen content per aortic dry weight is increased by 41% in SMC-Cat (n=3) compared to WT (n=5). Total collagen is reduced in WT+angII (n=5) by 31% compared to WT. Collagen content in SMC-Cat+angII (n=3) is reduced from SMC-Cat by 46% (*=P<0.05 compared to WT. #=P=0.1 compared to SMC-Cat).

Aortic rings isolated from the suprarenal and thoracic segments were bisected to quantify circumferential residual strain on the inner and outer aortic wall. Representative images of acute and obtuse opening angles are shown in Figure 4.4.5A and B. Both SMC-Cat and WT rings exhibited acute angles at baseline, which agreed with published residual strain characterization in apoE$^{-/-}$ mice (72). These authors studied the effect of ageing on spatial aortic remodeling observing conserved acute opening angle in the suprarenal aorta as late as 56 weeks of age. Our data, however, demonstrated that in the setting of angII, WT opening angle in the suprarenal region increased dramatically (Figure 4.4.5C) with some rings inverting to angles greater than 180˚. Similar differences were not detected in thoracic WT aorta or in either location in SMC-Cat (Figure 4.4.5D). Thus our results suggest that angII-mediated vascular hypertrophy promotes increased aortic opening angles specifically in the suprarenal region. Residual stress gradients

across the aorta, as manifest by an altered ratio of compressive inner strain to tensile outer strain, are therefore assumed to be a causal mechanical parameter that precipitates in aneurysm development. Most interesting, our results show that reducing H_2O_2 production in the vascular media blunts this suprarenal opening angle increase, imparting a mechanical advantage in circumferential stress gradients that inhibits AAA formation. Whether these protective mechanics were directed by medial or adventitial remodeling was subsequently addressed.

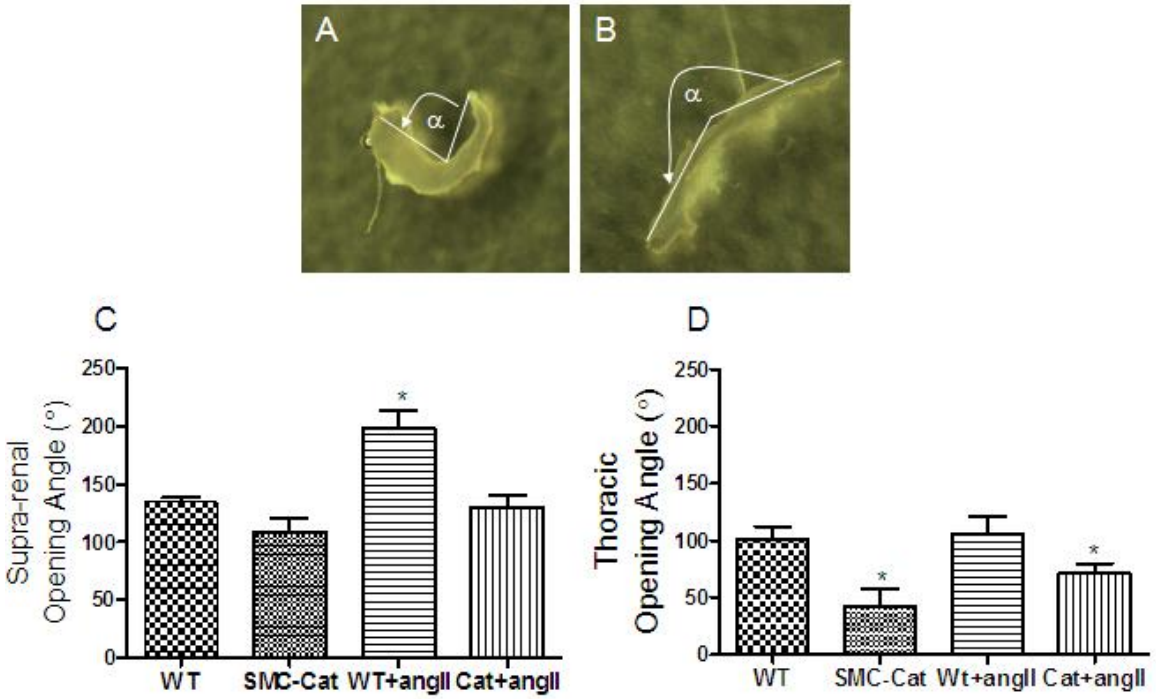

Figure 4.4.5. Representative images of A) acute opening angles and B) obtuse opening angles. C) Opening angle is specifically increased by 35% in the suprarenal region in aortic rings from WT mice treated with angII and HF diet. D) Opening angle of rings from the thoracic aorta is not significantly changed in any group. WT+angII opening angle in the suprarenal and thoracic region varies significantly (suprarenal 198±32.0 versus thoracic 105±38.1). n WT=5, n SMC-Cat=3, n WT+angII= 6, n Cat+angII=3, *P<0.05 compared to WT, Mann-Whitney test).

4.4.4 Integrity of media directs mechanical changes toward aneurysm formation

To determine if angII-mediated remodeling 1) is directed by the media or adventitia and/or 2) affects matrix reapportioning within the aortic wall, the overall

thickness of the media and adventitia were measured at baseline and after 7 days treatment with angII and HF diet. Medial hypertrophy was not apparent in any group, although the media remained thicker than the adventitia in all instances (Figure 4.4.6A). WT adventitial thickness was also unaffected by angII treatment (Figure 4.4.6B). As expected based on calculation of collagen/dry weight and Picro Sirius staining, SMC-Cat adventitia thickness was significantly greater than WT (44.8±14.7μm versus WT 31.0±9.55 μm; $P<0.05$) and showed a decreasing trend in the SMC-Cat +angII group (44.8±14.7 μm versus 33.2±7.3 μm; $P<0.06$). The behavior of the groups after angII treatment correlated with the data obtained in the above experiments to quantify total collagen content. There was increased total collagen content in the SMC-Cat group at baseline confounded with decreased total collagen after angII treatment. In addition the results demonstrate a lack of appreciable medial or adventitial material loss in WT at either baseline or 7 days angII treatment. This suggests an alternative mechanism other than reapportionment of aortic material density as the matrix-linked inducer of circumferential mechanical changes.

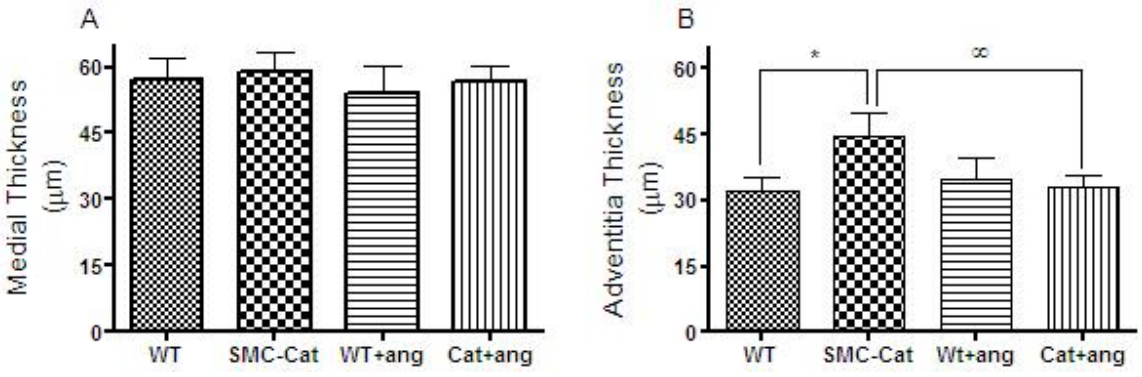

Figure 4.4.6. Thickness of aortic A) media and B) adventitia. Media thickness is not affected by angII treatment in WT SMC-Cat. SMC-Cat adventitia is 32% greater than WT; *$P<0.05$. AngII treatment promoted a decreasing trend in adventitial thickness in SMC-Cat; ∞$P<0.06$.

To determine whether the integrity of the media, rather than the density or thickness may direct angII-mediated mechanics, the number of elastin breaks per medial area was measured. WT aorta demonstrated a significant difference between the number of elastin breaks in the suprarenal and thoracic regions at baseline (Figure 4.4.7 A and B, 86 ±33 breaks/mm^2 versus 36±25 breaks/mm^2, respectively; $P<0.05$) and after angII treatment (133 ±105 breaks/mm^2 versus 37±21 breaks/mm^2, respectively; $P<0.05$). No marked spatial difference was detected in SMC-Cat. The striking finding in this analysis was that medial H_2O_2 scavenging significantly blunted the marked increase in elastin degradation observed in the WT+angII group. Thus, these data suggest that the connectivity and integrity of the elastic laminae within the media direct the spatial mechanics of the WT aorta. Furthermore, mitigation of H_2O_2 levels in the media prevents elastin degradation and blunts the mechanical propensity toward aneurysm.

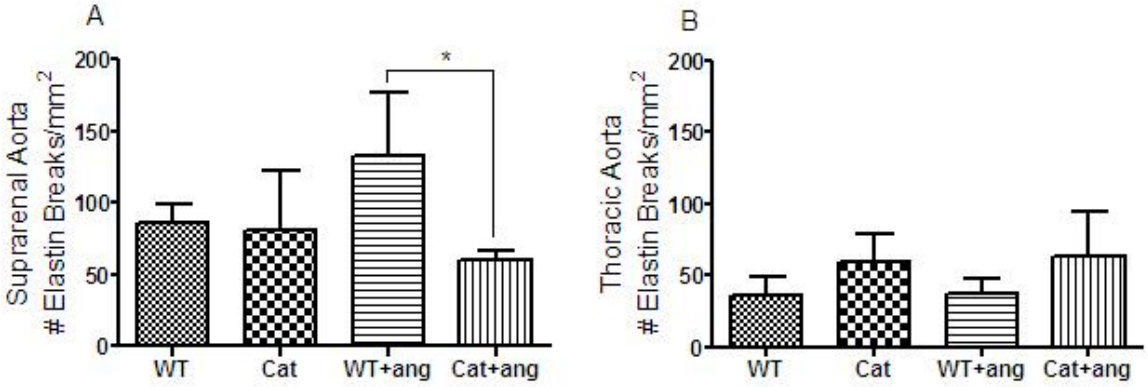

Figure 4.4.7. Elastin fragmentation within the suprarenal and thoracic aorta. Elastin fragmentation is expressed as the number of breaks in elastic laminae per medial area. Media area was calculated as the area enclosed by the inner and outer elastic laminae. A) Treatment with angII (ang) for 7 days induced elastin fragmentation in the WT suprarenal aorta that was significantly increased above the level of SMC-Cat. B) No difference in elastin fragmentation was detected in the thoracic aorta in any group (*$P<0.05$, WT n=6, SMC-Cat n=3, WT+angII n= 5, SMC-Cat+angII n=3, Mann-Whitney test).

4.4.5 Medial H_2O_2 scavenging-associated stabilization of aortic mechanics is associated with collagen gene transcription

To further investigate mechanisms by which H_2O_2 scavenging may alter angII-associated mechanical changes in this model, we analyzed expression of several specific matrix genes, specifically targeting the expression profiles of Col1a1, Col3a1, Col5a3, elastin, and fibronectin. These gene products were selectively targeted since Types I and III collagen dominate in the aortic wall (77). Type I collagen is found primarily in the adventitia and is secreted by fibroblasts (77). Type III collagen is associated with the medial layer and is the predominate collagen secreted by smooth muscle cells (78). Type V collagen plays a role in fibrillogenesis by incorporating into (79) and regulating the diameter (80) of Type I collagen fibrils. All groups within this gene expression analysis included a small sample number, n=3, due to small breeding numbers of SMC-Cat transgenic mice. Therefore even when large trends were detected among groups statistical significance did not exceed P=0.1. AngII stimulation failed to augment expression of proα1(III) collagen mRNA in WT or SMC-Cat aorta (Figure 4.4.B). Since type III collagen is associated with the medial layer (81) the result excludes type III collagen as a matrix protein regulated by angII. Within our investigation proα1(V) collagen mRNA was unchanged between WT and SMC-Cat, but showed a marked decreased upon WT stimulation with angII (Figure 4.4.8C). Catalase mitigation of VSMC H_2O_2 levels blunted significant reduction of proα1(V) collagen mRNA. Since proα1(V) collagen mRNA was downregulated upon angII treatment in WT, downregulation of proα1(I) collagen mRNA in this group was expected (Figure 4.4.8A). At baseline WT Type I expression was over 2-fold that of the SMC-Cat group. At 7 days

following angII and HF diet, WT expression decreased by half, while SMC-Cat expression increased over 2-fold to meet the level of baseline WT. This result indicated that angII-stimulation blunted Type I collagen production in WT, but effectively turned on *Col1a1* transcription machinery in the SMC-Cat aorta. It is speculated that the angII-mediated decrease in SMC-Cat collagen content detected at 7days by HP assay and morphologic analysis may be transient, and that later time points may reveal increased adventitial collagen in this group toward the abundant baseline SMC-Cat levels. Because Type I collagen is the main component of the adventitia, the data indicate that H_2O_2 scavenging augments adventitial associated ECM remodeling. In addition the analysis showed elastin mRNA was significantly reduced at baseline in SMC-Cat aorta, but was not significantly changed by angII in either group (Figure 4.4.8D). Fibronectin mRNA decreased comparably in both groups upon treatment with angII (Figure 4.4.8E), suggesting the elastin and fibronectin mRNA do not significant contribute to H_2O_2-induced ECM alteration at 7 days post angII infusion. Thus, in angII-mediated remodeling two main factors, 1) medial elastin integrity and 2) adventitial Type I collagen modulation, synergistically control circumferential wall mechanics.

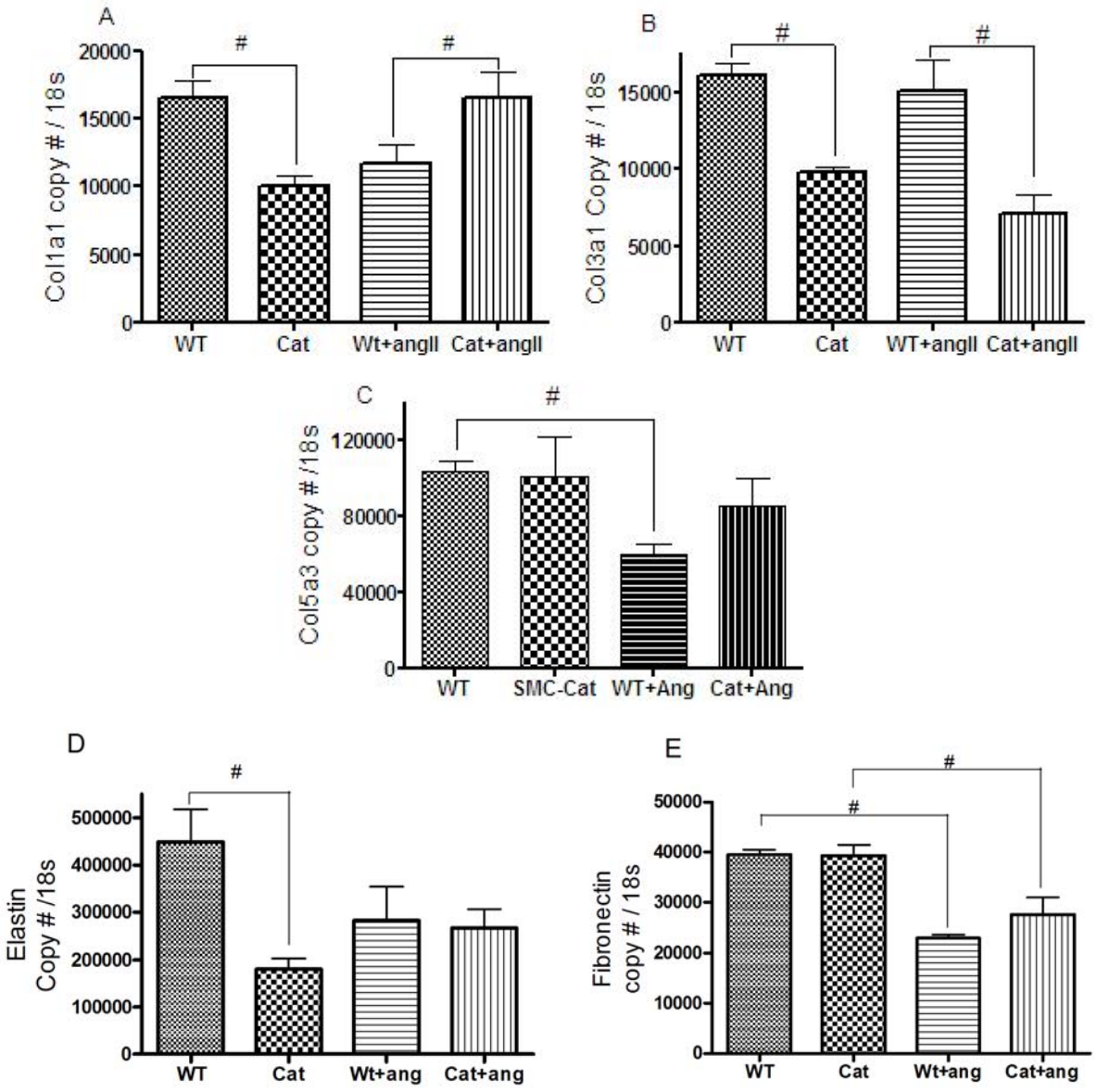

Figure 4.4.8. Quantitative RT-PCR measurement of A) *Col1a1*, B) *Col3a1*, C) *Col5a3, D) Eln, and C) Fbn* mRNA expression in WT, SMC-Cat, WT+angII, and SMC-Cat+angII treatment groups. Col1a1 expression is downregulated from baseline by angII in WT and upregulated by angII in SMC-Cat. Col3a1 is downregulated by angII treatment in both groups. Co5a3 expression is downregulated by angII in WT. Baseline elastin expression was downregulated by angII in WT and unchanged by angII in SMC-Cat. Fibronectin was downregulated by angII in both WT and SMC-Cat. (#P=0.1, n=3 in all groups, angII treatment for 7days, Mann-Whitney test).

4.4.6 MMP-9 activity is blunted in the aortas of SMC-Cat mice treated with angII and HF diet for 7 days

To determine if blunted elastolytic capacity was a plausible mechanistic link between increased elastin degradation and angII-mediated mechanics MMP-2/9 activity was measured. SMC-Cat and WT animals were treated with angII and HF diet for 7 days and the aortas were assayed for MMP-2/9 activity using gelatin zymography. No significant differences in proMMP-2 activity were observed between the groups at baseline and MMP-9 activity was absent (Figure 4.4.9A, B). MMP-2 activity was increased over WT in both groups after angII treatment (Figure 4.4.9C) and MMP-9 activity in WT+angII was detected at 4.5 times the level of SMC-Cat +angII (4.5±2.0 WT+angII versus Cat+angII, Figure 4.4.9D). These data suggest that angII-mediated upregulation of MMP-9 in the aorta of WT mice promoted elastolysis of the elastic laminae, which induced matrix and mechanical changes associated with early aneurysm formation. Moreover, the results demonstrated that H_2O_2 scavenging inhibits activation of MMP-2 and blunts activity of MMP-9 to conserve elastin integrity.

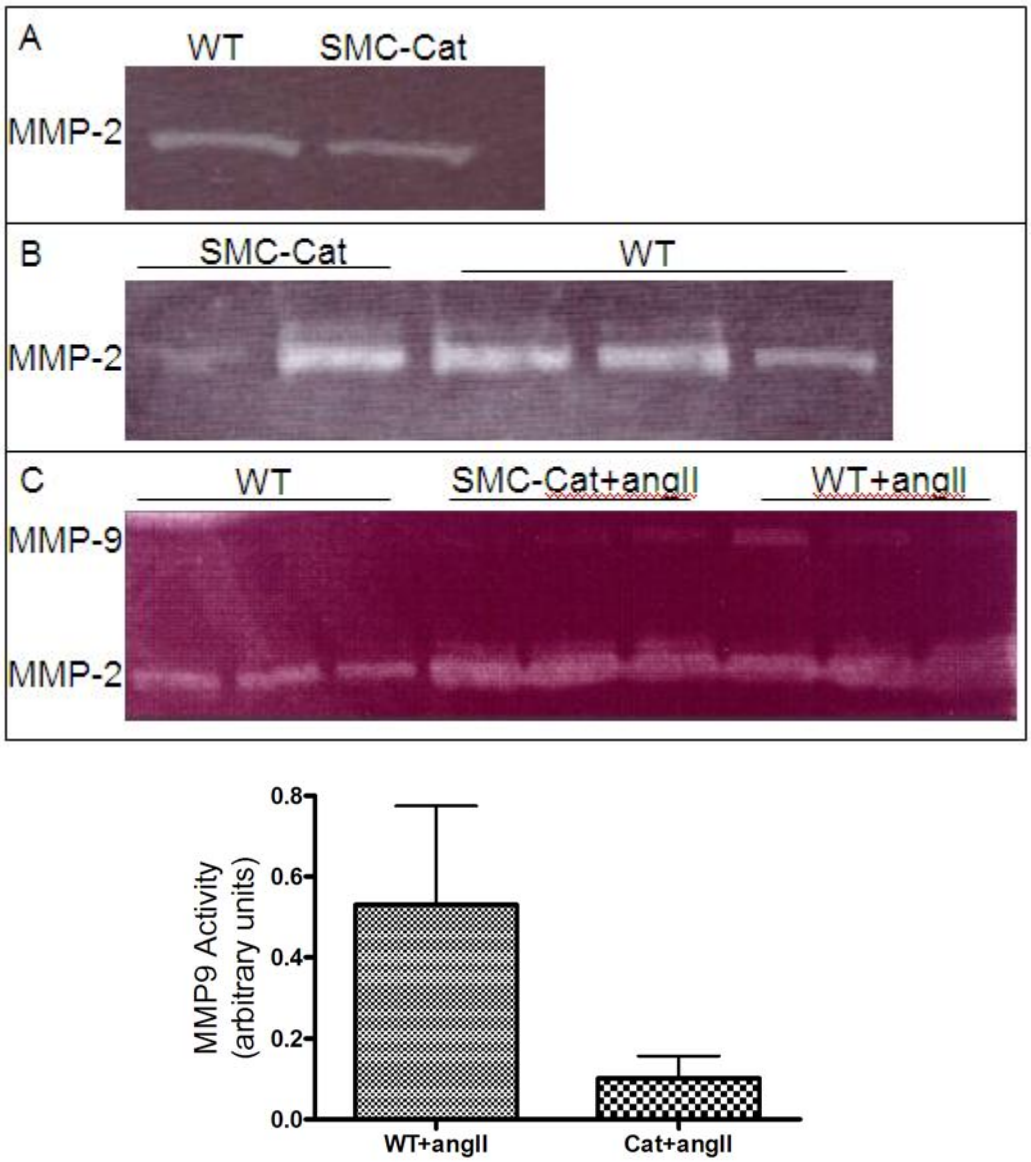

Figure 4.4.9. Representative blots of MMP-2 and -9 proteolytic activities within a gelatin impregnated 10% acrylamide gel. A,B) Aortic homogenates from WT and SMC-Cat groups demonstrate comparable MMP-2 activity and no MMP-9 activity. C) AngII stimulation of WT and SMC-Cat mice induced an upregulation of MMP-2 activity over WT. D) MMP-9 activity was upregulated in 3 out of 6 mice treated with angII and in 3 out of 3 SMC-Cat mice treated with angII. Those WT mice expressing MMP-9 had a 4.5 fold increase over MMP-9 activity in Cat+angII.

4.5 Discussion

In this study, we utilized an existing strain of transgenic mice that overexpressed catalase specifically in VSMCs. The working hypothesis for this study was that oxidative stress generated by H_2O_2 directs matrix remodeling, therefore is a molecular mediator of biomechanical remodeling involved in AAA formation. To test this hypothesis we measured both pressure versus diameter behavior and spatial residual strain, as well as characterized morphology and matrix changes in the aortas of our transgenic model in the setting of angII. Overall, the studies presented here demonstrate that oxidative stress ultimately alters mechanical behavior by affecting the composition of the aortic wall via mechanisms of matrix gene transcription and elastic laminae degradation. Specifically demonstrated are:

1) aortic matrix composition directs physiologic circumferential behavior
2) upregulation of the antioxidant catalase promotes increased collagen content at baseline and increased collagen transcription during angII-mediated pathology, and
3) elastin integrity within the tunica media protects against aneurysm formation.

Increased adventitial collagen is the phenotypic hallmark of the SMC-Cat aorta. Abundant collagen in the thickened adventitia augmented the diastolic behavior of the aorta compared to WT. The interesting question to pose within our study of the interplay between matrix composition, cell biology, and mechanics is whether altered diastolic behavior induced a thickened adventitia, or whether a thickened adventitia induced altered diastolic behavior. Our previous work in Chapter 3 indicated that in the setting of aneurysm development the molecular mediators arrive first and the mechanical result

second. However, in this model of catalase overexpression molecular and mechanical events evolved simultaneously throughout development and growth, making assignment of clear priority impossible.

Increased collagen in the SMC-Cat aorta at baseline could possibly be attributed to collagen production in embryonic or post natal development triggered by insertion of the human catalase gene. As previously demonstrated in this transgenic model, H_2O_2 levels are only reduced compared to WT upon stimulation with angII even though baseline catalase activity is elevated above WT (42). A possible mechanism for embryonic or post natal accumulation of adventitial collagen that is independent of H_2O_2 may be conferred by NF-Y, the transcription promoter of proα1(V) collagen mRNA. NF-Y has been detected at very high levels in vitro in H_2O_2-resistant cells that demonstrated abundant catalase activity (82). Therefore increased catalase expression in SMC-Cat may affect an increase in the NF-Y transcriptional binding factor to augment Type V and subsequently Type I collagen production preferentially within the aortic wall.

Our studies showed that angII treatment of SMC-Cat mice turned on Type I collagen transcription machinery compared to WT, blunted Type III in the same manner at WT, and conserved Type V expression over that of WT. Since VSMCs predominately synthesize Type III collagen (78) and fibroblasts predominately secrete Type I collagen (77), we speculate that fibroblast function is augmented in SMC-Cat aorta to secrete excess collagen at baseline and to compensate for degraded collagen at the expression level in the setting of catalase-induced H_2O_2 scavenging. This speculation is based on the fact that H_2O_2 in the aortic wall is freely diffusible and as such catalase activity could

have also reduced H_2O_2 levels in the adventitia, thereby affecting the oxidative environment of all vascular cells.

Previous studies in this same model (42) demonstrated that aorta from WT mice showed significant angII-mediated vascular hypertrophy after 14 days, an event which was blunted in the SMC-Cat mice. We did not observe this hypertrophic effect in the WT group by 7 days suggesting 1) a time course for normal angII-mediated vascular hypertrophy and 2) that H_2O_2 scavenging-induced alterations in collagen degradation and transcription may be temporally activated and mitigated as well. At the early time point investigated we cannot speculate that increased transcription of Type I collagen actually yielded a translated protein, nor can we validate that fibroblasts effectively compensated for lost collagen. Indeed to conclude that a catalase-mediated compensatory mechanism of collagen recovery exists we need to investigate the later time points for changes in aortic adventitial thickness and collagen content.

Particularly importantly for the purpose of this work, our data directly support the link between degradation of the medial elastic laminae and the potential for aneurysm formation. Residual stress gradients exist to effectively achieve equal stress distribution throughout the wall thickness during physiologic pressure loading. Increasing opening angle is canonically indicative of preferential growth in the vessel interior inducing increased inner compressive forces (83). The converse has been demonstrated by Greenwald *et al* (84) in which enzymatic degradation of medial elastin and collagen affected an opening angle decrease. In light of these hallmark experiments, detection of increased elastin degradation in our WT model should have achieved the same fate. However, this was not the case and opening angle increased dramatically. Moreover, in

the same paper Greenwald *et al* demonstrated that mechanically removing adventitial material in the presence of intact media did not affect any change in opening angle, preventing postulation that adventitial thinning induced the large opening angles observed. Perhaps the critical difference between previous characterization and that presented here is that in our model degraded elastin fibers remained embedded with a collagenous matrix, which may have increased the compressive stress within the media, therefore altering the balance between tensile force in the outer wall and compressive force in the inner wall. If the ratio of compressive stress to tensile stress was altered by angII-mediated elastin degradation to favor medial compression, release of the wall tension by aortic ring bisection would result in the obtuse opening angles observed. To describe this apparent discrepancy we consider the propensity of the unloaded elastic media to remain an open cylindrical tube even when the adventitia is surgically removed (85). This behavior suggests that tensile forces must exist within the media, at least in the unloaded configuration, to maintain an open lumen. We suggest that elastic laminae degradation may reduce this tensile force and perhaps even switch the polarity toward compressive forces that would generate the large opening angles seen in our studies.

Recently the heterogeneous distribution of proteoglycan (PG) within the aortic wall and their role in residual stress development has been investigated (86). Safranin O staining of rat aorta for proteoglycan showed concentration within the aortic intima and media and absence within the adventitia. When bisected rat aortic rings were placed in solutions of varying osmolarity, water adsorption to PGs induced differential osmotic pressure and swelling stress within the aortic wall that resulted in changes in opening angle. Hypotonic solutions induced opening angle increases implying based on our

discussion above that greater PG density in the media may promote generation of compressive forces. The link between PG content and opening angle is supported by combining the observations that biglycan, one of the most abundant vascular ECM PGs, is upregulated in the intimal wall of early and advanced atherosclerotic lesions (87) and that aortic rings containing atheromas exhibit larger opening angles compared to autologous non-atherosclerotic regions (88). While aneurysmal tissue on the other hand has a deficit of biglycan (89), our studies showing the increased opening angle in aortic rings from mice treated with angII for 7 days suggests an abundance of medial PGs in the early aneurysmal aorta.

It is well established that maintenance of arterial homeostatic mechanics induces differential response patterns throughout the vasculature. Likewise residual stress and strain vary in magnitude in the vasculature, from the aortic arch to the proximal femoral arteries (66, 72), as well as in the coronary arteries (88). These regional differences in mechanics alter the structural organization of the vessel and change the biomechanical response to hemodynamic forces (or vice versa). Preferential localization of disease, i.e. atherosclerosis at branch points and vessel osteum and aneurysm in the human infrarenal aorta, is a manifestation of these altered mechanics. Elastin and collagens have predominately been investigated as the important growth and remodeling-associated matrix proteins conferring such spatial distribution of the mechanical response. Indeed elastin and collagen have been the focus of the studies presented here. However, in light of recent data on the effects of osmotic pressure on arterial mechanical behavior (90, 91), spatial analysis of PG composition warrants equal attention and future directions for this project will include staining of aortic rings for PG content.

Increased ROS-mediated MMP activity has been conferred in other settings as discussed in Chapter 2 and therefore modulation of MMP activity in the SMC-Cat mice was expected. Interestingly the aorta of rats pretreated with tamoxifen in the setting of the elastase perfusion model of AAA formation showed 5-fold increase in catalase mRNA at 7 days and 8-fold increase in catalase protein localized in VSMCs at 14 days (34). Aortic diameters at 14 days were 50% smaller in the tamoxifen treated groups compared to control. The authors also demonstrated that MMP-9 activity was 2.4 times higher in the non-tamoxifen treated group. This is the only publication to our knowledge that has demonstrated AAA modulation mediated by catalase-induced decreases in MMP-9 activity. Although the authors did not investigate elastin fragmentation directly, based on the established effect of the elastase infusion model of AAA to directly degrade the elastic laminae, we can assume that mitigation of AAA dilation was produced by similar mechanisms as those describe in our study. Namely, increased H_2O_2 scavenging blunts normal redox sensitive transcription of MMP-9 and its subsequent activation, thereby preventing degradation of the elastic laminae, and preventing AAA formation.

In summary, we have shown that fragmentation of the elastic laminae is a causal event in angII-mediated augmentation of aortic mechanics. This result was demonstrated by means of a transgenic mouse model that has VSMC-specific catalase overexpression, which allowed us to target H_2O_2-mediated events in the setting of angII treatment. The combination of robustly altered matrix gene transcription and the complete absence of aneurysm incidence in all SMC-Cat treatment groups strongly suggest that VSMC-generated H_2O_2 is a pivotal molecular signal which induces aneurysm formation by regulating the matrix environment. The data provide critical linking

mechanisms between aortic composition, molecular events, and mechanical behavior. Interpretation of these early events in AAA pathogenesis is crucial to move toward detection and prevention of the disease.

CHAPTER 5

THE ADVENTITIA AS AN IMPORTANT LOAD BEARING CONSTITUENT OF THE ARTERIAL WALL

5.1 Introduction

Abdominal aortic aneurysms (AAA) are characterized in part by an inflammatory response in the aortic wall that includes dramatic growth and remodeling of the adventitia (44). Hallmarks of aneurysm pathology are degradation of elastin and deposition of collagen that displace the vessel from the homeostatic state and force it into the deleterious cycle of expansion. Collagen exhibits preferential turnover compared to elastin with a reported half life of as few as 3 and as many as 90 days (92, 93). Although elastin has greater longevity (12, 94), degradation of the elastic lamina is clearly linked to the manifestation of aortic dilation as shown in our work in Chapters 3and 4, as well as in the literature (12, 18). Indeed, targeting the elastic laminae via elastase infusion of the infrarenal aorta is an established model of reproducible AAA formation (46). The mechanical contribution of the adventitia, however, has not been demonstrated. Histological analysis of the "pre-aneurysm" in the accelerated (angII/βAPN/HF) and angII/HF models of AAA demonstrated that adventitial collagen may not play a major role in the initial remodeling response. However, the adventitia clearly appears as a significant matrix contributor to both small aortic dilatations and established aneurysms. Recent studies have shown that the tunica adventitia has a potentially important role in many aspects of vascular pathology via an "outside-in" mechanism of disease progression (73). The adventitia functions as a trafficking route for cellular infiltration to initiate inflammatory cascades, as well as a source of paracrine and humoral factors.

Therefore, the adventitia may be considered a temporally-dependent component to arterial remodeling and aneurysmal growth, and study of the natural history of AAA pathogenesis should include evaluation of the mechanical adaptation mediated by collagen-associated remodeling.

The individual mechanical properties of the arterial media and adventitia were first investigated in the 1980s (95). The major challenge of characterizing the composite mechanical properties of the aorta in the murine model is difficulty resolving the independent contributions of the adventitia and media in such small (diameter~1mm) vessels. To date the most accepted models of arterial mechanics are two-layer models which include contributions of the media and adventitia (96). Motivated by increasing interest in the functional relevance of the adventitia to cardiovascular disease, we hypothesize that effectively "knocking-out" the contribution of the adventitia in a control aorta modulates the mechanical behavior of the aorta. Our objective is to experimentally determine the passive mechanical response of the adventitia and media independently. We have employed an approach that allows subtractive evaluation of the mechanical contribution of the adventitia to the composite behavior of the aorta by "unshielding" the tunica media of its adventitial reinforcement.

5.2 Methods

5.2.1 Animals and Reagents

Male apolipoprotein E deficient ($apoE^{-/-}$) mice were bred in Emory University Department of Animal Research Facilities and allowed to age to 15-17 weeks for experiments. Mice were allowed free access to standard chow and water. All protocols were approved by the Institutional Care and Use Committee at Emory University. At the

time of experiment, animals were euthanized via carbon dioxide asphyxiation followed by perfusion and/or fixation methods. Dulbecco's Modified Eagles Medium without phenol red , HEPES buffer, sodium nitroprusside, HBSS without Mg^{2+} and Ca^{2+}, and phenylephrine hydrochloride were purchased from Sigma-Aldrich (St. Louis, MO). Collagenase Type 1 was purchased from Worthington (Lakewood, NJ).

5.2.2 Evaluation of circumferential mechanics by isolated vessel mechanical testing

After euthanasia, the thoracic cavity was opened and the vasculature perfused with 10mL of 0.9% saline via left ventricular puncture. Prior to dissection, the *in vivo* length of the aorta between the proximal thoracic to just above the iliac bifurcation was measured with digital calipers. The aorta was then excised and cleaned of loose connective tissue taking care not to disturb the intercostal arteries, superior mesenteric artery, celiac trunk, or renal arteries. All arteries were tied off with nylon filament, fastening each at least 1 mm away from the surface of the aorta. Aortas were cannulated with 200 μm diameter glass micropipettes in a vessel isolation chamber and stretched to the *in vivo* length. The cannulated aorta was continuously bathed with Dulbecco's Modified Eagle's Medium, pH 7.4, including 9mM HEPES and 10 μM sodium nitroprusside to prevent active contraction. The perfusate was maintained and delivered at 37°C. The vessel isolation chamber was mounted on the stage of a Nikon DIAPHOT 200 inverted microscope. After 20 minutes of equilibration, experiments to acquire the aortic pressure-diameter (P-D) response were performed as described in Chapter 3.

5.2.3 Collagenase digestion of adventitia

After the standard inflation protocol, the adventitial matrix was partially digested with collagenase Type 1 solution dissolved in Mg^{2+}- and Ca^{2+}-free HBSS at 175U/ml.

The perfusate media was replaced with the prepared collagenase solution for 20 minutes. Following wash out with fresh media, the vessel was equilibrated for 5 minutes and acquisition of P-D data was repeated as above.

5.2.4 Histological Analysis

The collagenase incubation time was optimized to provide maximum adventitial digestion without medial degradation. After the P-D studies were completed, aortic samples were pressure fixed with formalin and cut into two segments from the thoracic and suprarenal regions. Samples were embedded in paraffin and sectioned at 5 microns. Sections were stained with Verhoff's Van Geison Elastic stain for elastic fibers and with Picro Sirius Red Stain for fibrillar collagen. The latter was also analyzed under polarized light.

5.2.5 Vascular contractility after collagen digestion of adventitia

After normal aortic preparation including removal of perivascular fat and fastening of intercostal arteries, the end of the upper aorta from proximal thoracic to upper abdominal (approximately at the 7^{th} pair of intercostals arteries) were tied with suture to create a sealed tube. A cut was made just below the abdominal suture and the aorta was transferred to collagenase solution (175U/ml inMg^{2+}- and Ca^{2+}-free HBSS).The remainder of the abdominal aorta was transferred to fresh DMEM. Both aortic segments were incubated at 37˚C for 20 minutes. Two rings cut from each section were fastened onto stirrups in a 4-channel wire myograph (DMT, Denmark). The force reading for each channel was brought to 2mN and allowed to normalize independently for 30 minutes. After force normalization, 10μM phenylephrine was added to the bath and the developed force response recorded using MyoDAQ software.

5.2.6 Multiaxial Mechanical Testing

Because isolated vessel perfusion for P-D data evaluates circumferential mechanics under fixed length only, the contribution of longitudinal forces in the setting of adventitial collagenase digestion were measured with a multiaxial computer-controlled biomechanical testing device as previously described (70). The basic set-up is similar to our isolated vessel chamber with the addition of a force transducer at the distal end of the vessel. In this manner, axial force is simultaneously recorded during pressurization protocols. Control C57Bl/6 mice were used in these experiments.

5.3 Results

5.3.1 Adventitia digestion induces low pressure expansion and high pressure stiffening.

The relationship between circumferential strain and pressure in control mice is shown in Figure 5.3.1. The data presented in panel A demonstrate biphasic distensibility with increasing pressure. Percent diameter change with pressure in the physiological pressure range ($1\text{-}D_{@80mmHg}/D_{@120mmHg}$) was approximately 12% and overall diameter change throughout the entire pressure load ($1\text{-}D_{@130mmHg}/D_{@0mmHg}$) was 100%. The variation of local compliance with pressure in the control group demonstrated maximum pressure-induced distensibility (9.1±0.99 μm/mmHg) at 60mmHg and minimum distensibility (1.2±0.23 μm/mmHg) at 120mmHg (Figure 5.1, Panel B).

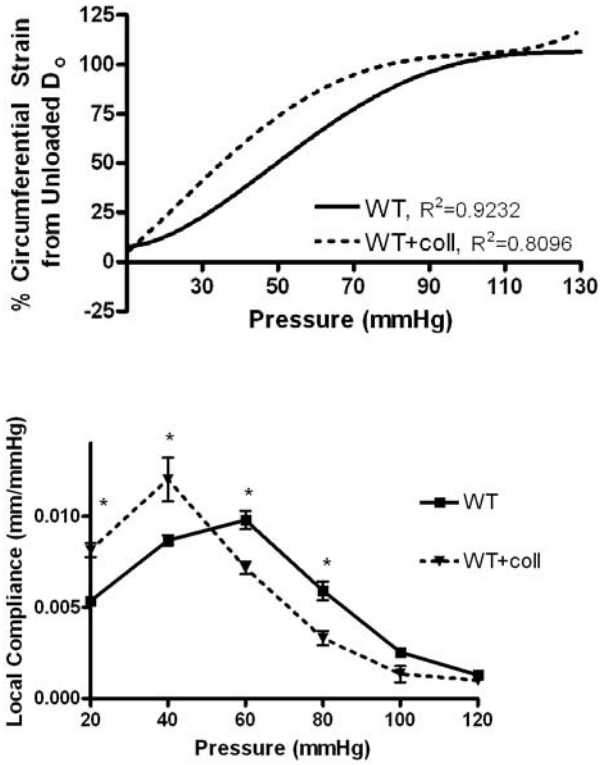

Figure 5.3.1. Circumferential strain and local compliance induction under transmural pressure. Panel A depicts the nonlinear regression line of the raw circumferential strain versus pressure data between control (▬) and post-collagenase aorta (----). Circumferential strain is calculated as $(D-D_0)/D_0*100$. A third order polynomial was fit to the data. Goodness of fit is indicated by the R^2 value included. Panel B shows a left shift of the compliance versus pressure response between control (▪) and post-collagenase aorta (▼). *P<0.05 compared to control at the pressure indicated.

After collagenase digestion the post-collagenase pressure versus strain data showed a marked left shift compared to control, demonstrating increased diameter expansion at all pressures. Overall strain versus pressure response was maintained in both groups. However, the response of the post-collagenase group did not demonstrate the region of minimal strain at pressures less than 40mmHg, as was observed in the control group (Figure 5.3.1, Panel A). Percent diameter change in the physiological pressure range decreased to approximately 7% while overall diameter change remained similar to control at 100%. The local compliance versus pressure curve of the post-

collagenase groups was also shifted to the left from control (Figure 5.3.1, Panel B), so that maximum compliance (7.1±0.66 μm/mmHg) occurred at 40mmHg and that minimum compliance (1.1±0.23 μm/mmHg) occurred at 100mmHg. Therefore adventitia digestion failed to change the magnitudes of the minimum and maximum compliance from control, but affected an overall shift of the aortic mechanical response to reduced pressures. These data closely mirrored deformation versus tension data obtained by VanBavel, *et al* (81) on rat mesenteric artery rings. In these experiments arterial rings subject to collagenase for 20-25 minutes exhibited low tension at submaximal strains and stiffening above control at maximal strains. Thus, our data suggest that the adventitia contributes significantly to the mechanical properties of the arterial wall by modulating normal physiologic vessel distensibility. The data suggest that if the tunica media were left unconstrained by the adventitia it would prematurely expand to maximum capacity at subphysiologic pressures.

Interestingly, collagenase digestion did not increase the maximum diameter achieved at peak pressure possibly due to compensatory recruitment of previously inactive fibrils. Evidence for this newly recruited population of fibrils is provided in the aforementioned experiment (81), which demonstrated that at maximum strain only 36% of collagen in mesenteric artery rings was in stretch, while 64% remained unloaded. Moreover the group who performed the first hallmark study to mechanically test arteries with and without adventitial attachment (97) indicated that the adventitia near the media became “much denser” and hard to remove, indicating tightly organized collagen at the adventitia/media boundary. These collagen fibrils may be protected from collagenase. Therefore our finding that aortas treated with collagenase did not expand beyond control

may be substantiated by a residual population of fibrils that are activated after collagenase digestion.

5.3.2 Collagenase digestion was specific to the adventitia and did not affect the tunica media.

Analysis of aortic cross sections by light microscopy verified that collagenase digestion specifically affected the adventitia, leaving the outer elastic laminae intact (Figure 5.3.2). Verhoff van Geison elastic staining confirmed the presence of a thick tunica media in the control groups composed of interstitial collagen and concentric elastic fibers forming concentric laminar rings (Figure 5.3.2A). Additionally, the adventitia showed intimate coherence to the outer elastic lamina. Picro Sirius stain viewed under polarized light confirmed normal appearing adventitia composed primarily of fibrillar collagen (Figure 5.3.2 C,E). After collagenase digestion (Figure 5.3.2 B,D,F) the morphology of the media appeared undisturbed and the elastic lamina remained intact. The desired alterations in fibrillar adventitial collagen post-collagenase were confirmed with picro-sirius stain (Figure 5.3.2 D,F). After collagenase digestion there was increased disorganization and "dispersion" of the fibers in the adventitia as well as localized detachment from the outer media. It is noted that we did not perform quantification of aortic collagen content before and after treatment to confirm degradation. Therefore, we referred to the effect of collagenase as dispersion, not degradation. Importantly, although not measured with high magnification microscopy, it is assumed that collagenase digestion degraded small collagen fibrils within the 20 minute incubation. Previous investigators using a similar model of collagenase digestion of rat mesenteric arteries (81) confirmed this assumption. Thus, external collagenase

incubation provided an effective method to specifically target and disperse the adventitia without disturbing medial microstructure.

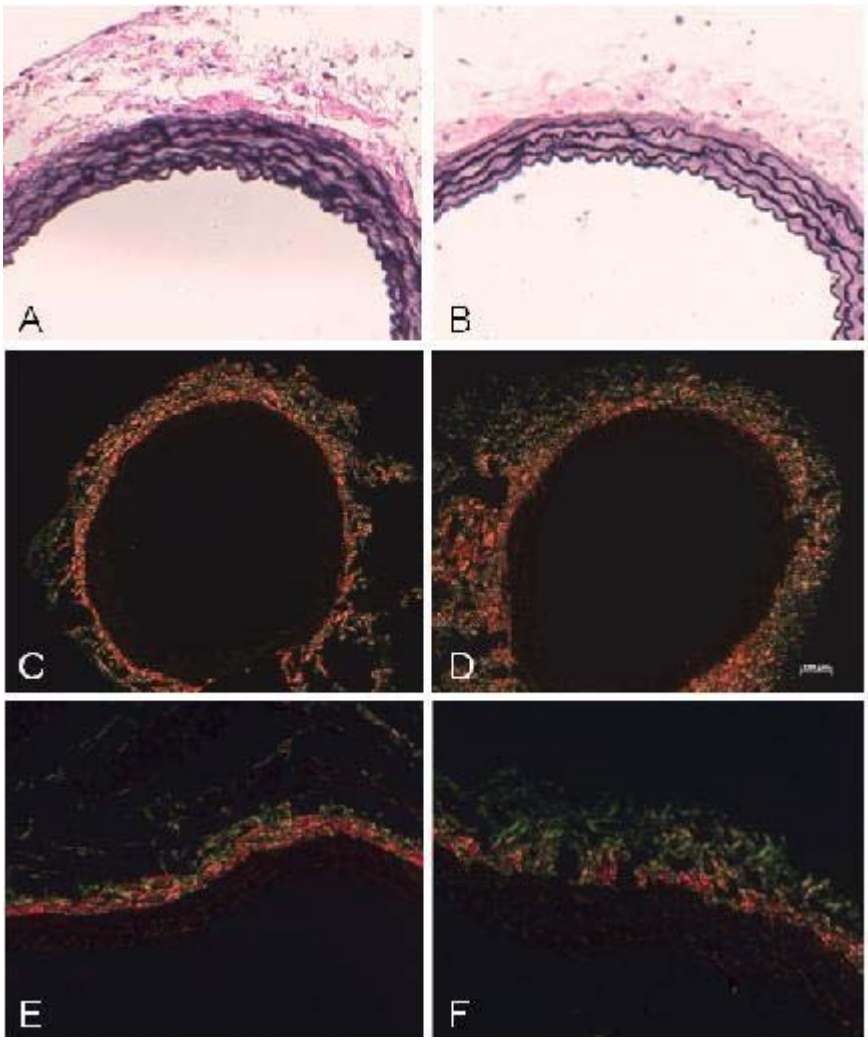

Figure 5.3.2. Histological analysis of control (A,C,E) and collagenase digested (B,D,F) aortas. Verhoff van Geison stain (A-B) showed that dispersion was specific to the adventitia and did not disrupt the elastic lamina or the media. Picro-sirius red stain (C-F) imaged under polarized light showed decreased red color and increased green color in the post-collagenase group compared to control indicating alterations in the organization of Type I and Type III collagen, respectively.

5.3.3 VSMC contractility is maintained after adventitia digestion.

To confirm that collagenase incubation did not compromise the media, smooth muscle cell contraction in response to phenylephrine (PE) constriction after collagenase treatment was measured using a myograph. After 30 minutes of equilibration the

baseline force tension in both control and post-collagenase group was less than 2mN (Figure 5.3.3 A and B). Addition of PE to the medium induced a contractile force of approximately 30% in each group (control, 26.6±7.74% versus post-collagenase, 34.71±14.2%, P=0.49) (Figure 5.3.4). In addition the post-collagenase group exhibited PE-induced contraction for up to 30 minutes that was similar to the response seen in control aorta (data not shown). Thus, controlled collagenase digestion selectively removed the mechanical effects of the adventitia without altering the structure or function of the tunica media.

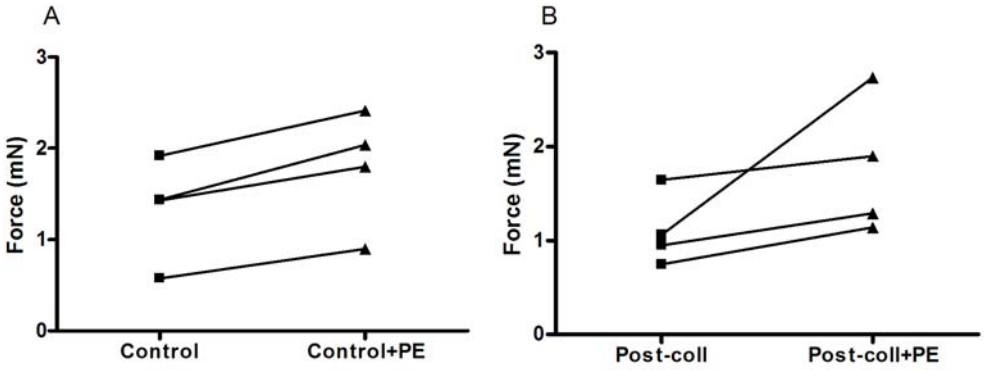

Figure 5.3.3. Baseline and PE-induced tension in A) control rings and B) rings from aortic segments treated with collagenase. Each ring was stretched to a force of 2mN and allowed to equilibrate for 30 minutes at which time PE was added to 10μM. Each data point represents the average of 2 paired rings from the same aortic segment. PE induced an increase in contractile force in all samples from all groups.

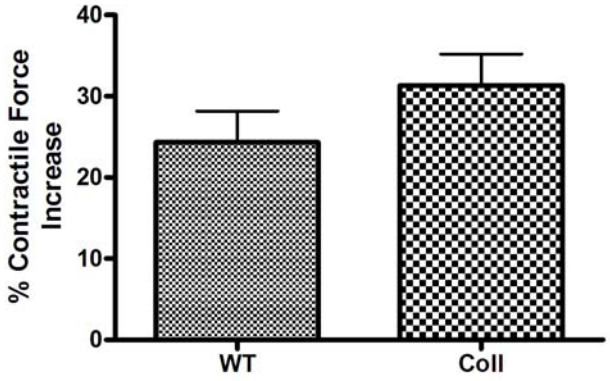

Figure 5.3.4. Contractile response to 10μM PE. After aortic harvest, the upper aorta from proximal thoracic to proximal abdominal was cleaned and tied to create a sealed tube which was exposed to 20 minutes of collagenase digestion. The remaining half above the renal arteries was incubated in DMEM. Two rings were cut from the collagenase digested segment and two from the incubated segment. The contractile response to PE of the 4 rings was evaluated in a 4-channel wire myograph. The percent increase in contractile force generation between the groups was not significantly different (P=0.49, N=4, Mann-Whitney test).

5.3.4 Normal aortic pressure versus diameter response to varied axial extension after adventitia digestion is altered.

To determine the effect of adventitia digestion on mechanical behavior we implemented our collagenase protocol in a multiaxial mechanical testing device. The mechanical properties of normal C57Bl/6 aortas were similar to values previously reported by other groups (54, 70). We were able to recapitulate published data by showing that there is range of axial stretch (stretch, $\lambda = L_{ex\ vivo}/L_{in\ vivo}$, L=length) in which the relationship between pressure and diameter did not change (Figure 5.3.5). Since increasing or decreasing stretch would alter the axial force on the vessel, we can assume, as did the previous authors, that near a target stretch the pressure-diameter response is independent of axial force. The range of axial extensions tested was λ_1 =1.9-2.3 for sample 1 and λ_2=2.7-3.0 for sample 2 (data not shown).

At the midpoint of the target stretch range, λ=2.2 in this case, a flat pressure versus force curve was recorded as shown in Figure 5.3.6. At extensions below this stretch, force dropped off considerably with pressure, while increasing extension beyond this stretch increased the resulting force. In the literature this target stretch corresponds to the *in vivo* length of the aorta. However, in our hands *in vivo* stretch was consistently measured as λ_{avg}= 1.5 and therefore our *ex vivo* result does not corroborate previous observations (54). This inconsistency is addressed in Appendix A.

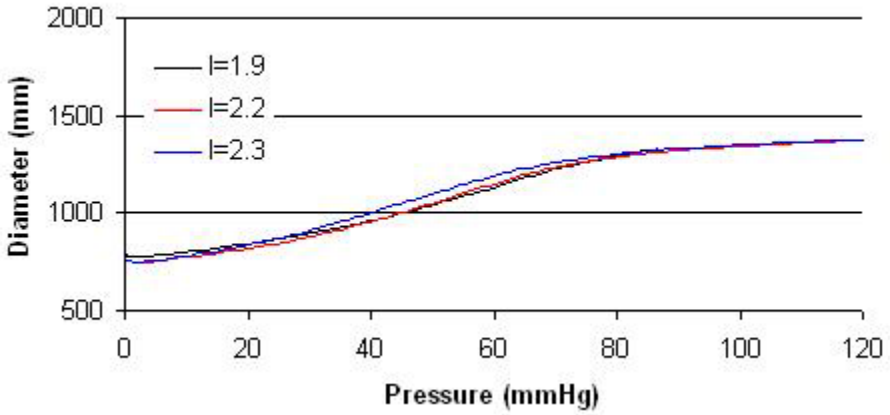

Figure 5.3.5. Biphasic diameter response to pressure at different axial stretch lengths. The normal diameter response is independent of stretch, and therefore independent of axial force, within the range of stretch applied, 1.9<λ<2.3.

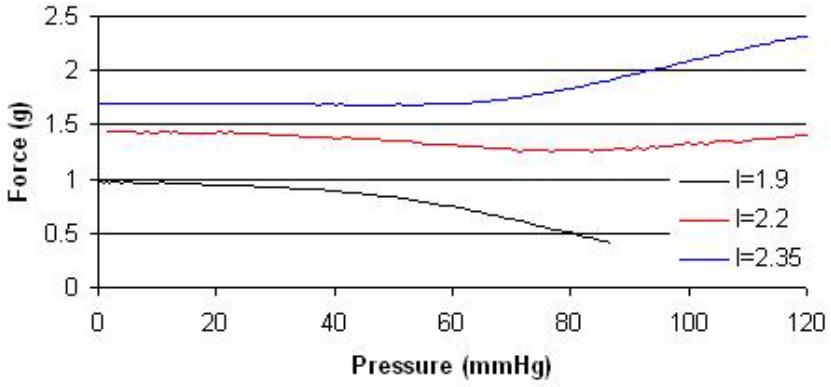

Figure 5.3.6. Representative example of pressure versus axial force behavior in the multiaxial vessel testing system. Force behavior was independent of pressure near the *in vivo* stretch, l=2.2. At stretch variations lower or greater than the target stretch the force generation decreased or increased, respectively, thus indicating a range of axial stretch in which the pressure versus diameter response is independent of axial force.

After the initial round of mechanical testing, the perfusate was replaced with collagenase solution for 20 minutes. After wash-out, the same mechanical tests were performed. Collagenase digestion of the adventitia induced a marked separation and increase of the diameter response at the same extensions (λ=1.9 and 2.2) (Figure 5.3.7). Moreover the diameter increase began immediately upon pressurization, rather than exhibiting sigmoidal behavior as observed in control. When collagenase treated vessels were stretched to λ=2.3 high axial force was recorded. As a result the experiment was stopped to prevent vessel tearing.

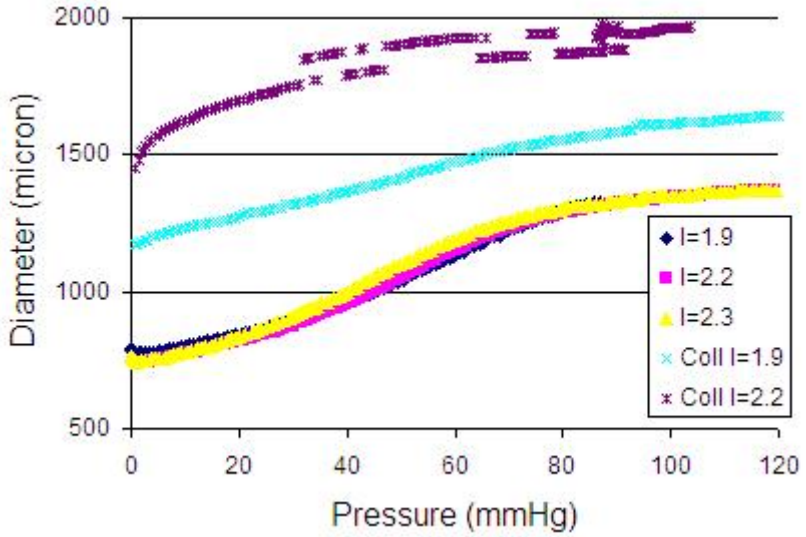

Figure 5.3.7. P-D response obtained after collagenase digestion of the adventitia Post collagenase at λ=1.9 (x) and at λ=2.2 (*). (The control data is included for reference). Dispersion of the adventitia induced greater diameter expansion under pressure than in control indicating that the adventitia prevents overexpansion of the elastic media. Diameter increased immediately upon pressurization indicating that dispersion of adventitia collagen removes the capacity for low pressure maintenance of unloaded diameter as observed in the control group.

Force versus pressure data after collagenase treatment shows comparable behavior to control. Force at the target stretch is constant and decreases at smaller extensions (Figure 5.3.8). These data indicate that the adventitia does not contribute

significantly to aortic axial force behavior, at least within the range of stretch investigated. Thus, biaxial characterization of the aorta after collagenase digestion of the adventitia demonstrated that the media alone does not determine the normal mechanical response of the vessel to altered axial loads. Conversely, the adventitia contributes significantly to the circumferential mechanical behavior of the arterial segment.

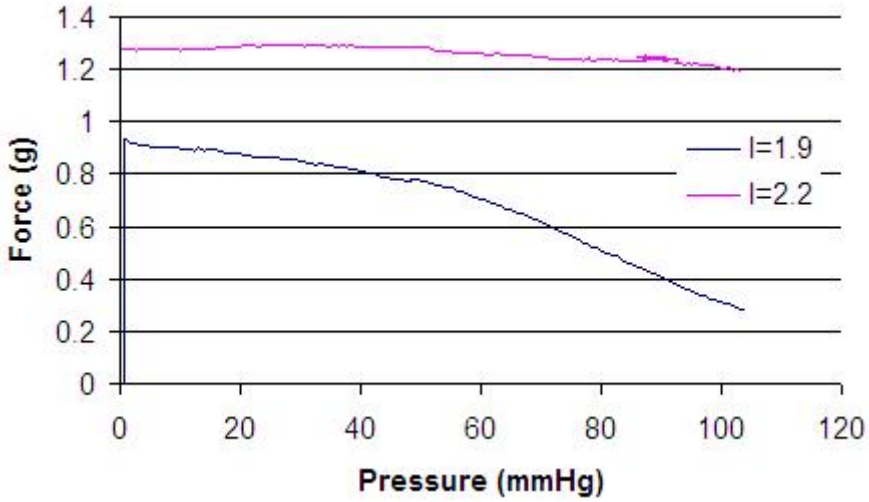

Figure 5.3.8. Pressure versus axial force behavior after collagenase digestion of the adventitia. At the target stretch λ=2.2 force does not vary with pressure. At the reduced extension λ=1.9 force decreases with pressure. These data show the same behavior as observed in control indicating that the adventitia does not contribute significantly to aortic axial force.

5.4 Discussion

In this study, our objective was to determine the independent mechanical contribution of the aortic adventitia and media tunica. To accomplish this goal we compared the circumferential and axial mechanical behavior of control aortas with and without collagenase treatment. Histological analysis and comparable contraction of control and post-collagenase aortic rings to PE confirmed that the mechanical differences detected were a result of dispersion of adventitial collagen and not from medial disruption. The data demonstrate that adventitia degradation significantly alters the

circumferential but not the axial behavior of the vessel. Specifically, the data demonstrate that the adventitia regulates the circumferential behavior of the aorta by preventing overstretch and the media regulates the axial behavior by maintaining tensile loading.

The finding that the adventitia reinforces the elastic media from overexpansion in the circumferential direction, but does not affect axial behavior is consistent with published roles for elastin and collagen at physiologic pressures (81, 98-100). Elastin imparts tensile strength, while collagen provides scaffold support (101). In the unloaded state collagen fibrils are very wavy (102), heterogeneous in size and length, and on account cannot bear loads. Collagen recruitment into the loaded state has been hypothesized to be responsible for the biphasic behavior (81, 103) observed in control P-D data. In this case, minimal recruitment at low pressure allows gradual increases in diameter mediated primarily by expansion of the aortic media. Maximum recruitment at high pressure affects rigidity and protection from overstretch. Dispersion of adventitial collagen blunted the normal diameter response at low pressure suggesting that collagenase digestion disturbed a population of collagen fibrils responsible for limiting diameter expansion at small loads.

Dispersion of the adventitia also altered the pressure versus diameter response at different axial extensions, therefore blunting axial force-independent diameter response as observed in control vessels. Based on the capacity of collagen to recruit from a heterogeneous population of fibrils, it is possible, although speculative, that in physiologic homeostasis a subgroup of small fibrils is synergistically recruited within the target range of stretches. The function of this subgroup is to maintain a constant diameter

upon altered axial extension. Collagenase treatment likely disrupted these small fibrils (as also suggested by (81)) and blunted their role in maintaining a constant diameter in this setting.

An alternative mechanism to maintenance of diameter is cellular regulation of ECM components. It is well established that vascular cells regulate their local matrix environment in part by mechanical cues. VSMCs have been shown to rapidly secrete collagen (104), MMPs (40), platelet-derived growth factor (105), and focal adhesion-related paxillin and vinculin (106), among other ECM-related factors in response to mechanical strain. It has also been demonstrated that fibroblasts can sense force-induced deformations (17), and in response can rapidly remodel the ECM (17, 107). Nonetheless, although the mechanism is not clear, adventitial collagen dispersion prevented normal homeostatic behavior. In this manner its capacity to control the diameter response to extension-induced variation in axial force was blunted.

Altering the mechanical environment via collagenase digestion is well suited to the study of vascular cell adaptation within the aortic wall. VSMCs, fibroblasts, and endothelial cells exist within a dynamic homeostatic state associated with cyclic axial and circumferential stretch and strain. In response to pathologic conditions, vascular cells rapidly modulate proliferative and contractile phenotypes in order to maintain continuity (93),(96). Isolated vessel culture studies have shown adaptation of intact arteries as early as 2 days in *ex vivo* organ culture (69, 70, 108-110). Indeed vessels maintained at axial lengths that deviated slightly from that experienced *in vivo* tend to actively remodel back to the *in vivo* configuration (70). Vessels subject to chronic large axial extensions exhibited lengthening (69, 108) to normalize axial force generation within the wall. In

each case the morphology of the arterial wall remained the same in structure and viability indicating cell-mediated mechanistic control of the microstructure. As suggested by our results, dispersion of the adventitia in these models of vascular adaptation reveals the role of the media to maintain axial force while experiencing altered circumferential strain and stress.

Interestingly, these results have relevance to adventitial and medial remodeling within the pathogenesis of AAA. Since disrupting adventitial collagen induces dilation of the aorta, the opposite effect may hold true as well. Thus, we speculate that deposition of adventitial collagen prevents aortic dilation in the setting of AAA. Based on this line of reasoning, these results suggest that adventitial collagen deposition may be a counter-regulatory adaptation to vascular expansion. The finding of increased adventitial collagen deposition in the setting of small aortic dilations and established AAA (Figures 3.4.5 and 3.4.7) supports this hypothesis. Carmo et al (12) have shown that endogenous collagen becomes highly crosslinked in aneurysm development with a concomitant deficiency in new collagen biosynthesis. Therefore, it is possible that at a critical stage of mechanical flux in early aneurysmal development, existing adventitial collagen becomes increasingly crosslinked in a counter-regulatory manner in order to stabilize the aortic wall. Indeed unpublished data from our lab has shown lysyl oxidase, which crosslinks elastin and collagen, is upregulated in the aorta of $apoE^{-/-}$ mice treated with angII/HF. Therefore AAA-induced mechanical alterations may be stabilized by lysyl oxidase mediated-crosslinking of endogenous collagen. The results of this study suggest that collagen remodeling is a critical mediator in the maintenance of homeostatic vascular

mechanics and that adventitial collagen crosslinking acts as a compensatory mechanism to prevent aortic dilation.

In summary, by implementing a technique of adventitial digestion by collagenase, we have demonstrated that the adventitia participates actively in the circumferential mechanical response to aortic loading, while the media participates in axial load bearing. We further demonstrated that normal vessel adaptation maintains a constant diameter in the presence of axial extension-induced changes in force within a target stretch range. Dispersion of adventitial collagen ablates this effect and causes the vessel to change diameter upon pressure loading at altered extensions. We can therefore conclude that the adventitia is an important load bearing constituent of the arterial wall, and plays a role in vascular adaptation to altered mechanical state. Finally, our interpretation of the results suggested a lysyl oxidase-mediated mechanism of increased collagen deposition in the adventitia of early and established AAA. Application of this collagenase-based technique to models of vascular adaptation and AAA formation will offer substantial insight into the individual function of the aortic layers, and their role in vascular growth, remodeling, and cellular mechanobiology.

CHAPTER 6

SUMMARY, LIMITATIONS, AND FUTURE CONSIDERATIONS

6.1 Summary

From the onset, our objective was to characterize the transition from a healthy aorta to an aneurysmal aorta. We hypothesized was that oxidative stress is mechanistically linked to the biomechanical remodeling involved in aneurysm formation. We tested this hypothesis in mouse models of accelerated and physiological AAA formation, as well as in transgenic mice that overexpress catalase, an antioxidant enzyme, in their vasculature. By means of mechanical testing of both aortic rings and intact aorta, morphologic and chemical characterization of aortic ECM composition, and protease activity and gene expression assays, this project has produced the following results.

1) Molecular events, specifically inflammatory cell infiltration, precede mechanical events, as detected by fixed-length mechanical testing, as the earliest modulators of aneurysm formation.

2) Aortic circumferential mechanics as measured by fixed-length mechanical testing are well conserved during the early physical changes of AAA matrix remodeling, including elastin fragmentation and adventitia thickening.

3) H_2O_2-mediated elastin degeneration within the aortic media is etiologic of altered aortic mechanics.

3) The adventitia modulates normal physiologic vessel distensibility and prevents overexpansion of the elastic media.

In summary, the major contributions of this work are both clinically and scientifically relevant and help to improve the understanding of the pathogenesis from a

healthy aorta to a pre-aneurysmal aorta. Based on the data obtained in Aim 1, we conclude that attempts to detect early aneurysm progression in the form of mechanical or geometric changes may miss the window in which aneurysm pathology may be potentially reversed. Based on the data obtained in Aim 2, we conclude that mitigating oxidative stress within the aortic wall, specifically targeting oxidative factors that degrade elastin fibers, may provide protection against AAA. And lastly based on our data from Aim 3, we conclude that that the adventitia is an important load bearing constituent of the arterial wall and plays an important role in vascular adaptation to an altered mechanical state. Overall our results impact the understanding of early AAA pathogenesis and in doing so may potentially participate in the development of preventative therapies for AAA.

6.2 Limitations and Future Directions

6.2.1 Aim 1 Define the fundamental biomechanical changes in the pre-aneurysmal aorta.

The primary limitation in Aim 1 was the inconsistent time course of AAA development with our models. Particularly in the accelerated model (angII/βAPN/HF diet) some AAAs were observed as early as 6 days, while others were observed as late as 21 days. The presentation of pronounced aortic dilations normally aborted mechanically testing as dilated aortas often did not hold pressure within our system. Therefore we cannot exclude that the mechanical data acquired at late time points were not biased by selectively testing only those aortas that demonstrated gradual AAA formation. We therefore suggest that future application of these techniques should focus on aortic diameter, rather than treatment time, as the end point. Doppler ultrasound proved an easy

tool to acquire aortic diameter. Therefore future mechanical or histological analysis in these models of AAA should include verification of aortic diameter first, before proceeding with experimentation. In addition, ultrasound would also provide measurement of *in vivo* compliance for each sample, which would greatly benefit subsequent analysis.

A second limitation of our analysis was lack of characterization of axial mechanics. As demonstrated in Chapter 3, our data showed that alterations in axial mechanics preceded circumferential changes. This finding suggests that the longitudinal force response in our models of AAA may be more sensitive to changes in the ECM. Characterization of axial force could be obtained in future experiments in a multiaxial computer controlled set-up such as that described by Gleason *et al* (70). Stress-strain relationships can be extracted after axial force is characterized and from these data, material properties can be obtained. In fact the optimization and data acquisition protocols for testing murine aortas with the multiaxial system were accomplished as part of this work, in the "collagenase" experiments in Chapter 5.

Another limitation in Aim 1 is a lack of a detailed understanding of the physical changes in ECM. Our histological analysis of elastin fragmentation and collagen turnover revealed general changes in aortic cross section, i.e. breaks in elastin fibers and thinning adventitia, but it does not provide a detailed description of how the ECM changes as a whole. Combining our isolated vessel perfusion with confocal microscopy may provide the opportunity to dynamically describe elastin and collagen behavior under simulated hemodynamic pressure *in situ*. We obtained trial images with this technique using a LSM 51 NLO META Multiphoton Excitation Confocal microscope (Carl Zeiss,

Inc) (Figure 6.2.1). Elastin fibers were large and undulating (left panel) while collagen fibers (right panel) appeared small, wavy, and required higher magnification. Description of the behavior and morphology of elastin and collagen fibers *in situ* would provide *in vivo* orientation angles of these constituents, which apply widely to theoretical modeling of aneurysmal mechanics.

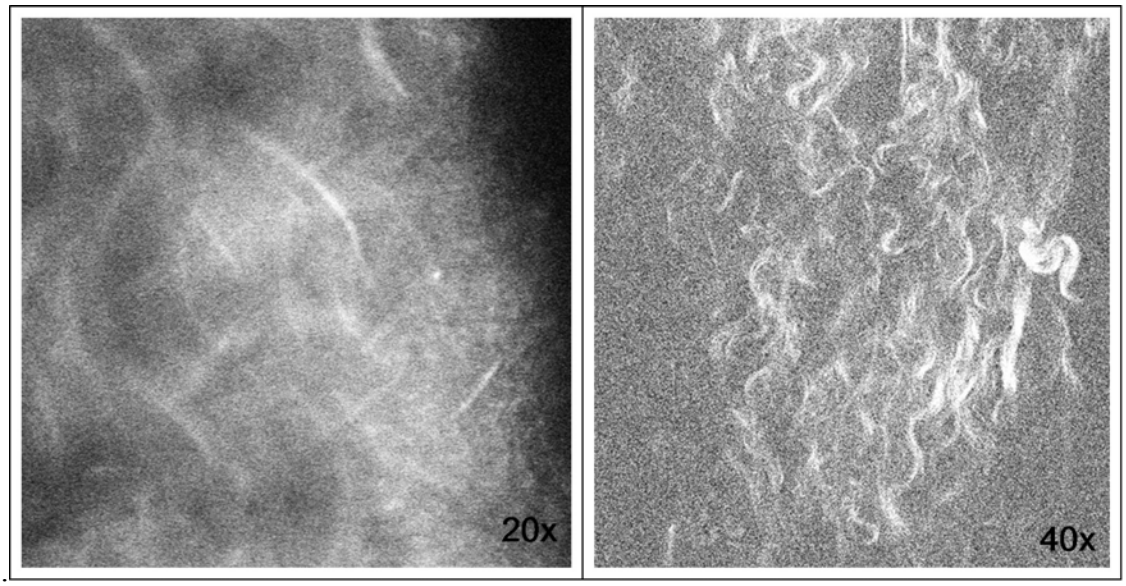

Figure 6.2.1. Multiphoton excitation confocal microscopy of aortic elastin fibers (left) and collagen fibers (right) *in situ*. Elastin fibers are visible at higher magnification than collagen. Collagen fibers appear more heterogeneous in size than elastin fibers and exhibit a high degree of waviness.

6.2.2 Aim 2: Determine the functional importance of oxidative stress in modulating the biomechanical changes in the aorta that occur prior to aneurysm formation

The results of Chapter 4 demonstrated that VSMC-derived H_2O_2 is an important mediator of aortic ECM organization and mechanical response. The primary limitation of this study is that it is not clear whether the events observed were driven by the source/location of H_2O_2 or due to globally increased levels of H_2O_2 within the aortic wall. Our lab has generated additional evidence in support of the latter hypothesis by demonstrating that a line of transgenic apoE$^{-/-}$ mice with macrophage-specific

overexpression of catalase is also completely protected from angII-induced AAA (data unpublished). Taken together these data strongly suggest that the ECM-degrading effects of reduced H_2O_2 levels within the aortic wall are independent of the source. To demonstrate this independence, *in situ* detection of H_2O_2 within the aortic wall can be performed by means of the oxidatively active fluorescent dye 2',7'-dichlorodihydrofluorescein diacetate (DCFDA), which stains for intracellular ROS. Briefly, DCFDA is applied to 30 μm thick aortic ring segments cut from frozen blocks and imaged with confocal microscopy. If H_2O_2 is present it will be visualized as green globules upon the otherwise smooth autofluorescent elastic laminae. Alternatively, since DCFDA staining is technically difficult, *in situ* zymography to determine regions of MMP activity may indirectly identify the location of H_2O_2 within the aortic wall, as H_2O_2 has been shown to upregulate MMP expression (14). Briefly, this technique consists of incubating sections of unfixed aortic tissue on slides coated with a gelatin-containing substrate (10, 111). Lysis of the substrate (which will appear black against a fluorescent substrate) indicates the focal areas of enzymatic activity in the tissue. Thus we speculate the targeting ROS production within the aortic wall is a potential mechanism for therapeutic management or prevention of AAA.

A second limitation in our investigation of Aim 2 is interpretation of the opening angle data which was measured in zero stress state of aortic rings. Vascular adaptation occurs at physiologic load and as such it could be argued that our analysis was misdirected as vascular cells never experience a zero load state. We refer to Figure 6.2.2 to help demonstrate how characterization of residual stress in the unloaded configuration is related to physiologic behavior. In Figure 6.2.2 the area indicated by grey shading

indicates the unloaded state and the area indicated by diagonal lines indicates the physiologic state. In the unloaded state, stretch, λ is close to 1, i.e. is under very small stretch. However, in the physiologic state stretch, λ^{phys} is much greater than 1. These two states are related by the stress-stretch behavior of the aorta. Thus the unloaded stress, $\sigma_{avg,\ unloaded}$ is related to the physiologic stress with the wall, $\sigma_{avg,\ phys}$ at all values of stretch. However, our analysis could be improved by performing isolated mechanical testing on aortas from angII treated SMC-Cat and WT mice. These experiments would allow for a detailed characterization of the role that H_2O_2 plays in alteration in the stress-stretch behavior of the early aneurysm.

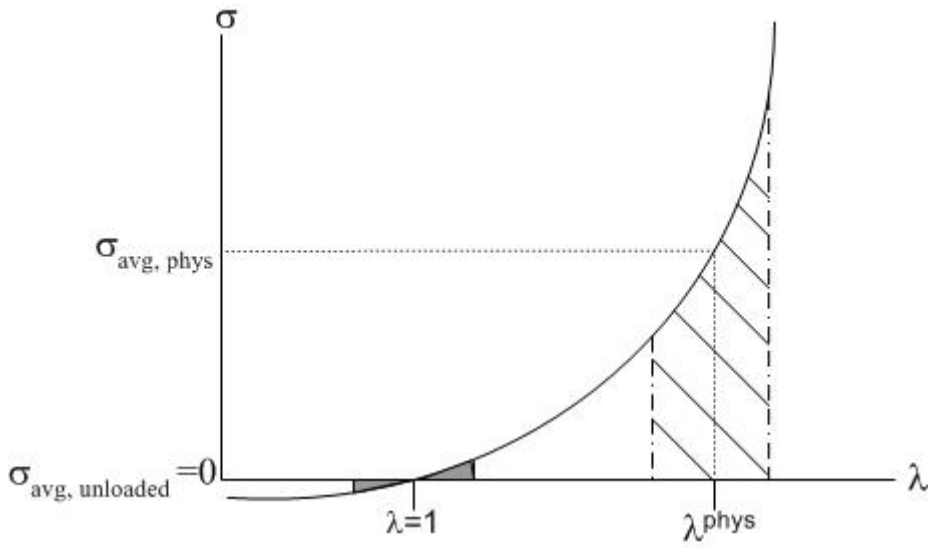

Figure 6.2.2. Illustration of the relationship between circumferential aortic stress (σ) and stretch (λ) in the zero load and physiologic configurations. In the zero stress range (grey shading) stretch values are very small and average stress is zero. Physiological loading (diagonal line) causes large deformations in diameter and due to the exponential relationship between stress and stretch the average stress ($\sigma_{avg,phys}$) is non-zero. The area shaded with diagonal lines shows the dynamic range in which slight variations of stretch induce large perturbations in stress. (Adapted from discussion with Alexander Rachev, Ph.D., Georgia Institute of Technology, Atlanta, Georgia).

6.2.3 Aim 3: Define the contribution of the tunica adventitia to the aortic mechanical response

A limitation in Aim 3 was the inability to completely remove the adventitia. Moreover we do not know exactly how much collagen was degraded and whether there was an overall loss of collagen content in the adventitia. An additional optimization step should be to quantify the percent collagen lost after collagenase digestion (if any). This test could easily be performed via the hydroxyproline assay outlined in Chapter 4.

As a future direction from Chapter 5, special focus should be given to the role of lysyl oxidase in AAA formation. The results of Chapter 5 clearly demonstrated that affecting collagen orientation within the adventitial layer modulates normal arterial mechanics. The results of the study allowed speculation on the link between lysyl oxidase and collagen biosynthesis in the adventitia of early and established aneurysmal dilations. Lysyl oxidase gene expression has been shown to be deficient in tissue from experimental AAA (65). We have substantial evidence from unpublished data in our laboratory showing that lysyl oxidase is upregulated in aortic tissue after 7 days of angII treatment (Figure 6.2.3 and 6.2.4). Our working hypothesis is that lysyl oxidase protects against early AAA disease, but that its activity is overwhelmed by ECM-degrading protease activity at later stages. To test this hypothesis, experimental design should include repetition of lysyl oxidase gene expression analysis at 10 or 14 days after angII treatment. This analysis would help to determine a time course of angII-mediated lysyl oxidase regulation. Additional analysis of protease expression should also be performed in order to determine the lysyl oxidase to protease mRNA ratio at different time points in AAA development. Activity assays for lysyl oxidase and proteases must be performed as

well since expression is not always indicative of protein activity. Thus investigating the temporal mechanism of lysyl oxidase regulation in AAA will provide an opportunity to investigate possible tissue repair mechanisms to counteract aneurysmal ECM-degradation.

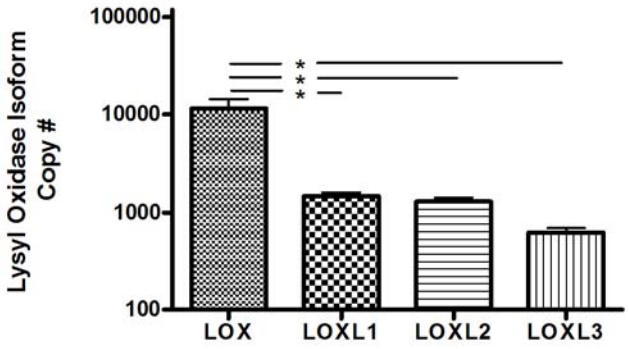

Figure 6.2.3. Lysyl oxidase isoform mRNA expression in aortic tissue. LOX demonstrates the highest expression at baseline. All other isoforms demonstrate significantly less expression than LOX (*P<0.05, Mann-Whitney test).

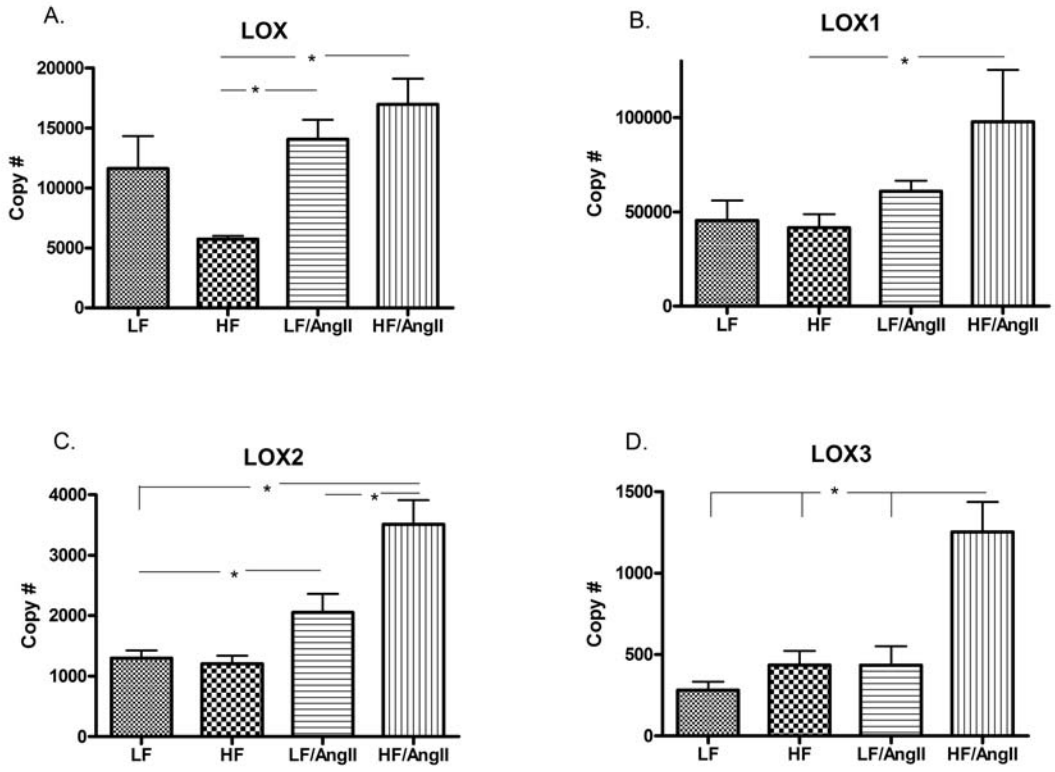

Figure 6.2.4. mRNA expression of lysyl oxidase isoforms at baseline (LF), and after 7days treatment with HF diet, standard diet and angII, or HF diet and angII. A) LOX expression after angII treatment did not increase significantly compared to baseline but was increase compared to HF diet condition. B) LOX1 also showed significant increase to angII when compared to HF diet condition. C) AngII treatment significant increased the expression of LOX2 regardless of diet. D) LOX3 expression was increased only after treatment with HF diet and angII. (*P<0.05, Mann Whitney test).

6.3 Conclusion

In conclusion, this work has provided a novel examination of molecular, matrix, and mechanical events that comprise the transition from healthy to aneurysmal aorta. We have identified elastin degradation as a critical event in the etiology of AAA and demonstrated a causal role for oxidative stress in that process. As discussed in this chapter, the results of this work present alternative directions and additional questions to address within the context of early AAA development. Our closing discussion of lysyl

oxidase provided encouragement that discovery of tissue repair mechanisms is possible. It is anticipated that the results of this work will lead to better understanding of aneurysm pathogenesis and help to define the associations between molecular and mechanical processes.

APPENDIX A

In Chapter 5 we described the force independent behavior of the P-D response at a target extension (Figure 5.3.5) showing that P-D behavior did not change with axial extension of the vessel. The pressure-force relationship in this target extension range is demonstrated in Figure A.1. At λ= 2.2 a relatively flat pressure-force curve was recorded.

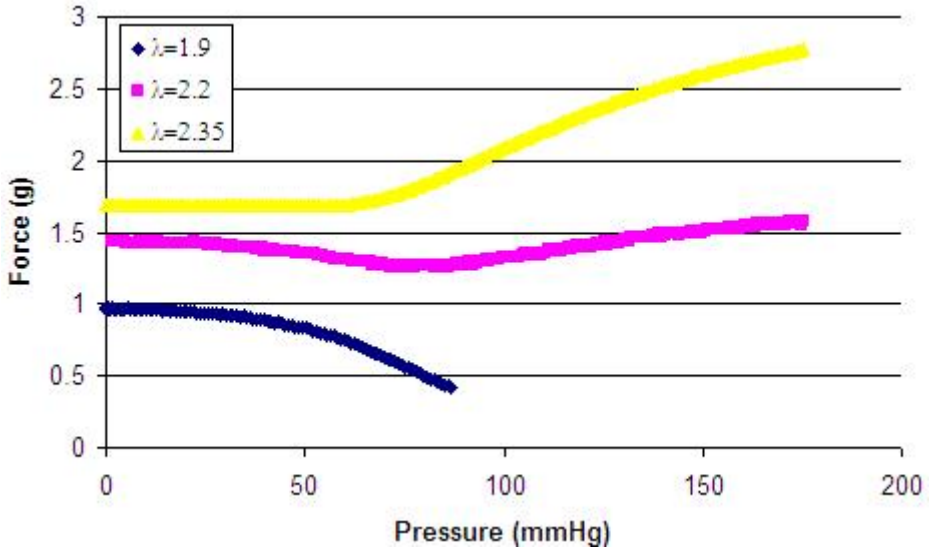

Figure A.1. Force versus pressure behavior of a murine aorta. At the target extension λ=2.2 the force does not increase with pressure. This extension corresponds to the *in vivo* stretch. At a small deviation below the target extension (λ=1.9) force drops of quickly with pressure and at deviations greater then the target extension (λ=2.35) force increases with pressure. The target/*in vivo* stretch indicates a period of uniform axial loading at all pressures.

At extensions below this set point the force measurement dropped off considerably with pressure, while increasing extension beyond this set point caused the force to increase with pressure. In the literature this extension set point is considered to match the *in vivo* stretch. However, λ=2.2 did not reflect the *in vivo* length of λ =1.5 measured at the time aortic harvest. We believe, however, that the output extension measured in this experiment is in error as the control system requires input of unloaded length as the

distance between the cannulated ends of the aorta. When this experiment was performed the unloaded length was input as the distance between two sets of markers on the aortic surface. As recalled from our discussion in Chapter 3, axial stretch ratio varies along the length of the aorta, i.e. the overall axial stretch is greater than the stretch between interior points. Therefore when the target stretch between our markers was reached, the overall stretch output by the controller was inaccurately elevated. Nonetheless, the desired force-pressure behavior was achieved in this preliminary study and validated the use of multi-axial mechanical data acquisition for future studies.

REFERENCES

1. Bergqvist, D., Björck, M., and Wanhainen, A. Abdominal Aortic Aneurysm - To Screen or Not to Screen. European Journal of Vascular and Endovascular Surgery, *35:* 13-18, 2008.

2. Iribarren, C., Darbinian, J. A., Go, A. S., Fireman, B. H., Lee, C. D., and Grey, D. P. Traditional and Novel Risk Factors for Clinically Diagnosed Abdominal Aortic Aneurysm: The Kaiser Multiphasic Health Checkup Cohort Study. Annals of Epidemiology, *17:* 669-678, 2007.

3. Powell, J. T., Worrell, P., Mac Sweeney, S. T., Franks, P. J., and Greenhalgh, R. M. Smoking as risk factor for abdominal aortic aneurysm. Ann N Y Acad Sci., *800:* 246-248, 1996.

4. Vande Geest, J. P., Sacks, M. S., and Vorp, D. A. The effects of aneurysm on the biaxial mechanical behavior of human abdominal aorta. Journal of Biomechanics, *39:* 1324-1334, 2006.

5. Vorp, D. A., Raghavan, M. L., Muluk, S. C., Makaroun, M. S., Steed, D. L., Shapiro, R., and Webster, M. W. Wall strength and stiffness of aneurysmal and nonaneurysmal abdominal aorta. Ann N Y Acad Sci., *800:* 274-276, 1996.

6. Vorp, D. A., Schiro, B. J., Ehrlich, M. P., Juvonen, T. S., Ergin, M. A., and Griffith, B. P. Effect of aneurysm on the tensile strength and biomechanical behavior of the ascending thoracic aorta. Ann Thorac Surg., *75:* 1210-1214, 2003.

7. Okamoto, R. J., Wagenseil, J. E., DeLong, W. R., Peterson, S. J., Kouchoukos, N. T., and Sundt, T. M. r. Mechanical properties of dilated human ascending aorta. Ann Biomed Eng., *30:* 624-635, 2002.

8. Zatina, M. A., Zarins, C. K., Gewertz, B., L., and Glagov, S. Role of medial lamellar architecture in the pathogenesis of aortic aneurysms. J Vasc Surg., *1:* 442-448, 1984.

9. Campa, J. S., Greenhalgh, R. M., and Powell, J. T. Elastin degradation in abdominal aortic aneurysms. Atherosclerosis., *65:* 13-21, 1987.

10. Lemaitre, V., Soloway, P. D., and D'Armiento, J. Increased Medial Degradation With Pseudo-Aneurysm Formation in Apolipoprotein E-Knockout Mice Deficient in Tissue Inhibitor of Metalloproteinases-1. Circulation, *107:* 333-338, 2003.

11. He, C. M. and Roach, M. R. The composition and mechanical properties of abdominal aortic aneurysms. J Vasc Surg., *20:* 6-13, 1994.

12. Carmo, M., Colombo, L., Bruno, A., Corsi, F. R. M., Roncoroni, L., Cuttin, M. S., Radice, F., Mussini, E., and Settembrini, P. G. Alteration of Elastin, Collagen and their Cross-links in Abdominal Aortic Aneurysms. European Journal of Vascular and Endovascular Surgery, *23:* 543-549, 2002.

13. Rajagopalan, S., Meng, X. P., Ramasamy, S., Harrison, D. G., and Galis, Z. S. Reactive Oxygen Species Produced by Macrophage-derived Foam Cells Regulate the Activity of Vascular Matrix Metalloproteinases In Vitro . Implications for Atherosclerotic Plaque Stability. J. Clin. Invest., *98:* 2572-2579, 1996.

14. Meli, D. N., Christen, S., and Leib, S. L. Matrix Metalloproteinase-9 in Pneumococcal Meningitis: Activation via an Oxidative Pathway. The Journal of Infectious Diseases, *187:* 1411-1415, 2003.

15. Gum, R., Lengyel, E., Juarez, J., Chen, J. H., Sato, H., Seiki, M., and Boyd, D. Stimulation of 92-kDa Gelatinase B Promoter Activity by ras Is Mitogen-activated Protein Kinase Kinase 1-independent and Requires Multiple Transcription Factor Binding Sites Including Closely Spaced PEA3/ets and AP-1 Sequences. J. Biol. Chem., *271:* 10672-10680, 1996.

16. Ungvari, Z., Orosz, Z., Labinskyy, N., Rivera, A., Xiangmin, Z., Smith, K., and Csiszar, A. Increased mitochondrial H2O2 production promotes endothelial NF-{kappa}B activation in aged rat arteries. Am J Physiol Heart Circ Physiol, *293:* H37-47, 2007.

17. Chiquet, M., Renedo, A. S., Huber, F., and Flück, M. How do fibroblasts translate mechanical signals into changes in extracellular matrix production? Matrix Biology, *22:* 73-80, 2003.

18. Miyake, T., Aoki, M., Masaki, H., Kawasaki, T., Oishi, M., Kataoka, K., Ogihara, T., Kaneda, Y., and Morishita, R. Regression of Abdominal Aortic Aneurysms by Simultaneous Inhibition of Nuclear Factor {kappa}B and Ets in a Rabbit Model. Circ Res, *101:* 1175-1184, 2007.

19. Gu, Z., Kaul, M., Yan, B., Kridel, S. J., Cui, J., Strongin, A., Smith, J. W., Liddington, R. C., and Lipton, S. A. S-Nitrosylation of Matrix Metalloproteinases: Signaling Pathway to Neuronal Cell Death. Science, *297:* 1186-1190, 2002.

20. Nishimura, K., Ikebuchi, M., Kanaoka, Y., Ohgi, S., Ueta, E., Nanba, E., and Ito, H. Relationships between matrix metalloproteinases and tissue inhibitor of metalloproteinases in the wall of abdominal aortic aneurysms. Int Angiol, *22:* 229-238, 2003.

21. Annabi, B., Shédid, D., Ghosn, P., Kenigsberg, R. L., Desrosiers, R. R., Bojanowski, M. W., Beaulieu, E., Nassif, E., Moumdjian, R., and Béliveau, R. Differential regulation of matrix metalloproteinase activities in abdominal aortic aneurysms. J Vasc Surg., *35:* 539-546, 2002.

22. Vinh, A., Gaspari, T. A., Liu, H. B., Dousha, L. F., Widdop, R. E., and Dear, A. E. A Novel Histone Deacetylase Inhibitor Reduces Abdominal Aortic Aneurysm Formation in Angiotensin II-Infused Apolipoprotein E-Deficient Mice. J Vasc Res, *45:* 143-152, 2008.

23. Goodall, S., Crowther, M., Hemingway, D. M., Bell, P. R., and Thompson, M. M. Ubiquitous Elevation of Matrix Metalloproteinase-2 Expression in the Vasculature of Patients With Abdominal Aneurysms. Circulation, *104:* 304-309, 2001.

24. Keeling, W. B., Armstrong, P. A., Stone, P. A., Bandyk, D. F., and Shames, M. L. An Overview of Matrix Metalloproteinases in the Pathogenesis and Treatment of Abdominal Aortic Aneurysms. Vascular and Endovascular Surgery, *39:* 457-464, 2005.

25. Petersen, E., Wågberg, F., and Angquist, K. A. Proteolysis of the abdominal aortic aneurysm wall and the association with rupture. Eur J Vasc Endovasc Surg, *23:* 153-157, 2002.

26. Pyo, R., Lee, J. K., Shipley, J. M., Curci, J. A., Mao, D., Ziporin, S. J., Ennis, T. L., Shapiro, S. D., Senior, R. M., and R.W., T. Targeted gene disruption of matrix metalloproteinase-9 (gelatinase B) suppresses development of experimental abdominal aortic aneurysms. J Clin Invest, *105:* 1641-1649, 2000.

27. Wilson, W. R. W., Anderton, M., Choke, E. C., Dawson, J., Loftus, I. M., and Thompson, M. M. Elevated Plasma MMP1 and MMP9 are Associated with

Abdominal Aortic Aneurysm Rupture. European Journal of Vascular and Endovascular Surgery, *35:* 580-584, 2008.

28. Sangiorgi, G., D'Averio, R., Mauriello, A., Bondio, M., Pontillo, M., Castelvecchio, S., Trimarchi, S., Tolva, V., Nano, G., Rampoldi, V., Spagnoli, L. G., and Inglese, L. Plasma Levels of Metalloproteinases-3 and -9 as Markers of Successful Abdominal Aortic Aneurysm Exclusion After Endovascular Graft Treatment. Circulation, *104:* I-288-295, 2001.

29. Basalyga, D. M., Simionescu, D. T., Xiong, W., Baxter, B. T., Starcher, B. C., and Vyavahare, N. R. Elastin Degradation and Calcification in an Abdominal Aorta Injury Model: Role of Matrix Metalloproteinases. Circulation, *110:* 3480-3487, 2004.

30. Longo, G. M., Buda, S. J., Fiotta, N., Xiong, W., Griener, T., Shapiro, S., and Baxter, B. T. MMP-12 has a role in abdominal aortic aneurysms in mice. Surgery, *137:* 457-462, 2005.

31. Silence, J., Collen, D., and Lijnen, H. R. Reduced Atherosclerotic Plaque but Enhanced Aneurysm Formation in Mice With Inactivation of the Tissue Inhibitor of Metalloproteinase-1 (TIMP-1) Gene. Circ Res, *90:* 897-903, 2002.

32. Griendling, K. K., Minieri, C. A., Ollerenshaw, J. D., and Alexander, R. W. Angiotensin II stimulates NADH and NADPH oxidase activity in cultured vascular smooth muscle cells. Circ Res., *74:* 1141-1148, 1994.

33. Griendling, K. K. and Fitzgerald, G. A. Oxidative Stress and Cardiovascular Injury Part I: Basic Mechanisms and In Vivo Monitoring of ROS. Circulation, *108:* 1912-1916, 2003.

34. Grigoryants, V., Hannawa, K. K., Pearce, C. G., Sinha, I., Roelofs, K. J., Ailawadi, G., Deatrick, K. B., Woodrum, D. T., Cho, B. S., Henke, P. K., Stanley, J. C., Eagleton, M. J., and Upchurch, J., Gilbert R. Tamoxifen up-regulates catalase production, inhibits vessel wall neutrophil infiltration, and attenuates development of experimental abdominal aortic aneurysms. Journal of Vascular Surgery, *41:* 108-114, 2005.

35. Deshpande, N. N., Sorescu, D., and Seshiah, P. Mechanism of Hydrogen Peroxide-Induced Cell Cycle Arrest in Vascular Smooth Muscle. Antioxidants and Redox Signaling, *4:* 845-854, 2002.

36. Miller, F. J., Jr, Sharp, W. J., Fang, X., Oberley, L. W., Oberley, T. D., and Weintraub, N. L. Oxidative Stress in Human Abdominal Aortic Aneurysms: A Potential Mediator of Aneurysmal Remodeling. Arterioscler Thromb Vasc Biol, *22:* 560-565, 2002.

37. Griendling, K. K. and Fitzgerald, G. A. Oxidative Stress and Cardiovascular Injury Part II: Animal and Human Studies. Circulation, *108:* 2034-2040, 2003.

38. Miller, F. J., Jr. Aortic Aneurysms: It's All About the Stress. Arterioscler Thromb Vasc Biol, *22:* 1948-1949, 2002.

39. Gavrila, D., Li, W. G., McCormick, M. L., Thomas, M., Daugherty, A., Cassis, L. A., Miller, F. J., Jr, Oberley, L. W., Dellsperger, K. C., and Weintraub, N. L. Vitamin E Inhibits Abdominal Aortic Aneurysm Formation in Angiotensin II-Infused Apolipoprotein E-Deficient Mice. Arterioscler Thromb Vasc Biol, *25:* 1671-1677, 2005.

40. Grote, K., Flach, I., Luchtefeld, M., Akin, E., Holland, S. M., Drexler, H., and Schieffer, B. Mechanical Stretch Enhances mRNA Expression and Proenzyme Release of Matrix Metalloproteinase-2 (MMP-2) via NAD(P)H Oxidase-Derived Reactive Oxygen Species. Circ Res, *92:* 80e-86, 2003.

41. Törnwall, M. E., Virtamo, J., Haukka, J. K., Albanes, D., and Huttunen, J. K. [alpha]-Tocopherol (vitamin E) and [beta]-carotene supplementation does not affect the risk for large abdominal aortic aneurysm in a controlled trial. Atherosclerosis, *157:* 167-173, 2001.

42. Zhang, Y., Griendling, K. K., Dikalova, A., Owens, G. K., and Taylor, W. R. Vascular Hypertrophy in Angiotensin II-Induced Hypertension Is Mediated by Vascular Smooth Muscle Cell-Derived H2O2. Hypertension, *46:* 732-737, 2005.

43. Tangirala, R., Rubin, E., and Palinski, W. Quantitation of atherosclerosis in murine models: correlation between lesions in the aortic origin and in the entire aorta, and differences in the extent of lesions between sexes in LDL receptor-deficient and apolipoprotein E-deficient mice. J. Lipid Res., *36:* 2320-2328, 1995.

44. Daugherty, A., Manning, M. W., and Cassis, L. A. Angiotensin II promotes atherosclerotic lesions and aneurysms in apolipoprotein E-deficient mice. J. Clin. Invest., *105:* 1605-1612, 2000.

45. Weiss D, K. J., Taylor WR Angiotensin II-Induced Hypertension Accelerates the Development of Atherosclerosis in ApoE-Deficient Mice. Circulation, *103:* 448-454, 2001.

46. Anidjar, S., Salzmann, J., Gentric, D., Lagneau, P., Camilleri, J., and Michel, J. Elastase-induced experimental aneurysms in rats. Circulation, *82:* 973-981, 1990.

47. Freestone, T., Turner, R. J., Higman, D. J., Lever, M. J., and Powell, J. T. Influence of Hypercholesterolemia and Adventitial Inflammation on the Development of Aortic Aneurysm in Rabbits. Arterioscler Thromb Vasc Biol, *17:* 10-17, 1997.

48. Di Martino, E. S., Bohra, A., Vande Geest, J. P., Gupta, N., Makaroun, M. S., and Vorp, D. A. Biomechanical properties of ruptured versus electively repaired abdominal aortic aneurysm wall tissue. Journal of Vascular Surgery, *43:* 570-576, 2006.

49. Truijers, M., Pol, J., Schultzekool, L., van Sterkenburg, S., Fillinger, M., and Blankensteijn, J. Wall stress analysis in small assymptomatic, symptomatic and ruptured abdominal aortic aneurysms. Eur J Vasc Endovasc Surg, *33:* 401-407, 2008.

50. Fillinger, M., Marra, S., Raghavan, M., and Kennedy, F. Prediction of rupture risk in abdominal aortic aneurysm during observation:wall stress versus diameter. J Vasc Surg., *37:* 724-732, 2003.

51. Rodríguez, J. F., Ruiz , C., Doblaré, M., and Holzapfel, G. A. Mechanical stresses in abdominal aortic aneurysms: influence of diameter, asymmetry, and material anisotropy. J Biomech Eng, *130:* 021023, 2008.

52. Watton PA and NA, H. Evolving mechanical properties of a model of abdominal aortic aneurysm. Biomechanical Model and Mechanbiolgy, 2007.

53. Hariton I, d. G., Gasser TC, Holzapfel GA. Stress-modulated collagen fiber remodeling in a human carotid bifurcation. J Theor Biol, *248:* 460-470, 2007.

54. Wagenseil, J. E., Nerurkar, N. L., Knutsen, R. H., Okamoto, R. J., Li, D. Y., and Mecham, R. P. Effects of elastin haploinsufficiency on the mechanical behavior of mouse arteries. Am J Physiol Heart Circ Physiol, *289:* H1209-1217, 2005.

55. Gasser, T. C., Ogden, R. W., and Holzapfel, G. A. Hyperelastic modelling of arterial layers with distributed collagen fibre orientations. J R Soc Interface, *22:* 15-35, 2006.

56. Coulson, R. J., Cipolla, M. J., Vitullo, L., and Chesler, N. C. Mechanical properties of rat middle cerebral arteries with and without myogenic tone. J Biomech Eng, *126:* 76-81, 2004.

57. Chesler, N. C., Thompson-Figueroa, J., and Millburne, K. Measurements of mouse pulmonary artery biomechanics. J Biomech Eng, *126:* 309-314, 2004.

58. Humphrey, J. D. and Na, S. Elastodynamics and arterial wall stress. Annals of Biomedical Engineering, *30:* 509-523, 2002.

59. Fung, Y. C., Fronek, K., Patitucci, P. Pseudoelasticity of arteries and the choice of its mathematical expression. American Jounral of Physiology, *237:* H620-H631, 1979.

60. Roach, M. R. and Burton, A. C. The reason for the shape of the distensibility curve of arteries. Canadian Journal of Biochemistry and Physiology, *35:* 681-690, 1957.

61. Weizsacker, H. W., Holzapfel, G. A., Desch, G. W., and Pascale, K. Strain energy density function for arteries from different topographical sites. Biomediz. Tech., *40:* 139-141, 1995.

62. Holzapfel, G. A. and Weizsacker, H. W. Biomechanical behavior of the arterial wall and its numerical characterization. Computers in Biology and Medicine, *28:* 377-392, 1998.

63. Matsumoto, T. and Hayashi, K. Stress and strain distribution in hypertensive and normotensive rat aorta considering residual strain. Journal of Biomechanical Engineering, *118:* 62-73, 1996.

64. Chuong, C. J. and Fung, Y. C. On residual stresses in arteries. Journal of Biomechanical Engineering, *108:* 189-192, 1986.

65. Yoshimura, K., Aoki, H., Ikeda, Y., Fujii, K., Akiyama, N., Furutani, A., Hoshii, Y., Tanaka, N., Ricci, R., Ishihara, T., Esato, K., Hamano, K., and Matsuzaki, M.

Regression of abdominal aortic aneurysm by inhibition of c-Jun N-terminal kinase. *11:* 1330-1338, 2005.

66. Guo, X. and Kassab, G. S. Variation of mechanical properties along the length of the aorta in C57bl/6 mice. Am J Physiol Heart Circ Physiol, *285:* H2614-2622, 2003.

67. Heng, M. S., Fagan, M. J., Collier, J. W., Desai, G., McCollum, P. T., and Chetter, I. C. Peak wall stress measurement in elective and acute abdominal aortic aneurysms. J Vasc Surg., *47:* 17-22, 2008.

68. Raghavan, M. L., Webster, M. W., and Vorp, D. A. Ex vivo biomechanical behavior of abdominal aortic aneurysm: assessment using a new mathematical model. Annals of Biomedical Engineering, *24:* 573-582, 1996.

69. Davis, N. P., Han, H.-C., Wayman, B., and Vito, R. Sustained Axial Loading Lengthens Arteries in Organ Culture. Annals of Biomedical Engineering, *33:* 867-877, 2005.

70. Gleason RL, G. S., Wilson E, Humphrey JD. A multiaxial computer-controlled organ culture and biomechanical device for mouse carotid arteries. Journal of Biomechanical Engineering, *126:* 787-795, 2004.

71. Sumitani, M., Cabral, A. M., Michelini, L. C., and Krieger, E. M. In vivo adaptive responses of the aorta to hypertension and aging. Am J Physiol Heart Circ Physiol, *273:* H96-103, 1997.

72. Gregersen, H., Zhao, J., Lu, X., Zhou, J., and Falk, E. Remodelling of the zero-stress state and residual strains in apoE-deficient mouse aorta. Biorheology, *44:* 75-89, 2007.

73. Maiellaro, K. and Taylor, W. R. The role of the adventitia in vascular inflammation. Cardiovasc Res, *75:* 640-648, 2007.

74. Manning, M. W., Cassis, L. A., and Daugherty, A. Differential Effects of Doxycycline, a Broad-Spectrum Matrix Metalloproteinase Inhibitor, on Angiotensin II-Induced Atherosclerosis and Abdominal Aortic Aneurysms. Arterioscler Thromb Vasc Biol, *23:* 483-488, 2003.

75. Woessner, J. The determination of hydroxyproline in tissue and protein samples containing small proportions of this imino acid. Arch Biochem Biophys, *93:* 440-447, 1961.

76. Junqueira, L. C. U., Cossermelli, W., and Brentani, R. Differential staining of collagens Type I, II, and II by sirius red and polarization microscopy. Arch Histol Jpn, *41:* 267-274, 1978.

77. Chatelain RE and BN., D. Increased DNA replication in the arterial adventitia after aortic ligation. Hypertension, *11:* I130-I134, 1988.

78. Burke, J. M., Balian, G., Ross, R., and Bornstein, P. Synthesis of types I and III procollagen and collagen by monkey aortic smooth muscle cells in vitro. Biochemistry, *16:* 3243-3249, 1977.

79. Andrikopoulos, K., Liu, X., Keene, D. R., Jaenisch, R., and Ramirez, F. Targeted mutation in the col5a2 gene reveals a regulatory role for type V collagen during matrix assembly. *9:* 31-36, 1995.

80. Birk, D., Fitch, J., Babiarz, J., Doane, K., and Linsenmayer, T. Collagen fibrillogenesis in vitro: interaction of types I and V collagen regulates fibril diameter. J Cell Sci, *95:* 649-657, 1990.

81. VanBavel, E., Siersma, P., and Spaan, J. A. E. Elasticity of passive blood vessels: a new concept. Am J Physiol Heart Circ Physiol, *285:* H1986-2000, 2003.

82. Nenoi, M., Ichimura, S., Mita, K., Yukawa, O., and Cartwright, I. L. Regulation of the Catalase Gene Promoter by Sp1, CCAAT-recognizing Factors, and a WT1/Egr-related Factor in Hydrogen Peroxide-resistant HP100 Cells. Cancer Res, *61:* 5885-5894, 2001.

83. Fung, Y. C. What are the residual stresses doing in our blood vessels? Annals of Biomedical Engineering, *19:* 237-249, 1991.

84. Greenwald, S. E., J. E. Moore, J., Rachev, A., Kane, T. P. C., and Meister, J.-J. Experimental Investigation of the Distribution of Residual Strains in the Artery Wall. Journal of Biomechanical Engineering, *119:* 438-444, 1997.

85. Holzapfel, G. A. and Gasser, T. C. A new constitutive framework for arterial wall mechanics and a comparative study of material models. journal of Elasticity, *61:* 1-48, 2000.

86. Azeloglu, E. U., Albro, M. B., Thimmappa, V. A., Ateshian, G. A., and Costa, K. D. Heterogeneous transmural proteoglycan distribution provides a mechanism for regulating residual stresses in the aorta
10.1152/ajpheart.01027.2007. Am J Physiol Heart Circ Physiol, *294:* H1197-1205, 2008.

87. Evanko, S., Raines, E., Ross, R., Gold, L., and Wight, T. Proteoglycan distribution in lesions of atherosclerosis depends on lesion severity, structural characteristics, and the proximity of platelet-derived growth factor and transforming growth factor-beta. Am J Pathol, *152:* 533-546, 1998.

88. Valenta, J., Svoboda, J., Valerianova, D., and Vitek, K. Residual strain in human atherosclerotic coronary arteries and age related geometrical changes. Bio-Medical Materials And Engineering, *9:* 311-317, 1999.

89. Tamarina, N. A., Grassi, M. A., Johnson, D. A., and Pearce, W. H. Proteoglycan Gene Expression Is Decreased in Abdominal Aortic Aneurysms. Journal of Surgical Research, *74:* 76-80, 1998.

90. Guo, X., Lanir, Y., and Kassab, G. S. Effect of osmolarity on the zero-stress state and mechanical properties of aorta. Am J Physiol Heart Circ Physiol, *293:* H2328-2334, 2007.

91. Azeloglu, E. U., Albro, M. B., Thimmappa, V. A., Ateshian, G. A., and Costa, K. D. Heterogeneous transmural proteoglycan distribution provides a mechanism for regulating residual stresses in the aorta. Am J Physiol Heart Circ Physiol, *294:* H1197-1205, 2008.

92. Nissen R, C. G., Udenfriend S. Increased turnover of arterial collagen in hypertensive rats. Proc Natl Acad Sci USA, *75:* 451-453, 1978.

93. Humphrey, J. Remodeling of a collagenous tissue at fixed lengths. J Biomech Eng, *121:* 591-597, 1999.

94. Perrin, S. and Foster, J. A. Developmental regulation of elastin gene expression. Critical Reviews in Eukaryote Gene Expression, *7:* 1-10, 1997.

95. vonMaltzahn, W. W., Warriyar, R. G., and Keitzer, W. F. Experimental measurements of elastic properties of media and adventitia of bovine carotid arteries. Journal of Biomechanics, *17:* 839-847, 1984.

96. Watton, P. and Hill, N. Evolving mechanical properties of a model of abdominal aortic aneurysm. Biomechanics and Modeling in Mechanobiology, 2007.

97. von Maltzahn, W. W., Warriyar, R. G., and Keitzer, W. F. Experimental measurements of elastic properties of media and adventitia of bovine carotid arteries. Journal of Biomechanics, *17:* 839-847, 1984.

98. Holzapfel, G. A. Determination of material models for arterial walls from uniaxial extension tests and histological structure. Journal of Theoretical Biology, *238:* 290-302, 2006.

99. Demiray H, V. R. A layered cylindrical shell model for an aorta. Int J Eng Sci, *29:* 47-51, 1991.

100. Guo, X., Lu, X., and Kassab, G. S. Transmural strain distribution in the blood vessel wall. Am J Physiol Heart Circ Physiol, *288:* H881-886, 2005.

101. Sverdlik A, L. Y. Time dependent mechanical behaviour of sheep digital tendons, including the effects of preconditioning. J Biomech Eng, *124:* 78-84, 2002.

102. Shadwick, R. Mechanical design in arteries. J Exp Bio, *202:* 3305-3313, 1999.

103. Sacks, M. Incorporation of experimentally derived fiber orientation into a structural consitutive model for planar collagenous tissues. ASME J Biomech Eng, *125:* 280-287, 2003.

104. Durante W, Liao L, Reyna SV, Peyton KJ, and AI, S. Physiological cyclic stretch directs L-arginine transport and metabolism to collagen synthesis in vascular smooth muscle. FASEB J., *14:* 1775-1783, 2000.

105. Wilson, E., Mai, Q., Krishnankutty, S., Weiss, R., and Harlan, E. I. Mechanical strain induces growth of vascular smooth muscle cells via autocrine action of PDGF. J Cell Biol, *123:* 741-747, 1993.

106. Na, S., Trache, A., Trzeciakowski, J., Sun, Z., Meininger, G., and Humphrey, J. Time-dependent Changes in Smooth Muscle Cell Stiffness and Focal Adhesion Area in Response to Cyclic Equibiaxial Stretch. Annals of Biomedical Engineering, *36:* 369-380, 2008.

107. Arora PD, M. C. Dependence of collagen remodelling on alpha-smooth muscle actin expression by fibroblasts. Journal of Cellular Physiology, *159:* 161-175, 1994.

108. Clerin, V., Nichol, J. W., Petko, M., Myung, R. J., Gaynor, J. W., and Gooch, K. J. Tissue Engineering of Arteries by Directed Remodeling of Intact Arterial Segments. Tissue Engineering, *9:* 461-472, 2003.

109. Han, H.-C., Ku, D. N., and Vito, R. P. Arterial Wall Adaptation under Elevated Longitudinal Stretch in Organ Culture. Annals of Biomedical Engineering, *31:* 403-411, 2003.

110. Jackson, Z. S., Gotlieb, A. I., and Langille, B. L. Wall Tissue Remodeling Regulates Longitudinal Tension in Arteries. Circ Res, *90:* 918-925, 2002.

111. Galis, Z., Sukhova, G., and Libby, P. Microscopic localization of active proteases by in situ zymography: detection of matrix metalloproteinase activity in vascular tissue. FASEB J., *9:* 974-980, 1995.

VITA

KATHRYN A. MAIELLARO

Katie was born in Pensacola, Florida to Edward and Rachel Maiellaro on June 29, 1978. She has two older bothers Matthew and Thomas. Katie attended St. Paul Catholic School from Kindergarten through 8th grade. She enrolled in the International Baccalaureate Program at Pensacola High School and graduated Valedictorian in May of 1996. Katie played varsity tennis throughout high school and won the district title her sophomore year. In August of 1997, she enrolled at the University of Florida, where she was a member of Chi Omega Sorority and studied Engineering Science with a focus in Biomechanics. Katie graduated with a Bachelor degree in Engineering Science in May of 2001 and remained at Florida to obtain a Master of Engineering in Biomedical Engineering, which she received in August of 2003. That same month Katie moved to Atlanta to pursue her doctorate in Biomedical Engineering in the Wallace H. Coulter Department of Biomedical Engineering at Georgia Tech and Emory University. Katie still lists tennis as one of her hobbies, and spends most of her free time playing with her dog Bodhi, planning a wedding to her handsome fiancé Tom Rafferty, and babysitting her six beautiful nephews.